Improving the Long-Term Condition of Pavements in Massachusetts and Determining Return on Investment: Implementing the AASHTO

Principal Investigator (s)
Walaa Mogawer

University of Massachusetts Dartmouth

Research and Technology Transfer Section
MassDOT Office of Transportation Planning

U.S. Department of Transportation
Federal Highway Administration

Technical Report Document Page

1. Report No. 24-067	2. Government Accession No. n/a	3. Recipient's Catalog No. n/a		
4. Title and Subtitle Improving the Long-Term Condition of Pavements in Massachusetts and Determining Return on Investment: Implementing the AASHTO Mechanistic-Empirical Pavement Design Guide - PHASE III		5. Report Date November 2024		
		6. Performing Organization Code n/a		
7. Author(s) Harold L. Von Quintus, Abu Sufian, Wouter Brink, Praveen Gopisetti & Walaa S. Mogawer		8. Performing Organization Report No. 24-067		
9. Performing Organization Name and Address University of Massachusetts Dartmouth 285 Old Westport Road North Dartmouth, MA 02747 & Applied Research Associates, Inc. 100 Trade Centre Drive, Suite 200 Champaign, IL 61820		10. Work Unit No. (TRAIS) n/a		
		11. Contract or Grant No.		
12. Sponsoring Agency Name and Address Massachusetts Department of Transportation Office of Transportation Planning Ten Park Plaza, Suite 4150, Boston, MA 02116		13. Type of Report and Period Covered Final Report - November 2024 [November 2022 – November 2024]		
		14. Sponsoring Agency Code n/a		
15. Supplementary Notes Project Champion – Edmund Naras, MassDOT				

16. Abstract

The Massachusetts Department of Transportation (MassDOT) has sponsored multiple projects to implement the Mechanistic-Empirical Pavement Design Guide (MEPDG). Due to the complexity of this research, a four-phase approach spanning several years was proposed. This report focuses on Phase 3.

In Phase 3, MassDOT concentrated on using the Long-Term Pavement Performance (LTPP) test pavements in Massachusetts and neighboring states. The LTPP projects provided readily available data on traffic, climate, subgrade, materials, structure, and performance. The objective was to verify the global flexible pavement calibration coefficients using LTPP test sections for predicting distresses and smoothness, and to locally/regionally calibrate the flexible pavement transfer functions (rutting, transverse cracking, fatigue cracking, reflection cracking, and smoothness) if necessary.

This report presents the 2024 regional calibration coefficients determined by distress type for new flexible pavements and asphalt overlays, along with a comparison to the global calibration coefficients of version 3 of the Pavement Mechanistic Empirical Design (PMED) software. It is recommended that MassDOT use these regional calibration coefficients for designing and evaluating flexible pavements, as they reflect the performance of flexible pavements and asphalt overlays in Massachusetts. Additionally, the default laboratory coefficients for dense-graded asphalt mixtures are suggested for predicting fatigue, thermal, and reflective cracking in Massachusetts until more comprehensive laboratory mixture test data can be collected. A future phase of this study, Phase 4, will address this shortcoming by incorporating additional roadway segments in Massachusetts and conducting laboratory tests on the asphalt mixtures used in these segments.

17. Key Word Mechanistic-Empirical, distress, prediction, pavement design, transfer function, Long-Term Pavement Performance, LTPP		18. Distribution Statement unrestricted		
19. Security Classif. (of this report) unclassified	20. Security Classif. (of this page) unclassified		21. No. of Pages 108	22. Price n/a

Form DOT F 1700.7 (8-72)   Reproduction of completed page authorized

This page left blank intentionally.

Improving the Long-Term Condition of Pavements in Massachusetts and Determining Return on Investment: Implementing the AASHTO Mechanistic-Empirical Pavement Design Guide - PHASE III

Final Report

Prepared By:

Harold L. Von Quintus, P.E.
Abu Sufian
Wouter Brink
Praveen Gopisetti

Applied Research Associates, Inc.
100 Trade Centre Drive, Suite 200
Champaign, IL 61820

Commonwealth Professor Walaa S. Mogawer, P.E., F.ASCE
Principal Investigator

University of Massachusetts Dartmouth
Highway Sustainability Research Center
151 Martine Street – Room 131
Fall River, MA 02723

Prepared For:

Massachusetts Department of Transportation
Office of Transportation Planning
Ten Park Plaza, Suite 4150
Boston, MA 02116

November 2024

This page left blank intentionally.

Acknowledgements

Disclaimer

This page left blank intentionally.

Executive Summary

The Massachusetts Department of Transportation (MassDOT) has sponsored multiple projects regarding use of the pavement mechanistic-empirical design (PMED) software. Due to the complexity of the research problem, a multi-phase (four phases) approach over several years was suggested to complete this research. This report focuses solely on Phase 3.

In this phase, MassDOT elected to initially focus on using the Long-Term Pavement Performance (LTPP) test pavements in Massachusetts and in adjacent states because the Long-Term Pavement Performance (LTPP) projects have readily available traffic, climate, subgrade, materials, structure, and performance data. This report describes and presents the results from using the LTPP sites to assess the global calibration coefficients and determine if adjustments to the global coefficients are needed for the region around Massachusetts.

A total of 18 new flexible and 48 asphalt overlay LTPP sections were used for the regional verification and calibration process of the flexible pavement transfer functions. All appropriate LTPP test sections were used in the verification and calibration process. The following sections summarize the results that are discussed in detail in the report.

Rut Depth
The total rut depth was predicted for the new flexible and asphalt overlay sites using the global calibration coefficients for the asphalt, aggregate base, and subgrade/embankment layers. Results from the verification concluded that the global rut depth calibration coefficients and the laboratory-derived plastic strain coefficients for dense-graded asphalt mixtures are acceptable for use in Massachusetts. The reliability equation, however, was different from the global equation. Results from the 2024 data found the standard deviation of residuals to be constant for all pavement layers, rather than a function of the predicted layer rut depths. The following summarizes the findings:

- Rut depth calibration coefficients:

    o For dense-graded asphalt mixtures, use the 2018 global calibration coefficients (β_{1r} = 0.40; β_{2r} = 0.52; and β_{3r} = 1.36). The 2018 default laboratory derived plastic strain coefficients for dense-graded asphalt mixtures were found to be representative for most asphalt mixtures included in the regional calibration using the LTPP sites in Massachusetts and adjacent states and are suggested for initial use (k_{r1} = -2.45; k_{r2} = 3.01; and k_{r3} =0.22).

    o For unbound aggregate base layers, use the 2018 global calibration coefficients (k_{s1} = 0.965 and β_{s1} = 1.0).

    o For unbound subgrade or embankment soils, use the 2018 global calibration coefficients that are soil dependent (coarse-graded soils, k_{s1} =

0.965 and $\beta_{s1} = 1.0$; fine-graded soils, $k_{s1} = 0.675$ and $\beta_{s1} = 1.0$; and sands, $k_{s1} = 0.635$ and $\beta_{s1} = 1.0$).

- Reliability equation/values: Different values than from the 2018 global values are suggested for initial use in Massachusetts, which are listed below.

  o Asphalt layer standard deviation of residuals for reliability is constant and is 0.060 inches.

  o Aggregate base layer standard deviation of residuals for reliability is constant and is 0.0079 inches.

  o Subgrade soil/embankment layer standard deviation of residuals for reliability is constant and is 0.029 inches.

Transverse Cracking

The total length of transverse cracks was predicted for the new flexible sites using the global calibration coefficient and an estimated asphalt mixture thermal coefficient of contraction. Many of the statistical values from the verification process comparing the predicted and measured values were good to fair, even considering the measurement error for transverse cracks. Thus, results from the verification concluded the global transverse cracking calibration coefficient are acceptable for use in Massachusetts. In addition, the global reliability equation was determined to be statistically the same for the 2024 data and is suggested for use in Massachusetts. The following summarizes the findings:

- Transverse cracking calibration coefficient: $\beta_t = 1.0$, which is the global calibration coefficient for dense-graded asphalt mixtures. The default laboratory adjustment factor, k_t which is mean annual air temperature dependent for dense-graded asphalt mixtures is suggested for use in Massachusetts.

- Reliability equation: found to be statistically the same as the global reliability equation.

$$\sigma_{TC-Level3} = 0.2386(TC) + 168$$

Where:

$\sigma_{TC-Level3g}$ = Standard deviation of residuals for transverse cracks, ft./mi.

TC = Predicted length of transverse cracks, ft./mi.

The results and suggestions are confined to the use of inputs level 3 asphalt mixture mechanistic properties (indirect tensile creep compliance and strength). A bias is noted and reported in the Mechanistic Empirical Pavement Design Guide (MEPDG) Manual of Practice between input level 3 and input level 1 or input level 2. As such, the calibration coefficient

derived using input level 3 asphalt mixture mechanistic properties does not apply to the use of input level 1 or input level 2 asphalt mixture mechanistic properties.

A 50 percent reliability level is suggested for transverse cracks. The suggestion is made because the transverse cracking model and transfer function do not consider the mechanisms of long-term shrinkage and asphalt absorption that can have an impact on the occurrence and propagation of transverse cracks.

Fatigue Cracking
The measured fatigue cracks recorded in the LTPP database were separated into bottom-up and top-down fatigue cracks using the procedure presented by FHWA (Von Quintus, et al., 2017). The procedure identifies characteristics of the crack initiation and growth patterns compared to the bottom-up fatigue damage index and groups the cracking into probable bottom-up or top-down cracks, as well as cracks initiating from construction and/or mixture anomalies.

Bottom-Up Fatigue Cracking
Results from the verification process concluded there was a statistical difference between the predicted and measured bottom-up fatigue cracks. The Calibration Assistance Tool (CAT) was used to optimize the regional bottom-up fatigue cracking calibration coefficients. The following are the optimized calibration coefficients.

- Bottom-Up fatigue cracking calibration coefficients: The bottom-up fatigue cracking calibration coefficients optimized from the CAT are: $C_1 = 1.11$, C_2 is mean annual air dependent in accordance with the global values, so there is no change, and C_3 remains unchanged from the global calibration. The default laboratory adjustment factors (k_f coefficients) were excluded from the optimization process using the CAT. The default laboratory coefficients for dense-graded asphalt mixtures are suggested for use in Massachusetts.

- Reliability equation: The 2024 reliability equation was found to be statistically different than for the 2018 global reliability equation. The following equation is suggested for initial use in Massachusetts.

$$\sigma_{BUC} = 3.5537 + 0.1496(FC_{BUC})$$

Where:

σ_{BUC} = Standard deviation of residuals for bottom-up fatigue cracks, percent total lane area.

FC_{BUC} = Predicted bottom-up fatigue cracks, percent lane area.

Top-Down Fatigue Cracking
Results from the verification process concluded there was a statistical difference between the predicted and measured top-down fatigue cracks. The CAT was used to optimize the regional

top-down cracking calibration coefficients. The following are the optimized calibration coefficients.

- Top-Down fatigue cracking calibration coefficients: The top-down fatigue cracking calibration coefficients optimized from the CAT are: $C_1 = 3.00$, $C_2 =$ is 0.60. The default laboratory adjustment factors (k_f coefficients) were excluded from the optimization process using the CAT. The default laboratory coefficients for dense-graded asphalt mixtures are suggested for use in Massachusetts.

- Reliability equation: The 2024 reliability equation was found to be statistically different than for the 2018 global reliability equation. The following equation is suggested for initial use in Massachusetts.

$$\sigma_{TDC} = 0.3667 + 0.1797(FC_{TDC})$$

Where:

σ_{TDC} = Standard deviation of residuals for top-down fatigue cracks, percent total lane area.

FC_{TDC} = Predicted top-down fatigue cracks, percent lane area.

Reflection Cracking

Fatigue and transverse cracks in the asphalt overlay are composed of new cracks and cracks from the original asphalt surface reflecting through the asphalt overlay. The reliability of cracking in the asphalt overlays is based on the total area of fatigue cracks, and total length of transverse cracks – not just the reflected cracks.

Total (New and Reflective) Bottom-Up Fatigue Cracks

Results from the verification process concluded there was a statistical difference between the predicted and measured bottom-up fatigue cracks. The CAT was used to optimize the regional bottom-up fatigue cracking calibration coefficients. The following are the optimized calibration coefficients.

Bottom-Up fatigue cracking calibration coefficients: The bottom-up fatigue cracking calibration coefficients optimized from the CAT are: $C_1 = 1.11$, C_2 is mean annual air dependent in accordance with the global values, so there is no change, and C_3 remains unchanged from the global calibration. The default laboratory adjustment factors (k_f coefficients) were excluded from the optimization process using the CAT. The default laboratory coefficients for dense-graded asphalt mixtures are suggested for use in Massachusetts. The 2018 global reflection fatigue cracking coefficients are listed in the following.

Reflection Cracking Variable Name	Term or Coefficient	Bottom-Up Fatigue Reflective Cracks
Damage Index Stress Intensity Coefficient	k_1	0.012
Damage Index Stress Intensity Coefficient	k_2	0.005
Damage Index Stress Intensity Coefficient	k_3	1.0
Damage Index Calibration Coefficient	c_1	0.38
Damage Index Calibration Coefficient	c_2	1.66
Damage Index Calibration Coefficient	c_3	2.72
Transfer Function Calibration Coefficient	c_4	105.4
Transfer Function Calibration Coefficient	c_5	-7.02

Reliability equation: The 2024 reliability equation was found to be statistically different from the 2018 global reliability equation. The following equation is suggested for initial use in Massachusetts.

$$\sigma_{RC-BUC} = 1.8387(FC_{RC-BUC})^{0.2093}$$

Where:

σ_{FC-BUC} = Standard deviation of residuals for total bottom-up fatigue cracks (new and reflective), percent total lane area.

FC_{RC-BUC} = Predicted total bottom-up fatigue cracks (new and reflective), percent lane area.

Total (New and Reflective) Transverse Cracks

The total length of transverse cracks was predicted for new and reflective transverse cracks. The global calibration coefficient and an estimated asphalt mixture thermal coefficient of contraction determined for new flexible pavements were used for the asphalt overlay sections. Many of the statistical values from the verification process comparing the predicted and measured values were fair to poor. Results from the verification concluded the global total transverse cracking calibration coefficient was acceptable for use in Massachusetts. In addition, the global reliability equation was determined to be statistically different from the 2018 global reliability equation. The following summarizes the findings:

Total transverse cracking (new and reflective) calibration coefficient: $\beta_t = 1.0$, which is the global calibration coefficient for dense-graded asphalt mixtures. The default laboratory adjustment factor, k_t which is mean annual air temperature dependent for dense-graded asphalt mixtures is suggested for use in Massachusetts. The 2018 global transverse reflection cracking coefficients are listed in the following.

Reflection Cracking Variable Name	Term or Coefficient	Transverse Reflective Cracks
Damage Index Stress Intensity Coefficient	k_1	0.012
Damage Index Stress Intensity Coefficient	k_2	0.005
Damage Index Stress Intensity Coefficient	k_3	1.0
Damage Index Calibration Coefficient	c_1	3.22
Damage Index Calibration Coefficient	c_2	25.7
Damage Index Calibration Coefficient	c_3	0.1
Transfer Function Calibration Coefficient	c_4	133.4
Transfer Function Calibration Coefficient	c_5	-72.4

Reliability equation: found to be statistically different than for the 2018 global reliability equation. The 2024 regional reliability equation for total transverse cracks is listed below.

$$\sigma_{RC-TC-Level3} = 69.61(TC_{RC})^{0.2893}$$

Where:

$\sigma_{RC\text{-}TC\text{-}Level3g}$ = Standard deviation of residuals for total transverse cracks (new and reflective), ft./mi.

TC_{RC} = Predicted total length of transverse cracks (new and reflective), ft./mi.

The results and suggestions are confined to the use of inputs level 3 asphalt mixture mechanistic properties (indirect tensile creep compliance and strength). A bias is noted and reported in the MEPDG Manual of Practice between input level 3 and input level 1 or input level 2. As such, the calibration coefficient derived using input level 3 asphalt mixture mechanistic properties does not apply to the use of input level 1 or input level 2 asphalt mixture mechanistic properties.

A 50 percent reliability level is suggested for transverse cracks. The suggestion is made because the transverse cracking model and transfer function do not consider the mechanisms of long-term shrinkage and asphalt absorption that can have an impact on the occurrence and propagation of transverse cracks.

Smoothness
The International Roughness Index (IRI) was predicted for new flexible pavement and asphalt overlay sites using the global calibration coefficients. Results from the verification concluded that the global IRI regression equation regression coefficients are acceptable for use in Massachusetts. The global reliability equation is also suggested for use in design. The following summarizes the findings:

- IRI regression coefficients: The 2018 global regression coefficients are: C_1 (rut depth coefficient) = 40.0; C_2 (total fatigue cracking coefficient) = 0.40; C_3 (transverse cracking coefficient) = 0.008, and C4 (site factor coefficient) = 0.015).

- Reliability equation/values: The 2024 regional standard deviation of residuals equation is suggested for use, which is listed below.

$$\sigma_{IRI} = 9.1082 * \text{Ln}(IRI) - 27.288$$

This page left blank intentionally.

Table of Contents

List of Tables

This page left blank intentionally.

List of Figures

This page left blank intentionally.

List of Acronyms

Acronym	Expansion
AASHTO	American Association of State Highway Transportation Officials
ANOVA	Analysis of Variance
CAT	Calibration Assistance Tool
FHWA	Federal Highway Administration
FY	Fiscal Year
IRI	International Roughness Index
JRCP	Jointed Reinforced Concrete Pavement
LTE	Load Transfer Efficiency
LTPP	Long-Term Pavement Performance
MassDOT	Massachusetts Department of Transportation
M-E	Mechanistic-Empirical
MEPDG	Mechanistic Empirical Pavement Design Guide
PMED	Pavement Mechanistic-Empirical Design
SEE	Standard Error of the Estimate
SPR	State Planning and Research

This page left blank intentionally.

1.0 Introduction and Objectives

This study entitled "Improving the Long-Term Condition of Pavements in Massachusetts and Determining Return on Investment: Implementing the AASHTO Mechanistic-Empirical Pavement Design Guide - PHASE III" was undertaken as part of the Massachusetts Department of Transportation (MassDOT) Research Program. This program is funded with Federal Highway Administration (FHWA) State Planning and Research (SPR) funds. Through this program, applied research is conducted on topics of importance to the Commonwealth of Massachusetts transportation agencies.

1.1 Introduction

MassDOT is striving to improve its highway infrastructure's resiliency to climate change, environmental impacts, and traffic loading by implementing new technologies that can provide valuable return on investment. These improvements should begin with the pavement design process which currently utilizes antiquated empirical design methods from the 1960's. Implementing the American Association of State Highway Transportation Officials (AASHTO) new Mechanistic-Empirical (M-E) pavement design method currently used by at least 33 state agencies would be a significant improvement. The M-E design method incorporates performance models which are tailored to the region and form an important component of the design process. Additionally, because the AASHTO M-E design can predict pavement distresses, it could be used as a tool by MassDOT to measure the return on investment when using new technologies such as warm mix, bio-asphalts, modified asphalts, mixtures with increased recycled (sustainable) materials, etc. Furthermore, based on the predicted distresses, MassDOT can make decisions on which pavement preservation strategies should be implemented to improve and extend the pavement life of its road network. The AASHTO M-E design method predicts pavement distresses utilizing prediction models that were developed and nationally calibrated using in-service pavements. To accurately predict the performance in Massachusetts, these models will need to be calibrated according to local conditions.

Due to the complexity of the research problem, a multi-phase (four phases) approach over several years was suggested to complete this research. This report focuses solely on Phase 3.

1.2 Background

The Mechanistic Empirical Pavement Design Guide (MEPDG) was released to the AASHTO in 2004 and adopted by AASHTO in 2012 to replace the empirical 1993 AASHTO Design Guide. Successful implementation of the MEPDG depends on an agency's resources to obtain accurate design inputs, and assessing and adjusting the calibration coefficients, if needed. Calibrating the transfer functions enables agencies to use the MEPDG for new construction and rehabilitation pavement design with higher confidence.

Since 2009, many states have performed calibrations specific to their state using various techniques and procedures. The process of calibration revolves around analyzing relevant data and establishing model coefficients that accurately predict pavement distresses. After the MEPDG was released, the performance data expanded over time and model accuracy was improved.

The flexible pavement transfer functions were recalibrated in 2018 using v2.6. Version 2.6 is directly compatible with v3.0 for flexible pavements. PMED version 3, a web-based application, was released in fiscal year (FY) 2022. The recent release of the pavement mechanistic-empirical deign (PMED) software in FY 2023 included enhancements to improve on the efficiency of the design for both flexible and rigid pavements.

Prior to using PMED version 3, the global calibration coefficients for flexible pavement design should be verified and adjusted to confirm the transfer functions predict rutting, transverse cracking, fatigue cracking and smoothness without bias and at a reasonable accuracy. Thus, a verification and calibration of the PMED flexible pavement transfer functions, if needed, for use in Massachusetts was completed.

MassDOT has sponsored multiple projects regarding use of the PMED software. MassDOT started the implementation process to accurately define the inputs and selecting roadway segments to be used in the verification-calibration process. The site selection process and defining the layer material and other inputs requires a high level of effort and can be time consuming. As such, MassDOT initially elected to focus on using the Long-Term Pavement Performance (LTPP) test pavements in Massachusetts and in adjacent states because the LTPP projects have readily available traffic, climate, subgrade, materials, structure, and performance data. Thus, verification and calibration are referred to as a regional verification and calibration for Massachusetts.

MassDOT can use the results from the regional LTPP sites to strategically and accurately determine the type and number of roadway segments needed to determine if adjustments are needed to the global calibration coefficients. This report describes and presents the results from using the LTPP sites to assess the global calibration coefficients and determine if adjustments to the global coefficients are needed.

1.3 Project Objective and Report Focus

The objective of this study was twofold:

1. Verify the global flexible pavement calibration coefficients using the LTPP test sections located in Massachusetts and in adjacent states for predicting distresses and smoothness.

2. Locally/regionally calibrate the flexible pavement transfer functions, if deemed necessary.

The verification and local calibration process was based on the AASHTO MEPDG Local Calibration Guide (AASHTO, 2010), with an objective to reduce the error in estimating pavement distresses and eliminating bias between measured and predicted pavement distresses.[1] The verification and local calibration of the flexible pavement transfer functions was completed using the AASHTOWare Calibration Assistance Tool (CAT). This document discusses the verification and recalibration of the flexible pavement transfer functions using v3.0 of the AASHTOWare PMED software.

1.4 Organization of Report

The report is organized into nine chapters, including the Introduction (Chapter 1). The following is an outline of the contents within each chapter.

- Chapter 2 summarizes the criteria used to determine the accuracy of the global calibration coefficients and determine if the coefficients need to be adjusted for use in Massachusetts.

- Chapter 3 lists and summarizes the roadway segments used and included in the verification and calibration of the pavement transfer functions for use in Massachusetts. As stated in Chapter 3, the sites used for the calibration are from Massachusetts and adjacent states.

- Chapter 4 discusses the verification and recalibration of the rut depth transfer function.

- Chapter 5 discusses the verification and recalibration of the transverse cracking transfer function.

- Chapter 6 discusses the verification and recalibration of the fatigue cracking (bottom-up and top-down) transfer functions.

- Chapter 7 discusses the verification and recalibration of the reflection cracking transfer functions for bottom-up fatigue and transverse cracks.

- Chapter 8 discusses the verification and recalibration of the flexible pavement International Roughness Index (IRI) regression equation.

- Chapter 9 presents the summary and conclusions from the regional calibration and a listing of the calibration coefficients for all transfer functions and regression equations.

---

[1] The AASHTO Local Calibration Guide is being updated. The second edition is expected to be published in fiscal year 2025.

This page left blank intentionally.

2.0 Verification and Calibration Criteria

The pavement distress prediction models, or transfer functions, are the key components of the MEPDG. The accuracy of the transfer functions depends on an effective process of calibration and subsequent validation with independent data sets. The goal of the calibration process is to confirm the transfer function can predict, without bias, pavement distress and smoothness, and to determine the standard error associated with the transfer function.

The MEPDG Local Calibration Guide provides suggested guidelines for verifying and calibrating the transfer functions (AASHTO, 2010). Results or the outcomes from the PMED software in predicting flexible pavement and asphalt overlay distress and performance measures are assessed to answer two questions:

1. Does the given global transfer function and model coefficients exhibit a reasonable goodness of fit between measured and predicted observations?

2. Are the distresses/performance measures predicted without significant bias?

Assessment on the adequacy of the calibration coefficients is based on selected diagnostic statistical variables, including the standard error of the estimate (SEE), s_e/s_y, bias, and R^2. A reasonable goodness of fit is typically defined through R^2. The s_e/s_y statistical term, however, is the standard error or the standard deviation of the residual errors divided by the standard deviation of the observations, which normalizes the error relative to the observations the model is predicting. The residual error is the predicted value minus the measured value.

The criteria used to determine the adequacy of the global model and transfer function coefficients for Massachusetts conditions are summarized in Table 1.[2]

---

[2] The criteria listed in Table 1 are the suggested values to assess the predicted performance measured in comparison to the measured values. Achieving a good to very good rating and accepting the null hypotheses for the slope, intercept, and bias for all performance measures is almost impossible considering the measurement error for the pavement performance indicators.

Table 1. Criteria for Assessing Adequacy of MEPDG Transfer Functions

Criterion of Interest	Test Statistic	Range of Statistical Value	Rating or Assessment
Goodness of fit	s_e/s_y, (all model)	< 0.35	Very good
Goodness of fit	s_e/s_y, (all model)	0.35 to 0.55	Good
Goodness of fit	s_e/s_y, (all model)	0.56 to 0.75	Fair
Goodness of fit	s_e/s_y, (all model)	0.76 to 1.0	Poor
Goodness of fit	s_e/s_y, (all model)	> 1.0	Very poor
Goodness of fit	Coefficient of determination (R^2), percent (all models)	81 to 100	Very good (strong relationship)
Goodness of fit	Coefficient of determination (R^2), percent (all models)	64 to 81	Good
Goodness of fit	Coefficient of determination (R^2), percent (all models)	49 to 64	Fair
Goodness of fit	Coefficient of determination (R^2), percent (all models)	< 49	Poor (weak relationship)
Goodness of fit	Global rut depth model SEE	< 0.1 in.	Good
Goodness of fit	Global rut depth model SEE	0.1 to 0.2 in.	Fair
Goodness of fit	Global rut depth model SEE	> 0.2 in.	Poor
Goodness of fit	Global fatigue cracking model SEE	< 5 percent	Good
Goodness of fit	Global fatigue cracking model SEE	5 to 10 percent	Fair
Goodness of fit	Global fatigue cracking model SEE	> 10 percent	Poor
Goodness of fit	Global transverse cracking model SEE[3]	< 300 ft./mi.	Good
Goodness of fit	Global transverse cracking model SEE	300 to 600 ft./mi.	Fair
Goodness of fit	Global transverse cracking model SEE	> 600 ft./mi.	Poor
Goodness of fit	Global IRI model SEE	< 20 in/mi	Good
Goodness of fit	Global IRI model SEE	20 to 35 in/mi	Fair
Goodness of fit	Global IRI model SEE	> 35 in/mi	Poor
Bias	Hypothesis testing of slope of the linear measured versus predicted values. H_0: slope = 1	p-value > 0.05 (i.e., a 5 percent significant level)	Accept
Bias	Hypothesis testing of slope of the linear measured versus predicted values. H_0: slope = 1	p-value > 0.05 (i.e., a 5 percent significance level)[4]	Accept
Bias	Hypothesis testing of intercept of the linear measured versus predicted values. H_0: Intercept = 0	p-value > 0.05	Accept
Bias	Paired t-test between measured and predicted values. H_0: Bias = 0	p-value > 0.05	Accept

---

[3] Values are provided for the transverse cracking model SEE but the distress mechanism in the MEDPG is restricted to low temperature cracking while transverse cracks are a result of low temperature events and other factors like shrinkage of the asphalt layer. See Chapter 5 on Transverse Cracks for more detailed discussion on this topic.

[4] A p-value or level of significance of 5 percent is suggested in the table. However, the Local Calibration Guide suggests a p-value 5 percent.

3.0 Flexible Pavement Test Sections

The roadway segments or test sections used for the verification and calibration of the MEPDG transfer functions for flexible pavements were restricted to those included in the LTPP program. Additional non-LTPP or roadway management sections were initially planned for use in Massachusetts, but the time required for extracting/reviewing the distress data and inputs to the MEPDG for each site was beyond the time frame initially set up for this phase of the project. As such, only LTPP sites located in Massachusetts and adjacent states were used.

A listing of the available LTPP sections is presented in Table 2, along with the number of observations or measurements. Maine is not adjacent to Massachusetts, but MassDOT suggested and agreed to the use of the LTPP sites located in Maine so they were included.

A total of 64 new flexible pavement sites and 48 asphalt overlay sites were identified from the LTPP database. The cells that are shaded in Table 2 identify the LTPP sites and data sets where only 1 measurement of the distress values were recorded in the LTPP database. Only 1 distress measurement restricts the prediction to 1 point in time and excludes information relative to the growth or increase in the distress or performance measure over time and traffic. Thus, the shaded LTPP test sections were not used in the verification.

Table 2. Flexible Pavement Test Sections Used for the Regional Calibration

State	LTPP Number	Data Sets with Total Number of Distress Observations New Flexible Rut Depth & IRI	Data Sets with Total Number of Distress Observations New Flexible Cracking	Data Sets with Total Number of Distress Observations Asphalt Overlay Rut Depth & IRI	Data Sets with Total Number of Distress Observations Asphalt Overlay Cracking
Connecticut	901	1	1	8	8
Connecticut	902	1	1	8	8
Connecticut	903	1	1	8	8
Connecticut	960	1	1	8	8
Connecticut	961	1	1	8	8
Connecticut	962	1	1	8	8
Connecticut	1803	23	8	12	7
Maine	501	13	9	None	None
Maine	502	1	1	12	8
Maine	503	1	1	12	8
Maine	504	1	1	12	8
Maine	505	1	1	12	8
Maine	506	1	1	12	8

State	LTPP Number	Data Sets with Total Number of Distress Observations New Flexible Rut Depth & IRI	Data Sets with Total Number of Distress Observations New Flexible Cracking	Data Sets with Total Number of Distress Observations Asphalt Overlay Rut Depth & IRI	Data Sets with Total Number of Distress Observations Asphalt Overlay Cracking
Maine	507	1	1	12	9
Maine	508	1	1	12	8
Maine	509	1	1	12	8
Maine	559	1	1	11	8
Maine	1001	5	1	5	3
Maine	1009	5	1	8	4
Maine	1012	8	2	None	None
Maine	1026	9	4	7	5
Maine	1028	4	1	10	7
Massachusetts	1002	18	10	None	None
Massachusetts	1003	7	2	None	None
Massachusetts	1004	9	2	6	5
New Hampshire	1001	16	9	4	4
New Jersey	501	17	9	None	None
New Jersey	502	2	1	18	10
New Jersey	503	2	1	17	11
New Jersey	504	2	1	17	10
New Jersey	505	2	1	17	10
New Jersey	506	2	1	17	10
New Jersey	507	2	1	17	10
New Jersey	508	2	1	17	10
New Jersey	509	2	1	17	10
New Jersey	559	2	1	17	10
New Jersey	560	2	1	17	10
New Jersey[5]	801	5	4	None	None
New Jersey	802	4	4	None	None
New Jersey	859	5	4	None	None
New Jersey	860	5	4	None	None
New Jersey	901	1	1	10	6
New Jersey	902	1	1	10	6
New Jersey	903	1	1	10	6

---

[5] The New Jersey LTPP SPS-8 sites do not include any traffic data, so these sites were excluded from the verification and calibration.

State	LTPP Number	Data Sets with Total Number of Distress Observations New Flexible Rut Depth & IRI	Data Sets with Total Number of Distress Observations New Flexible Cracking	Data Sets with Total Number of Distress Observations Asphalt Overlay Rut Depth & IRI	Data Sets with Total Number of Distress Observations Asphalt Overlay Cracking
New Jersey	960	1	1	10	6
New Jersey	961	1	1	10	6
New Jersey	962	1	1	9	5
New Jersey	1003	4	None	7	4
New Jersey	1011	6	1	6	4
New Jersey	1030	5	1	6	4
New Jersey	1033	6	1	9	7
New Jersey	1034	12	5	None	None
New Jersey	1638	12	5	None	None
New Jersey	6057	9	3	None	None
New York	801	20	18	None	None
New York	802	13	11	None	None
New York	859	12	10	None	None
New York	1008	1	None	8	3
New York	1011	5	1	6	3
New York	1643	8	4	4	3
New York	1644	8	4	5	3
Rhode Island	7401	None	None	None	None
Vermont	1002	23	16	None	None
Vermont	1004	10	4	7	6
Vermont	1681	3	1	9	3
Vermont	1683	4	1	14	8

The New Jersey LTPP SPS-8 sites do not include traffic data, so they were excluded from the calibration process. In addition, the Rhode Island LTPP test section is an asphalt overlay of a Jointed Reinforced Concrete Pavement (JRCP). JRCP is a rigid pavement design strategy that is not included in the MEPDG, so it was also excluded from the calibration process.

The data source for creating the .dgpx files was the LTPP database using the "best" available data. Input level 1 was used for many of the input variables for traffic, climate, the pavement layers, and subgrade soils. PMED global defaults were used for the inputs for which data were unavailable in the LTPP database. The asphalt dynamic modulus, indirect tensile creep compliance, IDT strength, plastic strain coefficients, and the fatigue strength are not included in the LTPP database, so input level 3 default values were used to predict flexible pavement distresses.

Appendix A includes a listing and basic structural information for each LTPP site. The original construction year for the new flexible pavement sections and the year of the asphalt overlays are included in Appendix A. Table 3 lists the age of the original construction sites and the age of the asphalt overlays. The age of the original construction or new flexible pavement is much higher than the age of the asphalt overlays. This is not considered detrimental to the verification-calibration of the flexible pavement transfer functions.

Table 3. Age of the LTPP Sites for the Last Cracking and/or Rutting Measurements Made and Included in the Regional Calibration

Age Parameter	New Flexible	Asphalt Overlays
Range of Age, years	1.06 to 44.2	0.04 to 21.6
Mean Age, years	16.6	6.5
Standard Deviation of Age	8.88	4.06

Appendix A also identifies when maintenance strategies were placed on the test sections. The application of some maintenance activities needs to be considered in verifying and/or recalibrating the transfer functions. Those maintenance activities considered by the PMED software were included in the calibration update where applicable. Repairs made to the test section are also recorded in the LTPP database. The repairs and localized maintenance activities were reviewed to determine how the activity affected the distress growth over time. The MEPDG does not include localized maintenance and repairs, so the distress values were generally removed for the full depth repairs and patches.

In summary, a total of 18 new flexible and 48 asphalt overlay LTPP sections were used for the regional verification and calibration process of the flexible pavement transfer functions. All appropriate LTPP test sections were used in the verification and calibration process. The number of new flexible sections is low using the standard split sampling technique for calibration and validation, while the number of asphalt overlay sections is adequate. The regional verification and calibration results using the LTPP sites was completed to provide MassDOT with information to determine an acceptable number of and inputs for the roadways segments to execute a calibration effort specific to Massachusetts. A validation of the revised or adjusted calibration factors was not included in the regional assessment on the accuracy of the distress transfer functions.

4.0 Rutting

4.1 Rut Depth Transfer Functions

The MEPDG computes rutting in flexible pavements by summing the plastic deformation in each pavement layer and the subgrade using two transfer functions: one for the asphalt layers and the other for unbound layers (aggregate base and subgrade layers).

4.1.1 Asphalt Layer Rut Depth Transfer Function

The plastic strain in the asphalt layer ε_p is computed in accordance with equation 1 as a function of the vertical elastic (resilient) strain ε_v calculated with elastic layered analysis.

$$\varepsilon_p = \varepsilon_v k_z \beta_{1r} 10^{k_{1r}} N^{k_{3r}\beta_{3r}} T^{k_{2r}\beta_{2r}} \qquad \text{(Eq. 1)}$$

Where:

N = Cumulative number of loading cycles.

T = Asphalt layer temperature (°F).

k_z = Confinement factor, which is a function of the depth D below the surface (inches):

$$k_z = (C_1 + C_2 D)0.328196^D \qquad \text{(Eq. 2)}$$

$$C_1 = -0.1039 (h_{ac})^2 + 2.4868 \ h_{ac} - 17.342 \qquad \text{(Eq. 3)}$$

$$C_2 = 0.0172 (h_{ac})^2 - 1.7331 \ h_{ac} + 27.428 \qquad \text{(Eq. 4)}$$

k_{1r}, k_{2r}, and k_{3r} = Plastic strain parameters derived from the repeated load plastic strain test: k_{1r} is the intercept and is -2.45, k_{3r} is the slope in the steady state zone of plastic strain versus number of load cycles and is 0.22, and k_{2r} is the temperature exponent or the impact of temperature on the intercept and is 3.01. Figure 1 includes a screen shot of the PMED software for the laboratory derived global default plastic strain coefficients for the asphalt layers.

β_{1r}, β_{2r}, and β_{3r} = Calibration coefficients with global default values of β_{1r} = 0.40, β_{3r} = 1.36, and β_{2r} = 0.52. Figure 1 includes a screen shot of the PMED software for the global calibration coefficients for predicting the rut depth in the asphalt layers.

Figure 1. Screen Shot of the PMED Software Displaying the Default Laboratory Plastic Strain Coefficients and Global Calibration Coefficients for Predicting the Rut Depth in the Asphalt Layers.

4.1.2 Unbound Layer Rut Depth Transfer Function (Aggregate Base and Subgrade Layers)

The plastic strain in the unbound layers (aggregate or granular base, subbase, and subgrade or embankment layers) is computed in accordance with equation 5 as a function of the vertical elastic (resilient) strain calculated from layered elastic analysis.

$$\varepsilon_p = \varepsilon_v \beta_{s1} k_{s1} \left(\frac{\varepsilon_0}{\varepsilon_r}\right) e^{-\left(\frac{\rho}{N}\right)^\beta} \tag{Eq. 5}$$

Where:

N = Number of load cycles.

k_{s1} = Laboratory derived plastic strain coefficient for unbound pavement materials. The global default values are 0.965 for unbound aggregate base layers and coarse-grained soils, 0.675 for fine-grained soils, and 0.635 for sandy soils. Figure 2 includes a screen shot of the PMED software for the laboratory derived default plastic strain coefficient for predicting the rut depth in the unbound aggregate base and subgrade layers.

β_{s1} = Local calibration factor with a default value equal to 1.0. Figure 2 includes a screen shot of the PMED software for the global calibration coefficient for predicting the rut depth in the unbound aggregate base and subgrade layers.

$\beta, \rho, \varepsilon_o$ are material properties obtained from laboratory repeated load tests at a resilient strain level of ε_r. The value of the exponent β (not a calibration coefficient) is

12

determined from the water content W_c (percent) in accordance with equation 6, and ρ is determined from β in accordance with equation 7.

$$log \ \beta = -0.61119 - 0.017638 \ W_c \qquad \text{(Eq. 6)}$$

$$\rho = 10^9 \left(\frac{C_0}{1-(10^9)\beta}\right)^{\frac{1}{\beta}} \qquad \text{(Eq. 7)}$$

Where:

$$C_0 = ln \left(\frac{\alpha_1 M_r^{b_1}}{\alpha_9 M_r^{b_9}}\right) \qquad \text{(Eq. 8)}$$

M_r = Resilient modulus,

b_1 and b_9 = Regression coefficients with values of 0, 0, respectively.

α_1, α_9 = Regression coefficients with values of 0.15 and 20, respectively.

AC Cracking Bottom Up	AC Cracking Top Down	AC Fatigue	AC Rutting	IRI	Subgrade Rutting	Thermal Fracture Level 1	Thermal Fracture Level 2	Thermal Fracture Level 3
Granular base rutting BS1					1			✓
Granular base rutting K1					0.965			✓
Granular Base rutting standard deviation					0.1477 * Pow(BASERUT,0.6711) + 0.001			✓
Subgrade A-3 rutting K1					0.635			✓
Subgrade coarse grained rutting K1					0.965			✓
Subgrade fine grained rutting K1					0.675			✓
Subgrade rutting BS1					1			✓
Subgrade Rutting standard deviation					0.1235 * Pow(SUBRUT,0.5012) + 0.001			✓

Figure 2. Screen Shot of the PMED Software Displaying the Default Laboratory Plastic Strain Coefficient and Global Calibration Coefficient for Predicting the Rut Depth in the Unbound Aggregate Base and Subgrade Layers.

4.2 Rut Depth Data Review

The total measured rut depth extracted from the LTPP database were reviewed for consistency of time-history values to identify potential anomalies or outliers and any bias between the two datasets (new flexible pavements and asphalt overlays). Figure 3 displays a cumulative

frequency diagram or distribution of rut depth for both data sets (new flexible and asphalt overlays). As displayed, the cumulative frequency of rut depth for both data sets is skewed to 0.

Table 4 compares the average (mean) and median rut depth measurements. Figure 4 displays the total rut depth as a function of test section age for all LTPP sections (original construction and asphalt overlays). As displayed, some of the new flexible sections and a few of the asphalt overlay sections have excessive rut depths. Figure 5 displays the measured total rut depths for the LTPP sections in States that exhibit the lower rut depths, while Figure 6 displays the measured total rut depths for the LTPP sections in the States with the higher or excessive rut depths.[6]
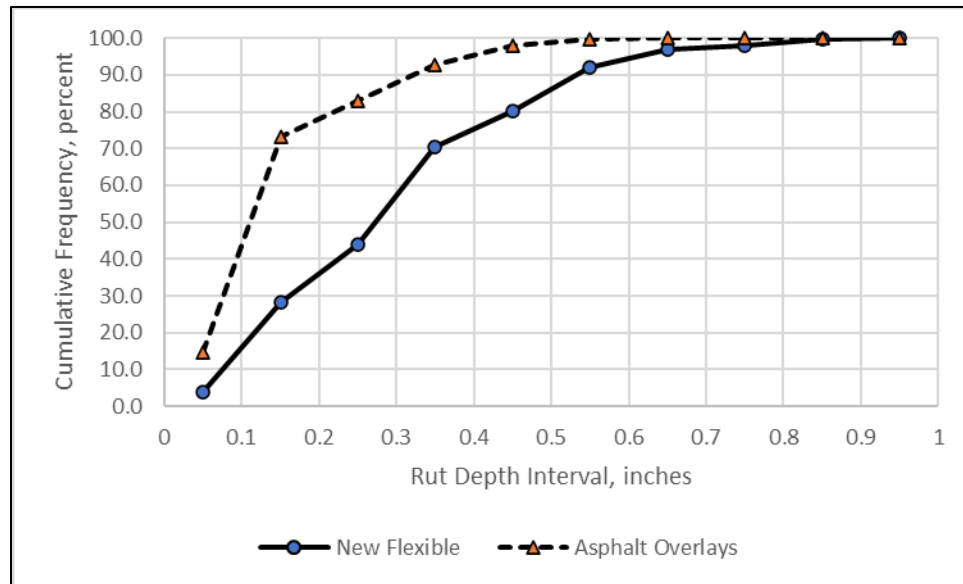
Figure 3. Cumulative Distribution of Total Rut Depth Data for the LTPP Sites Used in the Verification and Calibration Process.

---

[6] The intent of this comment is not to compare the rut depths measured on the LTPP test sections between states, but to categorize and identify the sections with different increases in rut depth over time. Traffic, subgrade, pavement structure, and other parameters have an impact on rutting.

Table 4. Mean, Median and Standard Deviation of the Measured Rut Depth

Statistical Value	Type of Section or Dataset	Type of Section or Dataset
	New Flexible	Asphalt Overlays
Total Number of Sections	64	48
Sections Applicable and Used in Verification/Calibration	18	48
Number of Measurements	345	521
Mean of Measured Total Rut Depth, inches	0.34	0.19
Median of Measured Total Rut Depth, inches	0.31	0.16
Standard Deviation of Measured Total Rut Depth, inches	0.117	0.114
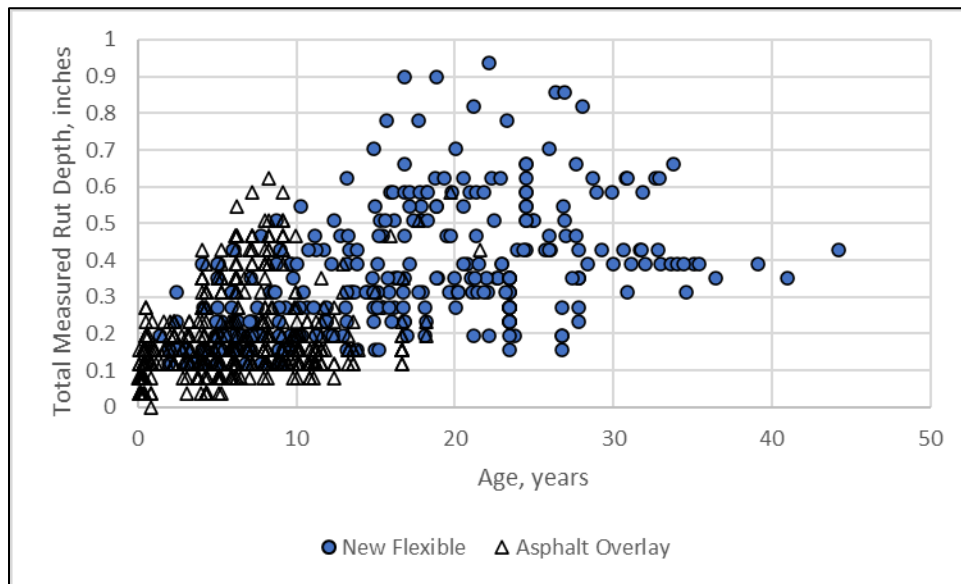
Figure 4. Increase in Total Rut Depth with Test Section Age.
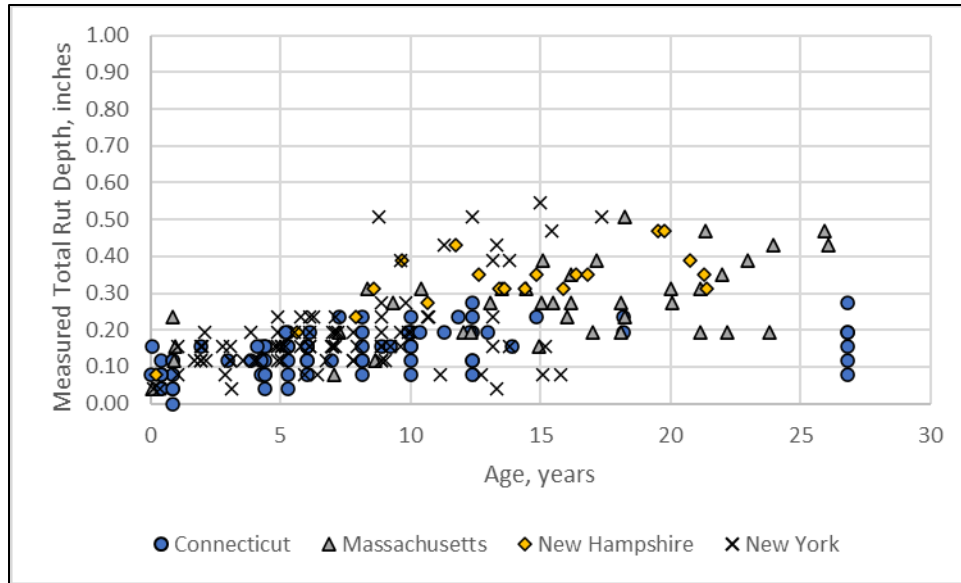
Figure 5. Increase in Total Rut Depth with Test Section Age for the Connecticut, Massachusetts, New Hampshire, and New York LTPP Sites.
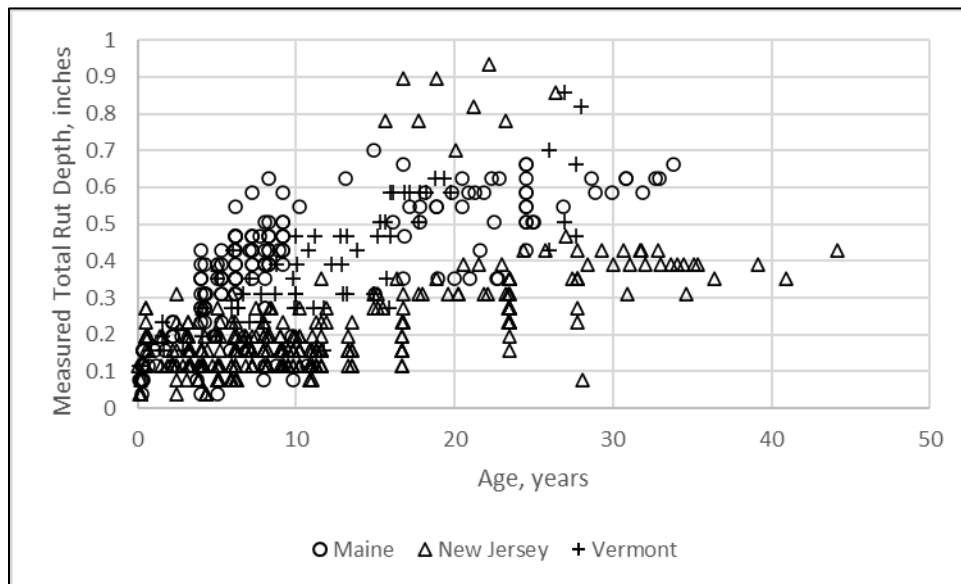
Figure 6. Increase in Total Rut Depth with Test Section Age for the Maine, New Jersey, and Vermont LTPP Sites.

16

The following are some points to be considered in the 2024 regional verification and calibration relative to the rut depth transfer functions.

1. As displayed in Figure 3 and Table 4, the total rut depth values for the asphalt overlays are skewed to 0, while the total rut depths for new flexible pavements have a more normal distribution. About half of the 18 LTPP new flexible sections and 4 of the 48 asphalt overlay sections exhibit rut depths higher than the typical threshold value of 0.5 inches.

2. Many of the new flexible and asphalt overlay sites exhibited typical rut depth growth over time. Figure 7 displays the measured rut depths for two LTPP sections, one in Massachusetts and one in New Hampshire. The measured rut depths for New Hampshire asphalt overlay of LTPP section 1001 is also displayed in Figure 7. An observation from Figure 7 is the variability in the measured rut depths over time. The measurement error is considered to be the larger component of the standard error of the estimate. The measurement error needs to be considered in assessing the accuracy of the transfer functions.

3. Some LTPP sites for both new flexible and asphalt overlays exhibited high rut depths indicating a deficiency of the asphalt mixtures. Figure 8 displays the measured rut depth for the original construction of the Maine SPS-5 project (LTPP section 0501) and the measured rut depths for selected sections with asphalt overlays (LTPP sections 0502, 0504, 0506, and 0508). The rutting of the original construction is high with values exceeding 0.5 inches after about 20 years, but the rutting of some of the asphalt overlay sections exceed 0.5 inches is less than 10 years. The rate of increase or growth in rut depth is considered significantly high and indicates a construction and/or material anomaly.

4. Figure 9 displays LTPP sections with a more gradual but continuous increase in the total rut depths for the original construction of Vermont section 1002 and the first and second asphalt overlay of Vermont section 1683. The rutting of the original construction of Vermont section 1683 is considered high with values exceeding 0.80 inches after 25 years. The rate of increase or growth in rut depth is considered moderate but continuous which can be characteristic of an asphalt mixture with poor strength or adhesion characteristics.
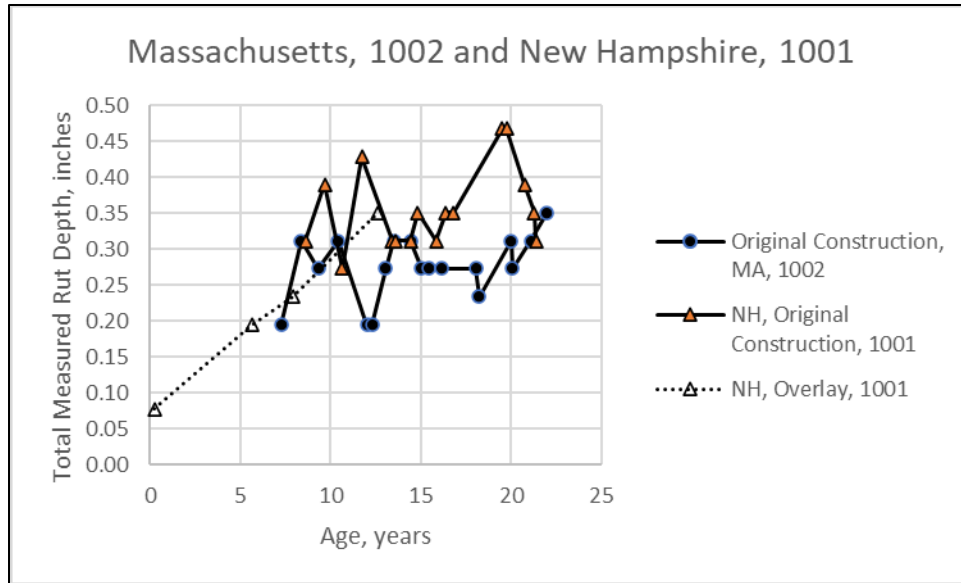
Figure 7. Increase in Total Rut Depth for Massachusetts New Flexible Section 1002 and the New Hampshire New Flexible and Asphalt Overlay for Section 1001 – Classified as Typical Rut Depths Growth Characteristics.
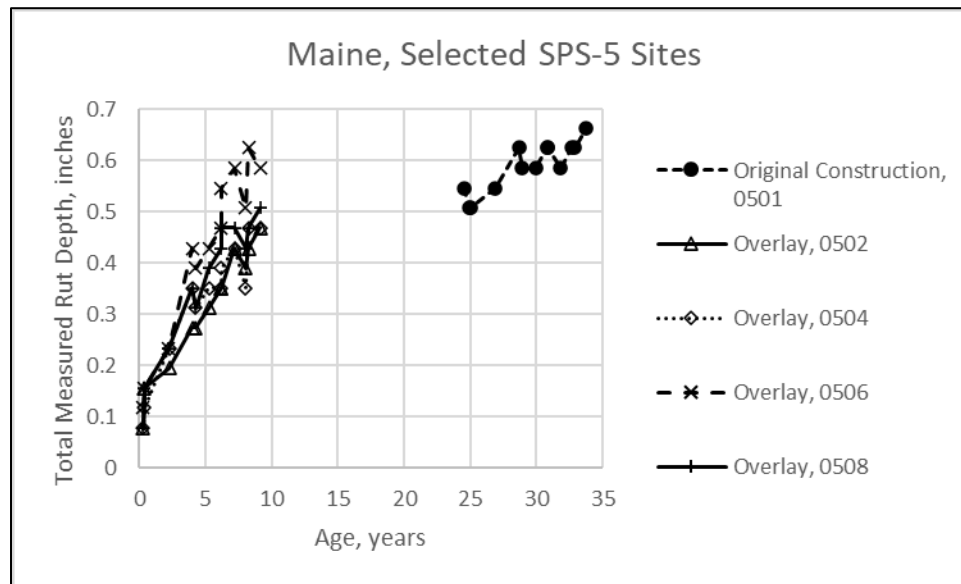
Figure 8. Increase in Total Rut Depth for the Maine New Flexible Section 0501 and Some of the Asphalt Overlay Sections – Classified as Excessive Rut Depths Growth Characteristics.
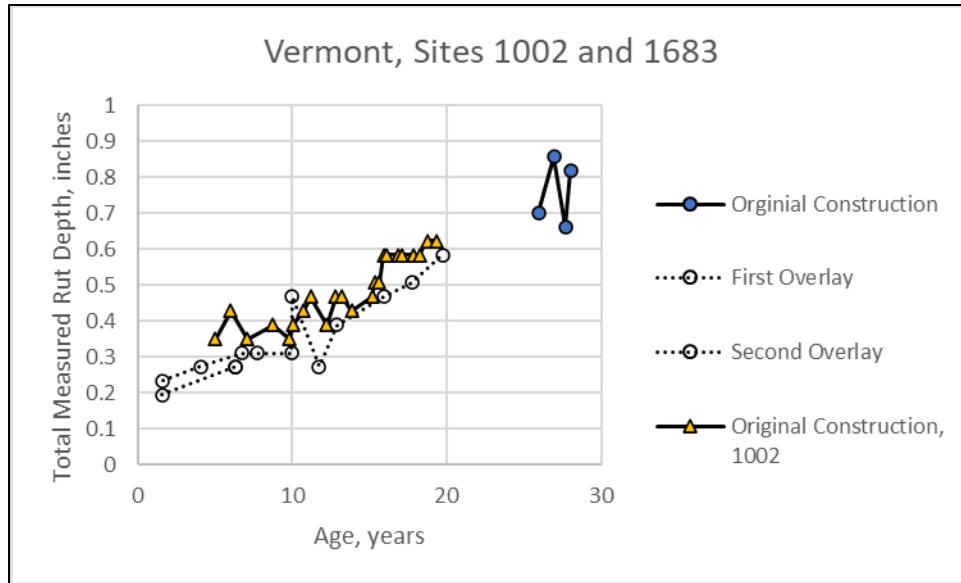
Figure 9. Increase in Total Rut Depth for the Vermont New Flexible and Asphalt Overlay of Section 1683 and the Vermont New Flexible Section 1002 – Classified as Moderate but Continuous Rut Depth Growth Characteristics.

5. Figure 10 displays two New Jersey LTPP new flexible sections and asphalt overlays of those sections (1003 and 1030). The rut depths for both new flexible sections are considered high with rut depths approaching 0.90 inches. The measured rut depths of the asphalt overlays of both sections, however, is considered low with an increase in rut depths but with decreasing rates. This characteristic suggests most of the rutting of the new flexible sections could be attributed to the underlying unbound layers.
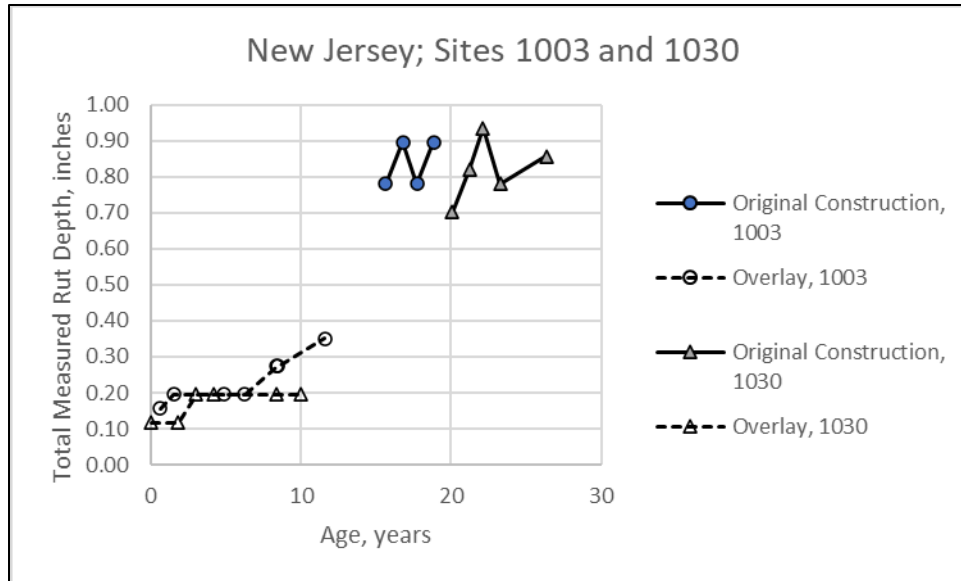
Figure 10. Increase in Total Rut Depth for the New Jersey New Flexible and Asphalt Overlay of Section 1003 and 1030 – Classified as Excessive Rutting for New Construction, but Typical Rutting for the Asphalt Overlay Growth Characteristics.

6. The distress measurement error is another point that needs to be considered in assessing the reasonableness of the calibration coefficients and accuracy of the distress models and transfer functions. Figure 7 through Figure 10 display the change in measured total rut depths over time for which the values increase and decrease and then increase. The measurement error can be the larger component of the standard error of the estimate, which complicates assessing the model's accuracy for which rut depths continually increase at a decreasing rate.

In summary, the measured rut depths for the LTPP sites included in the verification and calibration process were grouped into the following three categories for defining the laboratory-derived plastic strain coefficients for the asphalt layers and the unbound layers.

1. Low with typical rut depth growth characteristic: Rut depth is not excessive and increases over time but at a decreasing rate; considered to be representative of typical asphalt mixtures without construction or material anomalies.
2. Gradual but continuous rut depth growth characteristic: Rut depth continues to increase over time at the same rate or increasing rate; considered to be representative of asphalt mixtures with moisture damage, loss of adhesion between layers, etc.
3. Excessive rut depth growth characteristics: Rut depth increases at an increasing rate over time; considered to be representative of mixtures with stripping, loss of mixture adhesion, contaminated asphalt, loss of adhesion between layers, etc.

Appendix B identifies the LTPP sections included in the verification and the applicable rut depth growth category defined above. Forensic investigations of the LTPP sections with potential anomalies were performed on very few sections, so there is insufficient information within the LTPP database to determine the actual cause of the higher rut depths. Forensic investigations, however, have been performed on other calibration and research studies to measure the rut depth within each pavement layer through trenches and deriving the rut depth plastic strain coefficients of the different pavement layers and subgrade. The above rut depth growth categories and their laboratory-derived plastic strain coefficients are summarized in Table 5 that were estimated based on the results from these other forensic and research studies.

Table 5. Laboratory-Derived Plastic Strain Coefficients Assumed for the Rut Depth Categories and Suggested Based on Previous Forensic Investigation.

Rut Depth Growth Category	Lab-Derived Plastic Strain Coefficient k_{1r}	Lab-Derived Plastic Strain Coefficient k_{2r}	Lab-Derived Plastic Strain Coefficient k_{3r}
1. Rut depth increases over time but at a decreasing rate.	Global Default Value; -2.45	Global Default Value; 3.01	Global Default Value; 0.22
2. Rut depth continues to increase over time at the same rate or increasing rate.	-2.85	Global Default Value; 3.01	0.35
3. Rut depth increases over time at an increasing rate.	-3.25	Global Default Value; 3.01	0.43

4.3 Verification of the Rut Depth Transfer Function Global Coefficients

The total rut depth was predicted for the new flexible and asphalt overlay sites using the global calibration coefficients (see Figure 1 and Figure 2). Input level 3 for dynamic modulus and plastic strain coefficients was used because these asphalt properties are not included in the LTPP database.

Figure 11 displays a graphical comparison of the measured and predicted total rut depths using the global coefficients (laboratory strain and calibration). Figure 12 displays a graphical comparison of the measured and predicted total rut depth based on the plastic strain coefficients listed in Table 5. In summary, there was an improvement in the predicted rut depths using the values listed in Table 5 (see Appendix B). Figure 13 compares the predicted total rut depths to the residual errors (predicted minus measured value).
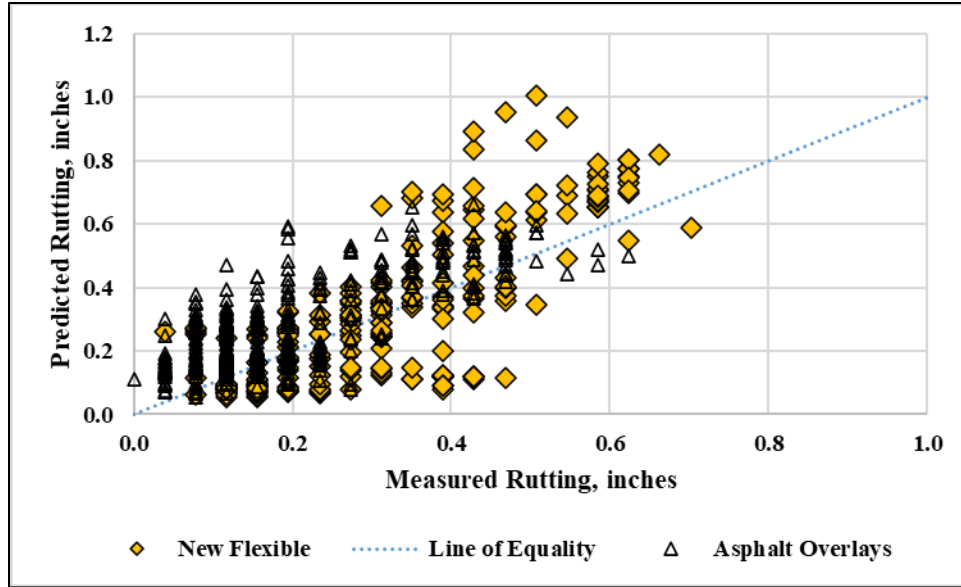
Figure 11. Predicted and Measured Total Rut Depths Using the 2018 Global Rut Depth Plastic Strain and Calibration Coefficients.

The data displayed in Figure 12 and Figure 13 are labeled as new flexible and asphalt overlay sections. No systematic difference in the residual errors or significant bias was observed between the two datasets when the difference in age is taken into consideration. Thus, the two datasets were combined.

The CAT was used to determine the statistical parameters between the predicted and measured total rut depth using the global calibration coefficients. Table 6 summarizes the statistical parameters using the laboratory-derived plastic strain and 2018 global calibration coefficients for the new flexible and asphalt overlay sites. As summarized, the s_e/s_y, R^2, bias, and SEE statistical parameters for rutting suggest a fair to good simulation or goodness of fit.

The hypothesis test for the slope being equal to 1 was accepted and with a low bias. However, the hypothesis test for the intercept and bias being equal to 0 based on the paired t-test between the predicted and measured total rut depths were rejected. The greater the number of observations, however, will result in a rejection even when the difference is less than the error of the measurement.

22
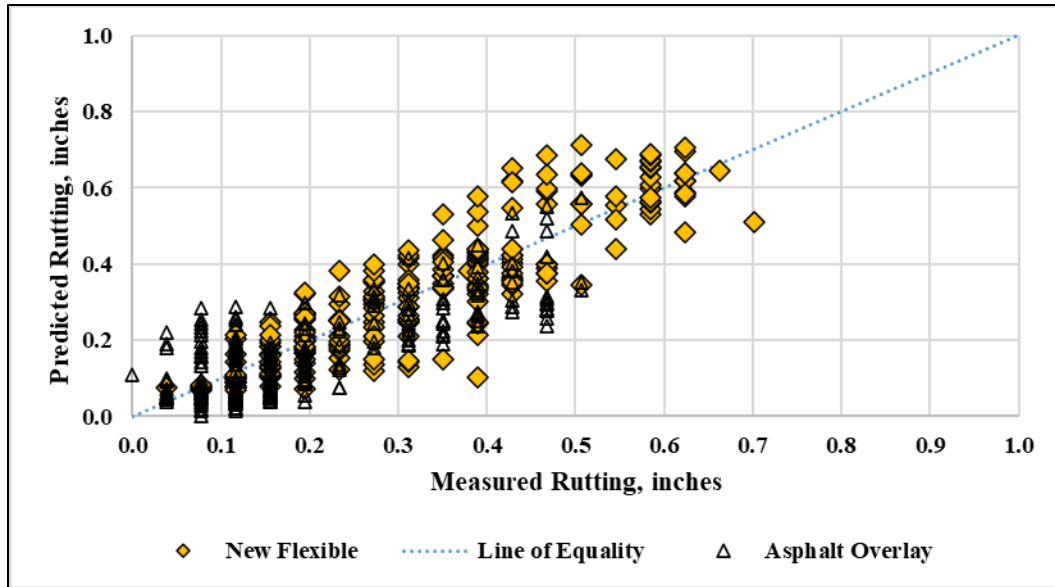
Figure 12. Predicted and Measured Total Rut Depths Using the Laboratory-Derived Plastic Strain Coefficients and the 2018 Global Calibration Coefficients.
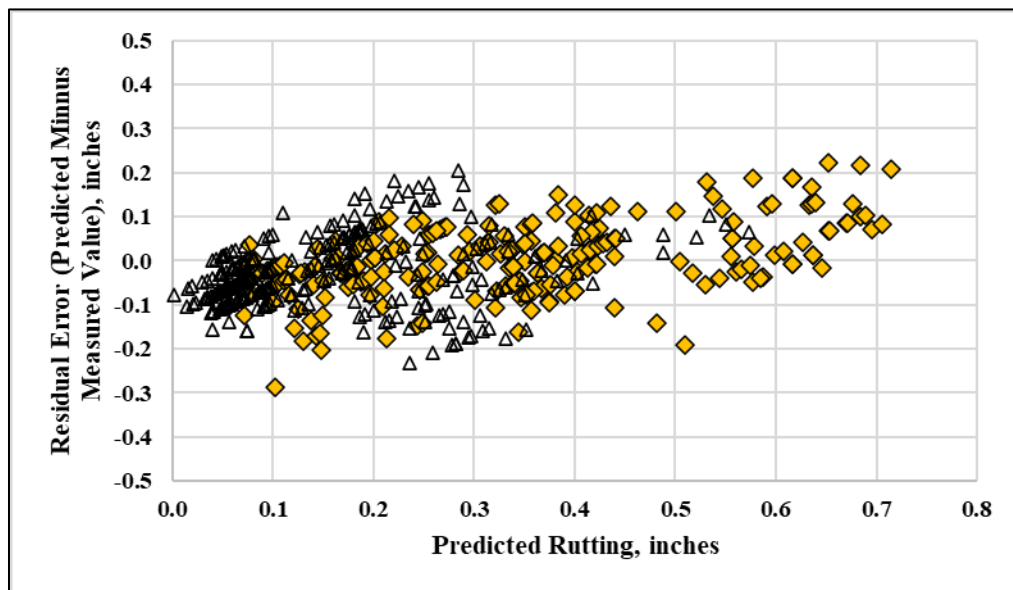
Figure 13. Predicted Total Rut Depths Using the Laboratory-Derived Plastic Strain Coefficients and the 2018 Global Calibration Coefficients as Compared to the Residual Error.

Table 6. Results from Using the 2018 Global Calibration Coefficients to Predict Total Rut Depth for Massachusetts.

Statistical Parameters for Total Rut Depth Model and Transfer Functions	PMED, Version 3.0; New Flexible and Asphalt Overlays
Number of Total Sections	66
Number of Observations	567
Goodness-of-Fit: R-squared	0.768 (Good)
Goodness-of-Fit: Se/Sy	0.568 (Fair)
Goodness-of-Fit: SEE, inches	0.0814 (Good)
Goodness-of-Fit: Standard Deviation of Residuals	0.0814
Goodness-of-Fit: Slope	0.971
Goodness-of-Fit: Intercept	-0.00854
Bias	-0.016 (Low)
Hypothesis Test; H_0 p-value: Slope = 1.0	Accept (p-value: 0.406)
Hypothesis Test; H_0 p-value: Intercept = 0.0	Reject (p-value: 0.0008)
Hypothesis Test; H_0 p-value: Paired t-test; Bias = 0.	Reject (p-value: 0.0000)

Overall, the verification suggests the rut depth model and transfer functions provide a good goodness of fit for explaining the total measured rut depths. In addition, no consistent difference exists between the new flexible and asphalt overlay sections. Even though the hypothesis for the intercept and bias were rejected, the global calibration coefficients of the rut depth transfer functions are considered adequate. It is difficult for the hypothesis test to be accepted for all three variables and result in a high goodness of fit considering the rut depth measurement error.

4.4 Reliability Equations for Rut Depth

The MEPDG estimates pavement design reliability, using the estimate of rutting in each pavement layer based on the average input values and the standard deviation of residual errors for rutting. However, the measured rut depth in the asphalt, aggregate base, and subgrade layers are not a measured value but are a calculated value based on the total rut depth measured at the surface. The rut depth standard deviation of residual errors prediction equation were developed as follows:

1. Divide the predicted rut depth into 4 or more intervals.

2. For each interval, determine mean predicted rut depth and standard deviation of residual errors (i.e., standard deviation of predicted minus measured rut depth values that fall within the given interval).

3. Develop a linear or nonlinear model to fit the mean predicted rut depth and standard deviation of the residual errors.

Figure 14 displays the standard deviation of residuals for the total predicted rut depth (cumulative rut depth in all layers) compared to the total predicted rut depth. A borderline between fair to good relationship exists between the standard deviation of the residuals and total predicted rut depth. More importantly, the slope is shallow and suggests that a constant or average standard deviation of residuals (0.0717 inches) applies to the total rut depth.

The PMED software, however, reports the predicted total and asphalt layer rut depth and the reliability of both variables. The rut depth reliability is based on the individual layers, rather than the total predicted rut depth.
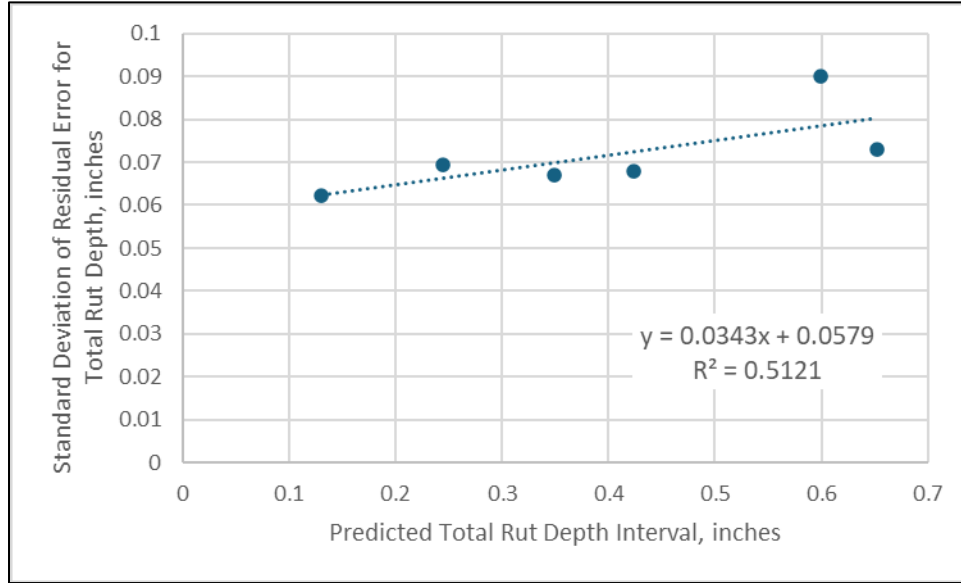
Figure 14. Standard Deviation of Residual Errors of the Predicted Total Rut Depths for all Pavement Layers.

The resulting standard deviation of the residual errors from the 2024 calibration data using v3.0 and the 2024 regional calibration coefficients is summarized below for each major type of materials in a flexible pavement.

- Asphalt Layers: Figure 15 displays a comparison of the predicted asphalt layer rut depth and residual error. As shown, the residual error increases with increasing predicted asphalt layer rut depth. Equation 9 is the standard deviation of residuals for predicted rut depths in the asphalt layers, which is displayed in Figure 16 in comparison to the global standard deviation of residuals equation. As displayed, the regional asphalt layer standard deviation of residuals is statistically constant throughout the range of predicted asphalt layer rutting. Although the residual errors are related to the predicted asphalt layer rut depth, the variability of the residual errors are the same throughout the predicted values.

$$\sigma_{RD-Asphalt} = 0.060(RD_{Asphalt})^{0.00} + 0 = 0.060 \qquad \text{(Eq. 9)}$$

25

Where:

$\sigma_{RD\text{-}Asphalt}$ = Standard deviation of residual errors (predicted minus measured rut depth) for the asphalt layers.

$RD_{Asphalt}$ = Average rut depth predicted for all asphalt layers.
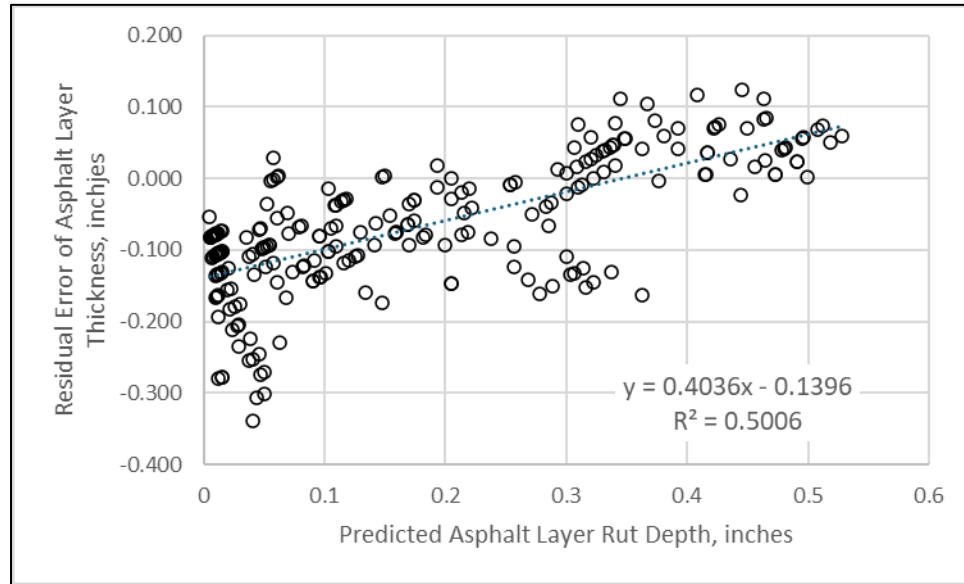
Figure 15. Residual Error Compared to the Predicted Rut Depth for the Asphalt Layers.
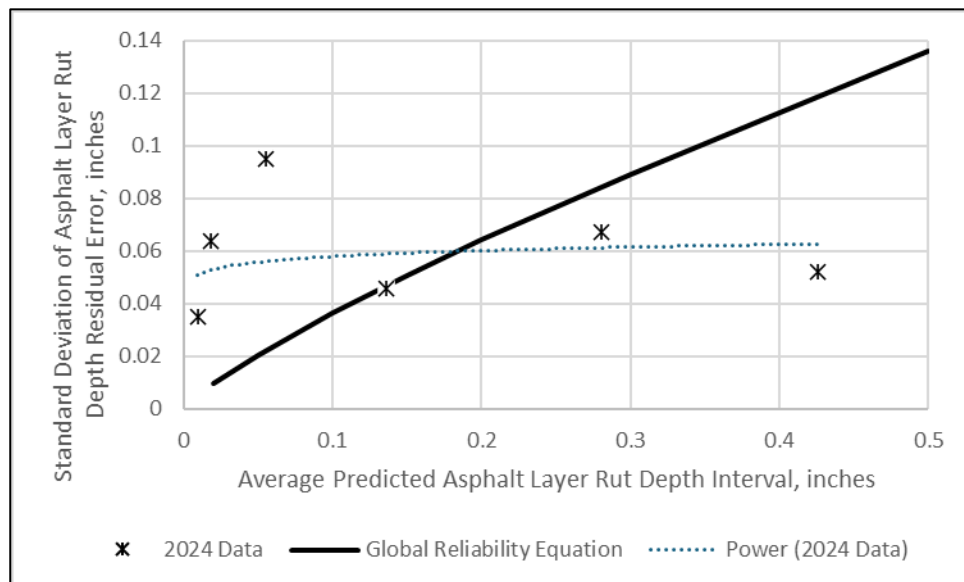
Figure 16. Standard Deviation of Residual Errors Equation for Estimating the Reliability of the Predicted Rut Depths for the Asphalt Layers.

26

- Unbound Aggregate Layers: Figure 17 displays a comparison of the predicted unbound aggregate base layer rut depth and residual error. As shown, the residual error increases with increasing predicted rut depth in the unbound aggregate base layers. Equation 10 is the standard deviation of residuals for predicted rut depths in the unbound aggregate base layers, which is displayed in Figure 18 in comparison to the global standard deviation of residuals equation. As displayed, the regional unbound aggregate base layer standard deviation of residuals is statistically constant throughout the range of predicted values. Although the residual errors are related to the predicted unbound aggregate base layer rut depth, the variability of the residual errors are the same throughout the predicted values.

$$\sigma_{Unbound\ Base} = 0.0079(RD_{Unbound\ Base})^{0.00} + 0.0 = 0.0079 \quad\quad\text{(Eq. 10)}$$

Where:

$\sigma_{RD\text{-}Unbound\ Base}$ = Standard deviation of residual errors (predicted minus measured rut depth) for the unbound aggregate base layers.

$RD_{Unbound\text{-}Aggregate}$ = Average rut depth predicted for all unbound aggregate base layers.

- Unbound Subgrade/Embankment Layers: Figure 19 displays a comparison of the predicted unbound subgrade and embankment layer rut depth and residual error. As shown, the residual error increases with increasing predicted rut depth in the unbound subgrade and embankment layers. Equation 11 is the standard deviation of residuals for predicted rut depths in the unbound subgrade/embankment layers, which is displayed in Figure 20 in comparison to the global standard deviation of residuals equation. As displayed, the regional unbound subgrade/embankment standard deviation of residuals have a negative slope. However, it is suggested that MassDOT simply use the average of the standard deviation throughout the predicted subgrade rut depths.

$$\sigma_{Unbound\ Subgrade} = 0.029(RD_{Unbound\ Subgrade})^{0.00} + 0.0 = 0.029 \quad\quad\text{(Eq. 11)}$$

Where:

$\sigma_{UnboundSubgrade}$ = Standard deviation of residual errors (predicted minus measured rut depth) for the unbound subgrade/embankment layers.

$RD_{UnboundSubgrade}$ = Average rut depth predicted for all subgrade/embankment layers.
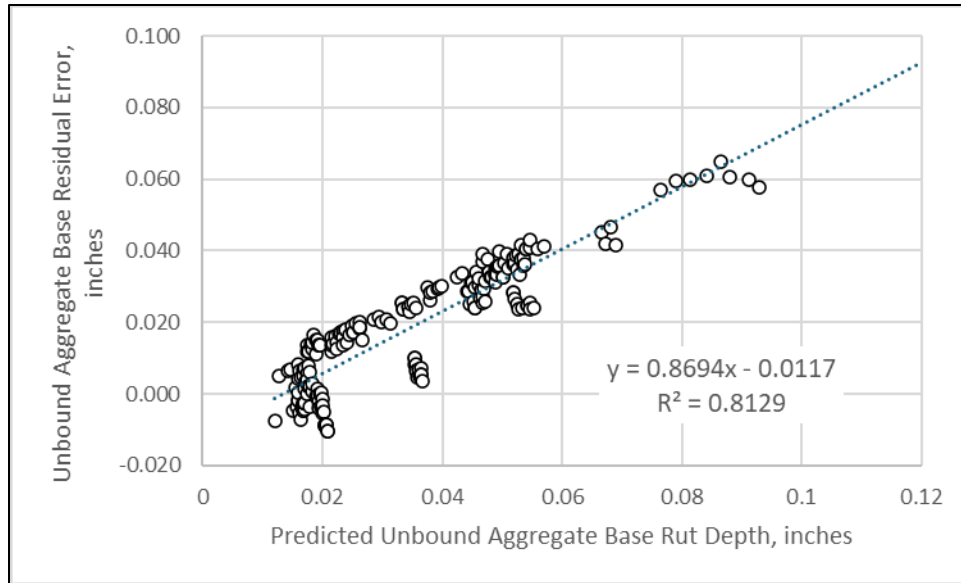
Figure 17. Residual Error Compared to the Predicted Rut Depth for the Unbound Aggregate Base Layers.
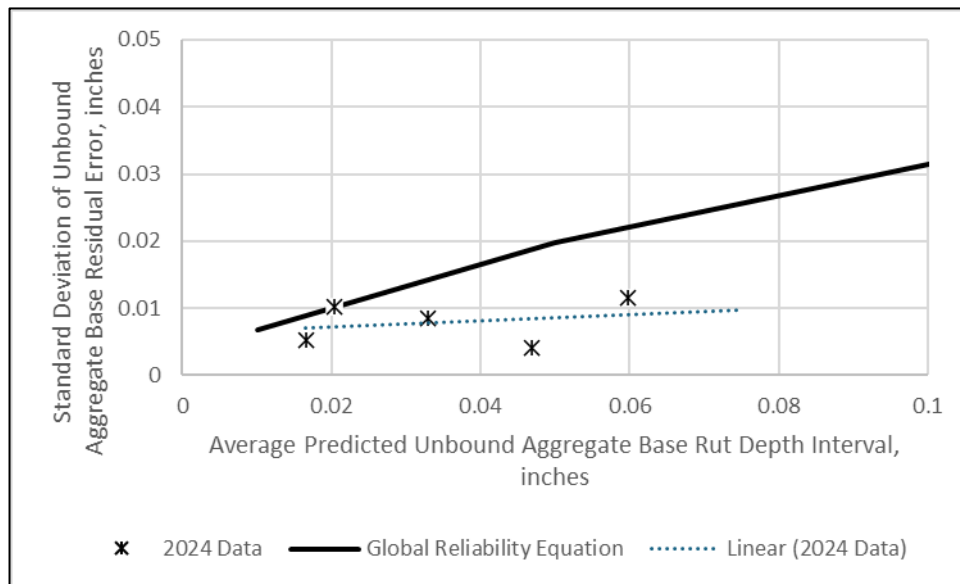
Figure 18. Standard Deviation of Residual Errors Equation for Estimating the Reliability of the Predicted Rut Depth for the Unbound Aggregate Base Layers.
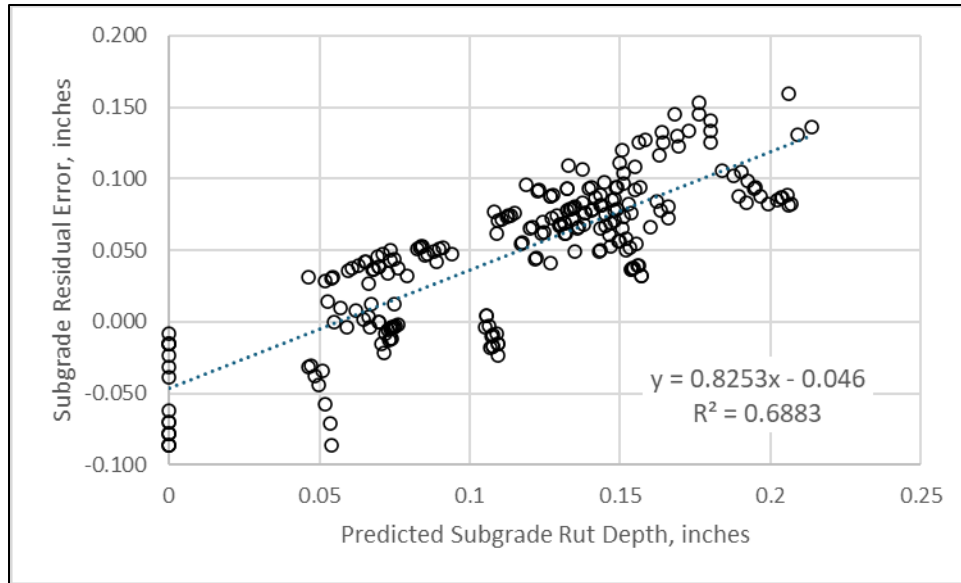
Figure 19. Residual Error Compared to the Predicted Rut Depth for the Unbound Subgrade and Embankment Layers.
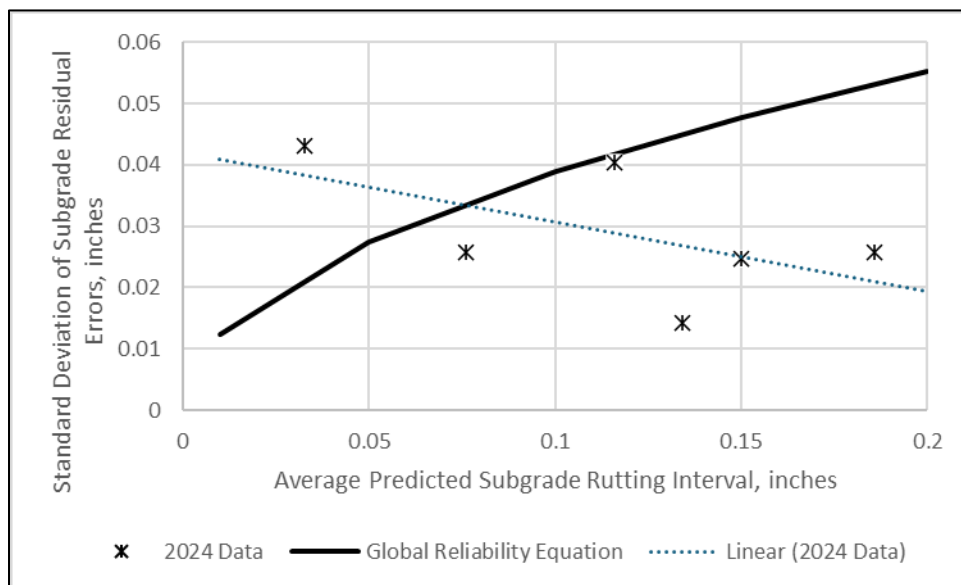
Figure 20. Standard Deviation of Residual Errors Equation for Estimating the Reliability of the Predicted Rut Depths for the Unbound Subgrade/Embankment Layers.

This page left blank intentionally.

5.0 Transverse Cracking

5.1 Transverse Cracking Transfer Functions

A detailed description of the transverse cracking prediction methodology is presented in the MEPDG Manual of Practice (AASHTO, 2020). The initial methodology for predicting transverse thermal cracks was based on thermal events or temperature changes. Based solely on temperature events, transverse cracks are never predicted using the PMED software in mild to warm climates. Transverse cracks, however, do occur in these climates so adjustments to the methodology were integrated through a correction factor (k_t as defined below). The following paragraphs explain the prediction of transverse cracks in the current version of the PMED software.

In summary, thermal transverse cracking is initiated when the thermal stresses exceed the tensile strength of the asphalt mixture. Crack propagation is calculated using the Paris law displayed in equation 12.

$$\Delta C = A\ (\Delta K)^n \tag{Eq. 12}$$

Where ΔC is the increase in crack length due to cooling, ΔK is the change in the stress intensity function, and n and A are fracture parameters. The stress intensity function is displayed in equation 13.

$$K = \sigma\left(0.45 + 1.99\ C_0^{\ 0.56}\right) \tag{Eq. 13}$$

Where, C_0 is the original crack length and σ is the stress (psi) in the asphalt layer at the depth of the crack tip. The parameter n is estimated from the creep compliance master curve. The cracking parameter n is related to the slope m of the linear part of the $\log D(\xi)$ versus $\log \xi$ creep compliance master curve, as displayed in equation 14.

$$n = 0.8\left(1 + \frac{1}{m}\right) \tag{Eq. 14}$$

The parameter A is estimated through calibration using the measured transverse cracking data by equation 15.

$$A = \beta_t k_t 10^{4.389 - 2.52\ log(E_{AC}\ S_t\ n)} \tag{Eq. 15}$$

Where, E_{AC} and S_t are the indirect tensile modulus and the tensile strength (psi) of the asphalt mixture, respectively, k_t is a laboratory to field fracture correction factor, and β_t is a local calibration factor. The k_t laboratory factor was found to be dependent on the mean annual air temperature (MAAT) during the 2018 global calibration to reduce the bias between the measured and predicted transverse cracks in cold to warm climates. The calculation methodology was not changed, only MAAT was introduced to increase the k_t variable in

warmer climates. The distress mechanism introduced was to account for factors such as long-term shrinkage of the asphalt mixture and asphalt absorption.

The relationship between k_t and MAAT changes at a MAAT of 57°F, which was based on an analysis of variance of the residual errors between the predicted and measured transverse cracks during the 2018 global calibration. It was hypothesized that in colder climates (MAAT < 57°F) cold temperature events control the occurrence of transverse cracks, but in warmer climates (MAAT > 57°F) other factors like shrinkage and asphalt absorption control the occurrence of transverse cracks.

All sites included in this regional verification/calibration have a MAAT less than 57°F. The relationship between MAAT and k_t for climates with a MAAT less than 57°F is displayed in equation 16. Figure 21 includes a screen shot of the PMED software for the global calibration coefficient for predicting the length of transverse cracks.

$$k_t = 3 * (10)^{-7} * (MAAT)^{4.0317} \qquad \text{(Eq. 16)}$$

AC Cracking Bottom Up	AC Cracking Top Down	AC Fatigue	AC Rutting	IRI	Subgrade Rutting	Thermal Fracture Level 1	Thermal Fracture Level 2	Thermal Fracture Level 3
AC thermal cracking level 3 K (MAAT <= 57 deg F)						((3 * Pow(10,-7)) * Pow(MAAT,4.0319)) * 1 + 0		✓
AC thermal cracking level 3 K (MAAT > 57 deg F)						(0.13 * Pow(MAAT,2) - 11.68 * MAAT + 244.14) * 1 + 0		✓
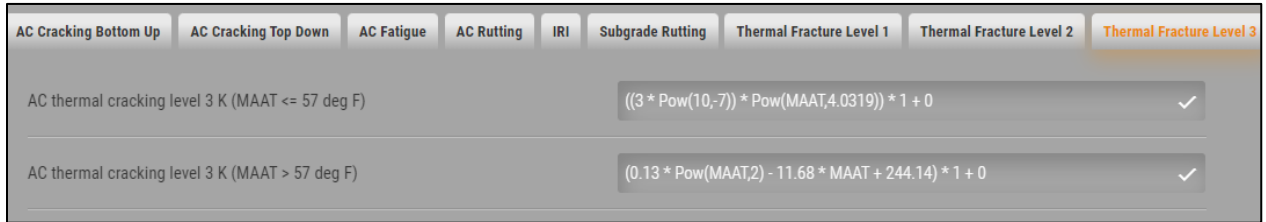
Figure 21. Screen Shot of the PMED Software Displaying the Global Calibration Coefficient for Predicting Transverse Cracks.

Finally, the extent of transverse thermal cracking in asphalt mixtures TC (in linear feet/mile) is computed from the probability that the thermal crack depth C_d (inches) exceeds the thickness of the asphalt layers, h_{ac}, as expressed in equation 17.

$$TC = \beta_{t1} N \left(\frac{1}{\sigma_d} log \left(\frac{C_d}{h_{AC}} \right) \right) \qquad \text{(Eq. 17)}$$

Where:

N = Standard normal probability function.

σ_d = Standard deviation of the log of the depth of thermal cracks in asphalt pavements (i.e., taken as 0.769 inches).

β_{t1} = Regression constant, which has a default value of 400.

5.2 Transverse Cracking Data Review

The transverse cracking data extracted from the LTPP database were reviewed for consistency and to identify potential errors, outliers, and any bias. Figure 22 displays the cumulative

frequency diagram of the transverse cracking values measured for the LTPP new flexible and asphalt overlay sections. The new flexible and asphalt overlay data sets exhibit similar characteristics, but the transverse cracking measurements are consistently higher for the new flexible sections. The new flexible sections are consistently older than the asphalt overlay segments (see Table 3). Figure 23 displays the measured length of transverse cracks as a function of age. The older new flexible sites exhibit greater lengths of transverse cracks in comparison to the asphalt overlay sites at the same age.
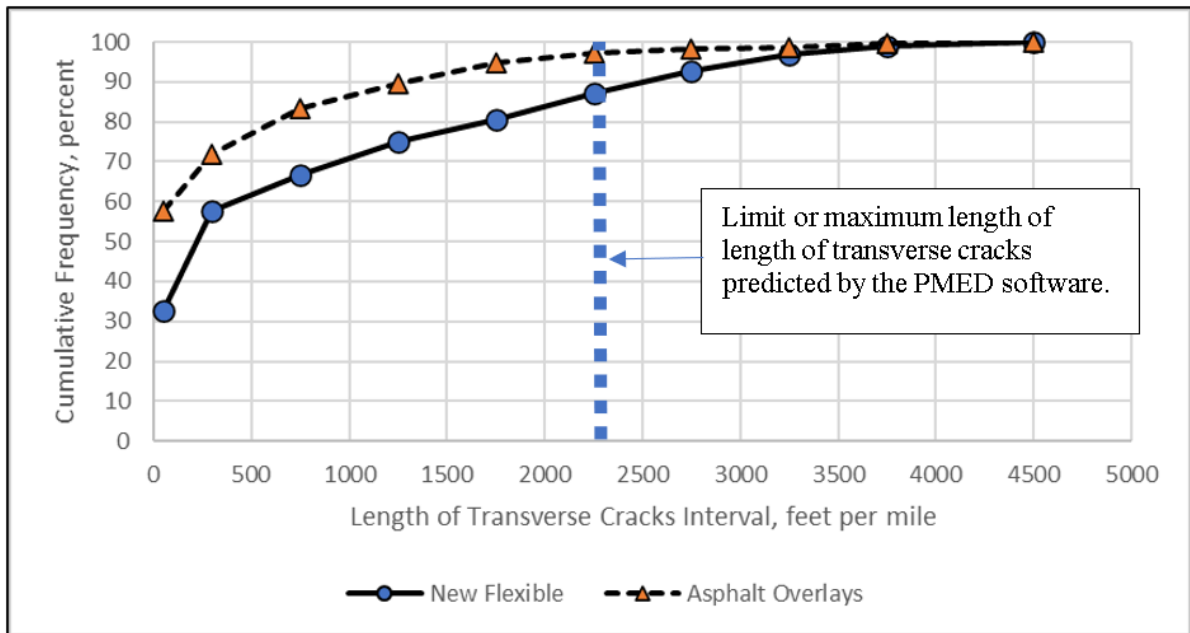
Figure 22. Cumulative Frequency Diagram of Transverse Cracking Measurements for the LTPP Sites Used in the Verification and Calibration Process.
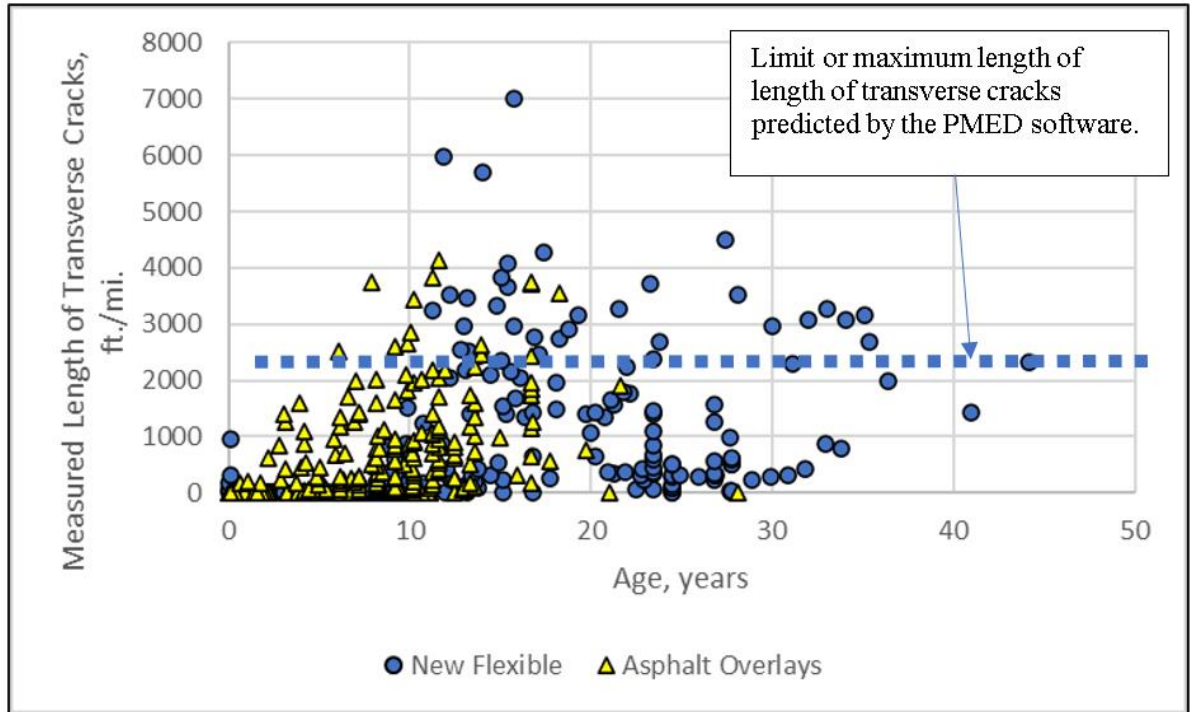
Figure 23. Increase in Measured Length of Transverse Cracks with Test Section Age.

Table 7 compares the mean, median, and standard deviation of the transverse cracking measurements. As shown in Figure 22 and Table 7, the transverse cracking measurements are skewed towards the lower values, especially for the asphalt overlays. All segments (new flexible and asphalt overlay sections), however, exhibit average transverse cracking measurements higher than the threshold value typically used to design flexible pavements (1,000 to 1,500 feet per mile).

An important point is there is a limit or maximum length of transverse cracks calculated by the PMED software (see Figure 22 and Figure 23). More of the new flexible pavement sites in comparison to the asphalt overlay sites exhibit transverse cracks that exceed the limit predicted by the PMED software. Thus, the maximum length of measured transverse cracks was set at 2,200 feet per mile for the new flexible sites to be consistent with the limit applied in the PMED software to assess the accuracy of the global calibration coefficient. The limit for the asphalt overlay sites was not applied because of reflection cracking. The length of transverse cracks in the asphalt overlay can exceed 2,200 feet per mile and is another reason for keeping the two data sets separate in the initial verification and calibration.

Table 7. Mean, Median, and Standard Deviation of the Transverse Cracking Measurements

Statistical Value	Type of Section New Flexible	Type of Section Asphalt Overlays
Number of Sections	18	48
Number of Observations	196	336
Mean of Measured Faulting, inches	1,017	453
Median of Measured Faulting, inches	367	17
Standard Deviation of Faulting Value, inches	1,321	794

Figure 24 displays the measured length of transverse cracks as a function of age of the LTPP new flexible pavement sites and applying the limit on the length of transverse cracks included in the PMED software. The new flexible pavement sites can be grouped into two categories: one where the transverse cracks start to occur around year 10 and propagate or increase rapidly to the maximum limit and the other where the transverse cracks start to occur after year 10 but increase more gradual over time. Figure 25 includes examples from each group.

Figure 26 displays the measured length of transverse cracks as a function of age for the LTPP new flexible pavement sites located in Connecticut, New Jersey, New York, and Vermont, while Figure 27 displays the measured transverse cracks as a function of age for the LTPP sites located in Maine, Massachusetts, and New Hampshire. The LTPP new flexible pavement sites located in Maine, Massachusetts, and New Hampshire exhibit much less transverse cracks.[7] An analysis of variance (ANOVA) of the residual errors and length of transverse cracks did not identify any specific variable that would explain this difference between the two transverse cracking categories.

---

[7] The intent of this comment is not to compare the transverse cracking measured on the LTPP sections between states, but to categorize and identify the sections with different sections when transverse cracks start to occur and how they propagate over time. Climate, asphalt properties, asphalt layer thickness, and other parameters have an impact on the occurrence of transverse cracks.
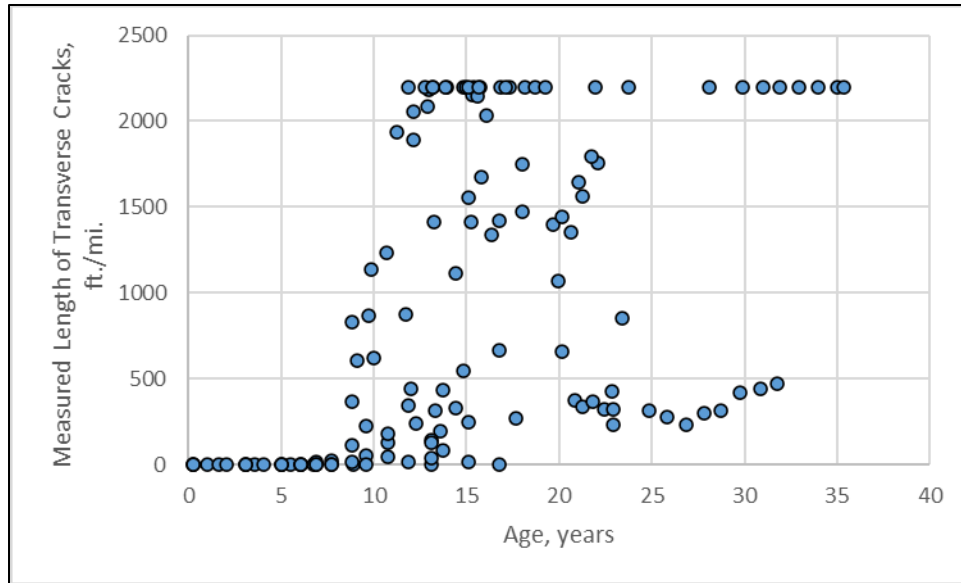
Figure 24. Increase in Measured Length of Transverse Cracks with Test Section Age and Applying the Limit included in the PMED Software.
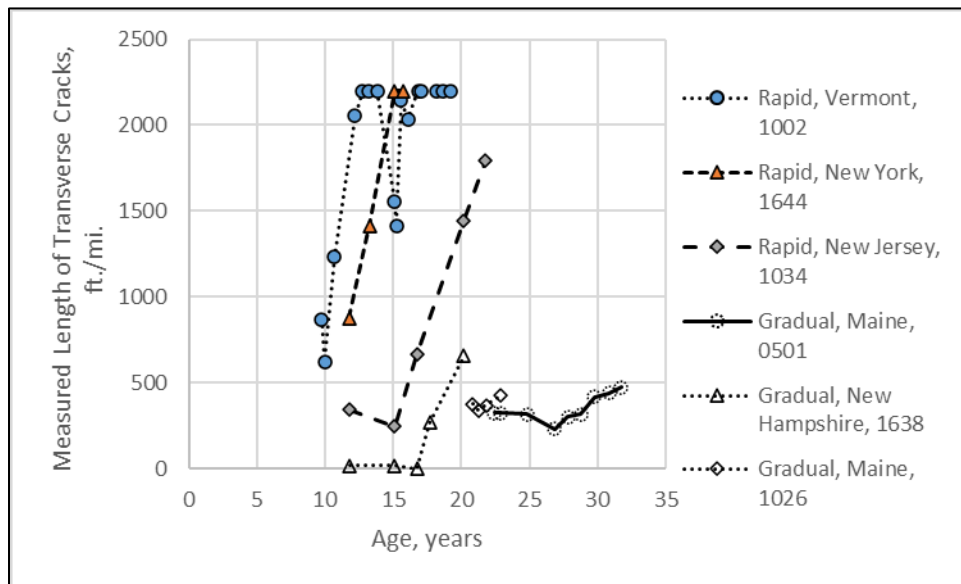
Figure 25. Increase in Measured Length of Transverse Cracks with Test Section Age for Sites Exhibiting a Rapid to Gradual Increase in Transverse Cracks when Applying the Limit included in the PMED Software.
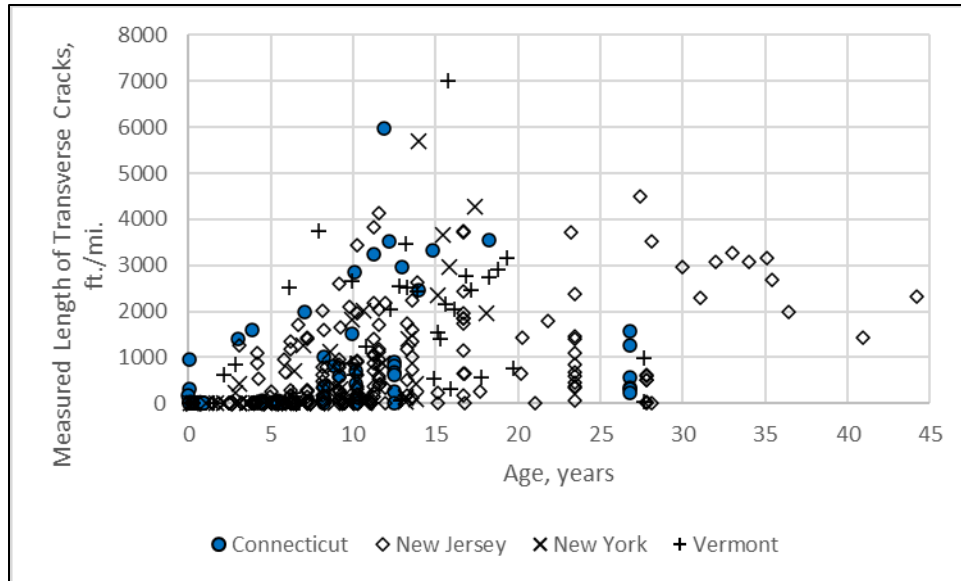
Figure 26. Increase in Measured Length of Transverse Cracks with Test Section Age for the Connecticut, New Jersey, New York, and Vermont LTPP Sites.
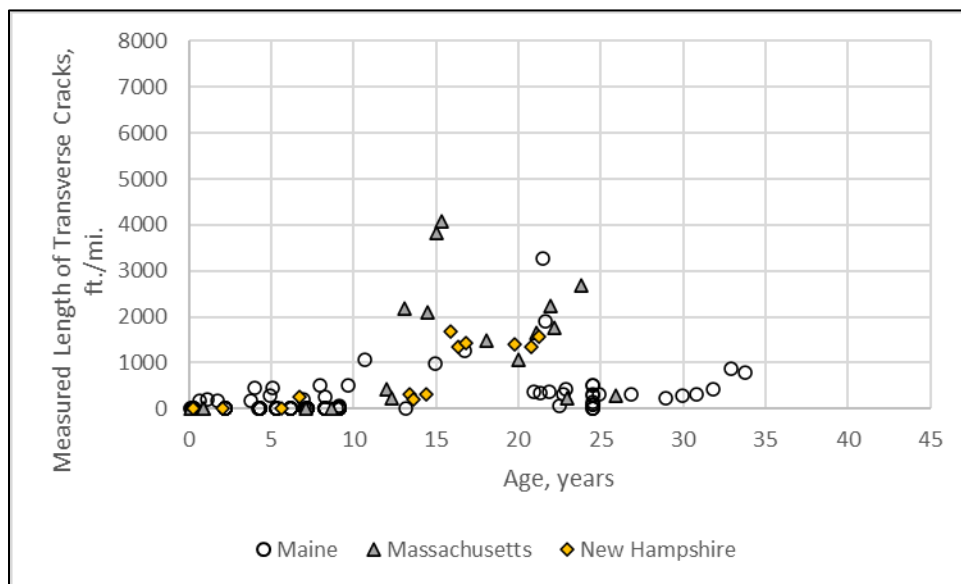
Figure 27. Increase in Measured Length of Transverse Cracks with Test Section Age for the Maine, Massachusetts, and New Hampshire LTPP Sites.

5.3 Verification of the Global Transverse Cracking Transfer Function Calibration Coefficients

The length of transverse cracks was predicted for the new flexible and asphalt overlay sites using the global calibration coefficients (see Figure 21). The new flexible and asphalt overlay sites, however, were kept separate because of reflection cracking. Reflection transverse cracks are discussed and evaluated in Chapter 7.

The "best" available data from the LTPP database was used to determine the inputs for the asphalt wearing surface for the new flexible sites. Input level 1 was used for many traffic, climate, and layer inputs. Input level 3 for dynamic modulus, indirect tensile creep compliance, and indirect tensile strength was used because these asphalt properties are not included in the LTPP database.

Figure 28 displays a graphical comparison of the measured and predicted transverse cracking values for the new flexible pavement sites. As displayed, transverse cracks were predicted for only a few of the new flexible sites so there is a significant bias between the predicted and measured length of transverse cracks.

Figure 29 shows the measured length of transverse cracks as a function of age. The measured length of transverse cracks is highly variable. Some sections exhibit transverse cracks prior to 10 years and exhibit the maximum length of cracks predicted by the PMED software in just over 10 years, while other sections do not exhibit transverse cracks until after 20 years and do not exhibit the maximum length of transverse cracks predicted by the PMED software even after 30 years. The amount of variability cannot be accurately predicted within a region using the default asphalt surface layer properties.
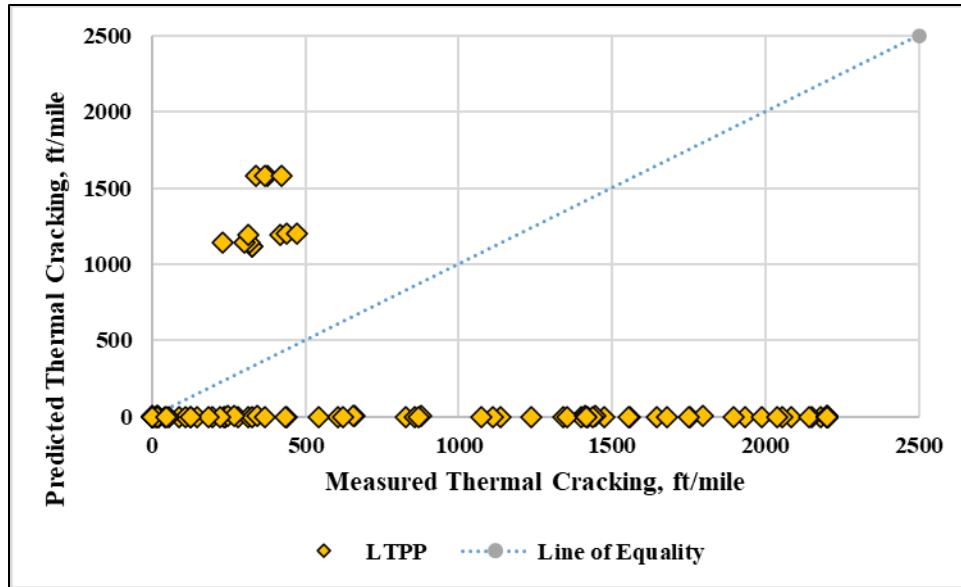
Figure 28. Graphical Comparison of the Predicted and Measured Transverse Cracking using the 2018 Default Asphalt Mixture Properties and Global Transverse Cracking Calibration Coefficient.
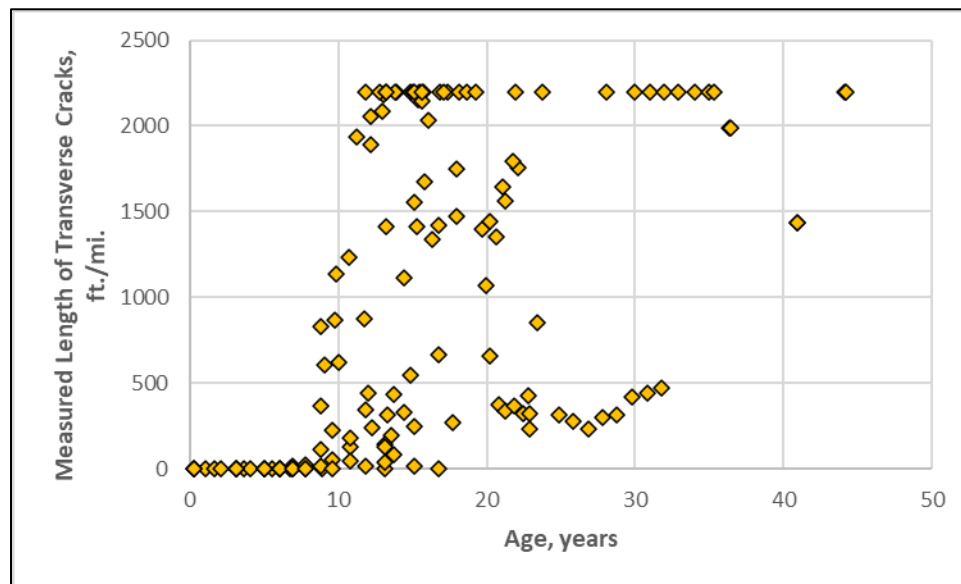
Figure 29. Measured Length of Transverse Cracks over Time or Age of the Section.

The creep compliance and strength values were calculated by the MEDPG regression equations (input level 3) because they are not included in the LTPP database. The volumetric properties of the asphalt layers are variable, with air voids varying from over 11 percent to under 5 percent. The initial air voids at the time of construction are not measured values – they have to be backcasted from when they were measured years after construction. The backcasting process introduces additional error.

The variation of the asphalt content and air voids may not capture the true properties of the asphalt layers at the extreme volumetric values. As such, the asphalt mixture coefficient of thermal contraction was estimated and used in the revised verification. Appendix C lists the asphalt mixture coefficient of thermal contraction for each of the sections, which represent the impact of thermal contraction, shrinkage, and asphalt absorption for the different volumetric properties.

Figure 30 displays a graphical comparison of the measured and predicted transverse cracking values for the new flexible pavement sites using the revised asphalt mixture coefficient of thermal contraction, while Figure 31 compares the predicted transverse cracking to the residual error. As displayed, there is a significant improvement between the predicted and measured values.

The statistical parameters between the predicted and measured average transverse cracking values using an estimated asphalt mixture thermal coefficient of contraction and the 2018 global calibration coefficient in v3.0 are listed in Table 8. The R-squared, s_e/s_y, and standard error of the estimate terms are considered good to fair, and the bias is low. The hypothesis test for the bias being equal to 0 using the paired t-test was accepted, but the hypothesis tests for the slope equal to 1 and the intercept equal to 0 were rejected. Possible reasons the hypothesis tests for the intercept and slope were rejected is related to the measurement error of transverse cracks and estimating the asphalt mixture thermal coefficient from backcasted initial air voids.
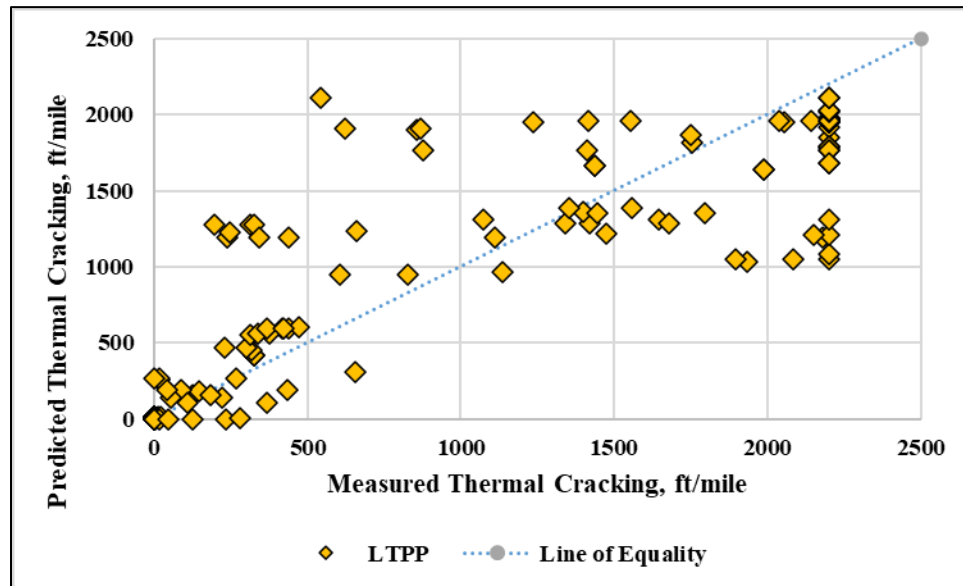
Figure 30. Graphical Comparison of the Predicted and Measured Transverse Cracking using an Estimated Thermal Coefficient and the 2018 Global Transverse Cracking Calibration Coefficient.
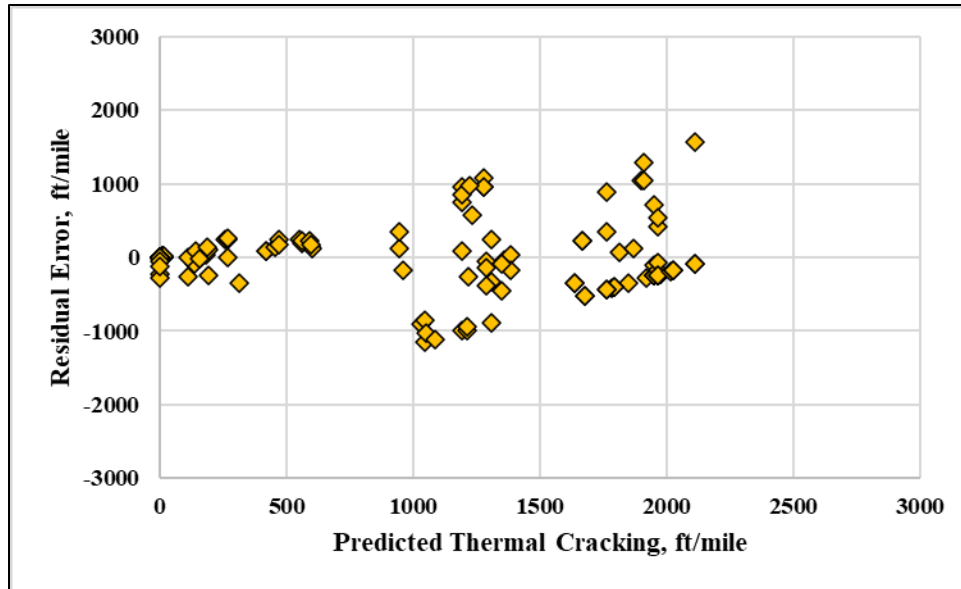
Figure 31. Graphical Comparison of the Predicted Transverse Cracking and Residual Error using an Estimated Thermal Coefficient and the 2018 Global Transverse Cracking Calibration Coefficient.

Table 8. Verification Results Using the 2018 Global Calibration Coefficient to Calculate Transverse Cracking.

Statistical Parameters for New Flexible Transverse Cracking Transfer Function	PMED, Version 3.0; New Flexible
Number of Total Sections	18
Number of Observations	137
Goodness-of-Fit: R-squared	0.746 (Good)
Goodness-of-Fit: Se/Sy	0.438 (Good)
Goodness-of-Fit: SEE, feet per mile	394.8 (Fair)
Goodness-of-Fit: Standard Deviation of Residuals	454.8
Goodness-of-Fit: Slope	0.747
Goodness-of-Fit: Intercept	237.7
Bias	-7.79 (Very Low)
Bias Test: H_0 p-value: Slope = 1.0	Reject (p-value: 0.0000)
Bias Test: H_0 p-value: Intercept = 0.0	Reject (p-value: 0.00004)
Bias Test: H_0 p-value: Paired t-test	Accept (p-value: 0.841)

Figure 32 and Figure 33 display a comparison of the predicted and measured lengths of transverse cracks for a LTPP section located in Massachusetts (25-1002) and Vermont (50-1002). These two figures are examples that illustrate the variability in the length of measured cracks over time for which no model can predict. Figure 25 also illustrated the variation in measured transverse cracks over time for selected LTPP sites. Overall, the standard error and bias are lower than the measurement error for transverse cracks on a ft./mi. basis. Thus, the

41

transverse cracking transfer function calibration coefficient was considered appropriate for use in Massachusetts.

The results are confined to the use of inputs level 3 asphalt mixture mechanistic properties (indirect tensile creep compliance and strength). A bias was noted and reported in the Mechanistic Empirical Pavement Design Guide (MEPDG) Manual of Practice between input level 3 and input level 1 or input level 2 in 2023 when the input level 2 for creep compliance of asphalt mixtures was replaced. As such, the calibration coefficient derived using input level 3 asphalt mixture mechanistic properties does not apply to the use of input level 1 or input level 2 asphalt mixture mechanistic properties.[8]
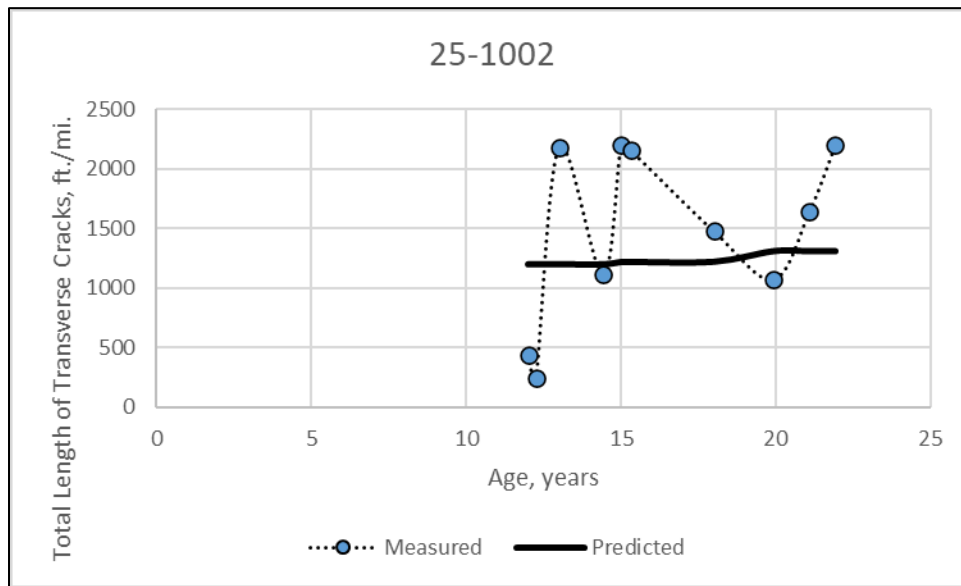
Figure 32. Graphical Comparison of the Predicted and Measured Length of Transverse Cracks in Verification for the LTPP Site in Massachusetts (25-1002).

---

[8] An addendum to the MEPDG Manual of Practice was submitted and balloted for revising the input level 2 inputs for creep compliance of asphalt mixtures. The addendum has yet to be published by AASHTO.
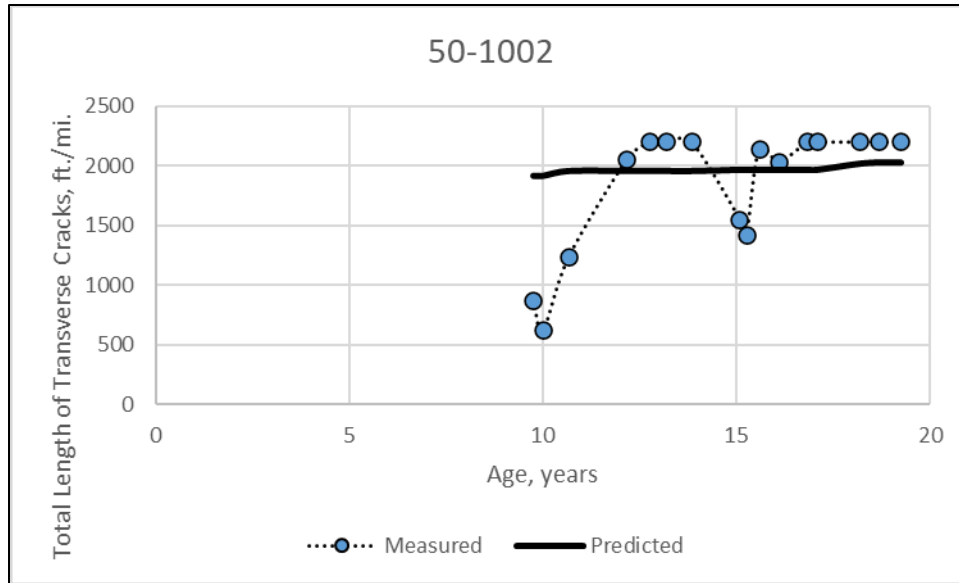
Figure 33. Graphical Comparison of the Predicted and Measured Length of Transverse Cracks in Verification for the LTPP Site in Vermont (50-1002).

5.4 Reliability Equation for Transverse Cracking

The MEPDG estimates pavement design reliability using the predicted length of transverse cracking based on the average input values and the standard deviation of residual errors. The transverse cracking standard deviation of residual errors prediction equation was developed as follows:

1. Divide the transverse cracking values into 4 or more intervals.

2. For each interval, determine the mean predicted average transverse cracking and standard deviation of residual errors (i.e., standard variation of predicted – measured transverse cracking for all predicted transverse cracking values that fall within the given interval).

3. Develop a linear or nonlinear model to fit the mean predicted transverse cracking values and standard deviation of the residual errors.

Figure 34 displays a comparison of the predicted length of transverse cracks and residual error. As shown, the residual error significantly increases beyond a predicted length of transverse cracks of 1,000 ft./mi. Figure 35 displays the standard deviation of residual errors of the predicted length of transverse cracks in comparison to the predicted length of transverse cracks using the global calibration coefficient of $\beta_t = 1.0$. The 2018 global standard deviation of residuals equation is displayed in Figure 35 in comparison to the 2024 regional calibration data using v3.0. As shown, the reliability equation using the 2024 data included as equation 18 is

statistically the same as the global reliability equation for transverse cracks. Thus, the global reliability equation is suggested for use in Massachusetts.

$$\sigma_{TC-Level3} = 0.2845(TC) + 76.62 \qquad\qquad \text{(Eq. 18)}$$

Where:

$\sigma_{TC\text{-}Level3g}$ = Standard deviation of residuals for transverse cracks, ft./mi.

TC = Predicted length of transverse cracks, ft./mi.
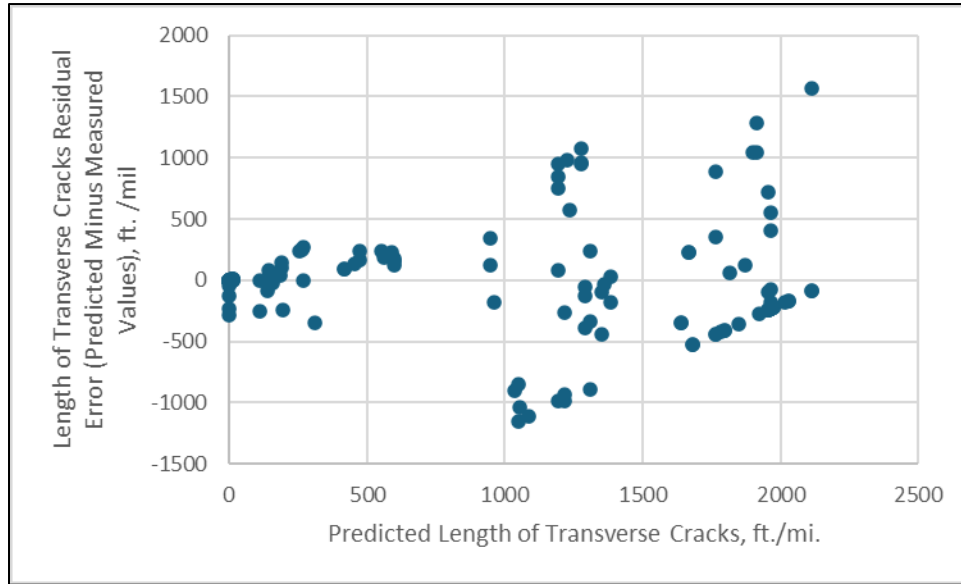
Figure 34. Residual Error Compared to the Predicted Length of Transverse Cracks.
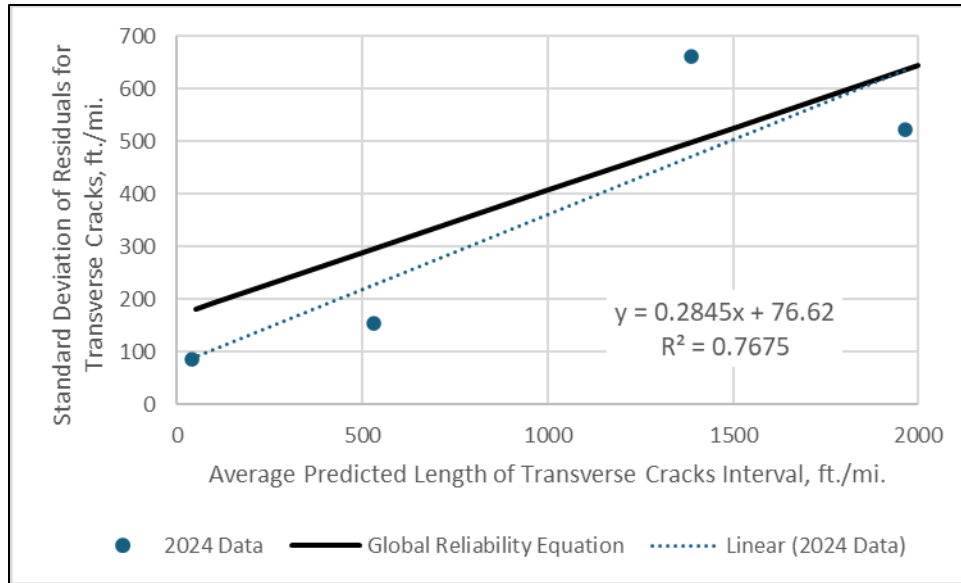
Figure 35. Standard Deviation of Residual Errors Equation for Estimating Transverse Cracking Reliability.

A 50 percent reliability level is suggested for transverse cracks in judging the adequacy of a design in Massachusetts. The reason for a 50 percent reliability level is transverse cracks can be a result of low temperature events (included in the model), as well as long-term shrinkage of the asphalt mixture and asphalt absorption which are not directly considered in the PMED software. These other transverse cracking mechanisms excluded from the software can result in high standard errors and conservative designs with the use of higher reliability levels.

This page left blank intentionally

6.0 Fatigue Cracking

6.1 Fatigue Cracking Transfer Functions

The MEPDG predicts two forms of fatigue cracking in flexible pavements, one defined as bottom-up fatigue cracks and the other as top-down fatigue cracks. The LTPP database, however, does not distinguish between bottom-up and top-down fatigue cracks.

6.1.1 Bottom-Up Fatigue Cracks

Bottom-up fatigue cracks are predicted using two primary equations. The first equation is referred to as the fatigue strength of asphalt layers or mixtures and is used to calculate the fatigue life of the asphalt layer (or number of load repetitions to failure, N_f) when subjected to repeated loads. The fatigue strength is displayed in equation 19.

$$N_f = k_{f1} C \; C_H \; \beta_{f1} \left(\frac{1}{\epsilon_t}\right)^{k_{f2}\beta_{f2}} \left(\frac{1}{E}\right)^{k_{f3}\beta_{f3}} \qquad \text{(Eq. 19)}$$

Where:

ε_t = Tensile strain at the bottom of the asphalt layer.

E = Dynamic modulus of the asphalt layer (psi).

k_{f1}, k_{f2}, and k_{f3} = Laboratory derived fatigue strength coefficients. The global input level 3 values for the laboratory fatigue strength coefficients are: 3.75 mils/in. for k_{f1}; 2.87 for k_{f2}; and 1.46 for k_{f3}. Figure 36 includes a screen shot of the PMED software for the global laboratory derived fatigue strength coefficients for predicting the fatigue strength (N_f).

β_{f1}, β_{f2}, and β_{f3} = Calibration regression coefficients for the laboratory defined fatigue strength. The global default values are: β_{f1} is thickness dependent which is defined below; 1.38 for β_{f2}; and 0.88 for β_{f3}. Figure 36 includes a screen shot of the PMED software for the global calibration regression coefficients for predicting the fatigue strength (N_f).

- $\beta_{f1} = 0.02054$ for a total thickness of the asphalt layers less than 5 inches.
- $\beta_{f1} = 5.012(h_{ac})^{-3.416}$ for a total thickness of the asphalt layers greater than 5 inches but less than 12 inches.

- $\beta_{f1} = 0.001032$ for a total thickness of the asphalt layers greater than 12 inches.

h_{ac} = Total thickness of the asphalt layers.

C = A volumetric correction factor defined by equation 20.

$$C = 10^M \qquad \text{(Eq. 20)}$$

Where:

$$M = 4.84 \left(\frac{V_{be}}{V_a + V_{be}} - 0.69 \right) \qquad \text{(Eq. 21)}$$

V_{be} = Effective volume of the asphalt binder.

V_a = Volume of the air as percentages of the total mix volume (air voids).

C_H = Thickness correction factor between stress and strain-controlled conditions, defined by equation 22:

$$C_H = \frac{1}{0.000398 + \frac{0.003602}{1 + e^{11.02 - 3.49\, h_{ac}}}} \qquad \text{(Eq. 22)}$$

AC Cracking Bottom Up	AC Cracking Top Down	AC Fatigue	AC Rutting	IRI	Subgrade Rutting	Thermal Fracture Level 1	Thermal Fracture Level 2	Thermal Fracture Lev

AC fatigue BF1: < 5 in.	0.02054	✓
AC fatigue BF1: 5 in. <= hac <= 12 in.	(5.014 * Pow(hac,-3.416)) * 1 + 0	✓
AC fatigue BF1: > 12 in.	0.001032	✓
AC fatigue BF2	1.38	✓
AC fatigue BF3	0.88	✓
AC fatigue K1	3.75	✓
AC fatigue K2	2.87	✓
AC fatigue K3	1.46	✓

Figure 36. Screen Shot of the PMED Software Displaying the Global Laboratory Fatigue Strength and Global Calibration Regression Coefficients for Calculating the Fatigue Strength (N_f).

Fatigue damage FD_{Bottom} (percent) is accumulated for bottom-up cracking according to Miner's hypothesis as defined by equation 23.

$$FD_{Bottom} = \sum \frac{n_{i,j,k,l,m}}{N_{i,j,k,l,m}} \, 100 \qquad \text{(Eq. 23)}$$

Where:

$n_{i,j,k,...}$ = Applied number of load applications at condition i, j, k, l, m, n.

$N_{i,j,k,...}$ = Number of axle load applications to cracking failure under conditions i, j, k, l, m.

i = Month, which accounts for monthly changes in the resilient modulus of the aggregate base and subgrade due to moisture variations and asphalt due to temperature variations.

j = Time of the day, which accounts for hourly changes in the modulus of the asphalt layer.

k = Axle type, (i.e., single, tandem, triple and quad).

l = Load level for each axle type.

m = Traffic path, assuming a normally distributed lateral wheel wander.

Temperature and moisture changes are computed using the Enhanced Integrated Climatic Model and weather data for the location of the pavement. The fatigue damage computations in the PMED software involves a series of layered elastic analysis solutions to compute the tensile strains at the bottom of the asphalt layer and the number of repetitions to fatigue failure for each axle configuration and load magnitude using equation 19 and equation 23. The bottom-up fatigue cracking area FC_{bottom} (i.e., alligator cracking in percent of total lane area) is computed as:

$$FC_{bottom} = \frac{1}{60} \frac{C_3}{1+e^{(C_1 C_1^* + C_2 C_2^* \, log \, (FD_{bottom}100))}} \qquad \text{(Eq. 24)}$$

Where:

C_1, C_2 and C_3 = Calibration coefficients of the transfer function. The default values are: 1.31 for C_1; C_2 is thickness dependent as defined below; and 6,000 for C_3. Figure 37 displays a screen shot of the PMED software showing the global bottom-up fatigue cracking C_1, C_2 and C_3 calibration coefficients.

- $C_2 = 2.1585$ for a total thickness of the asphalt layers less than 5 inches.
- $C_2 = 0.867 + (0.867 * h_{ac})$ for a total thickness of the asphalt layers greater than 5 inches but less than 12 inches.
- $C_2 = 3.9666$ for a total thickness of the asphalt layers greater than 12 inches.

C_1^*, C_2^* = Coefficients defined by the total asphalt layer thickness as displayed in equation 25 and equation 26.

$$C_1^* = -2C_2^* \qquad \text{(Eq. 25)}$$

$$C_2^* = -2.40874 - 39.748 \, (1 + h_{ac})^{-2.856} \qquad \text{(Eq. 26)}$$

49

Figure 37. Screen Shot of the PMED Software Displaying the Global Bottom-Up Fatigue Cracking Global Calibration Coefficients.

6.1.2 Top-Down Fatigue Cracks

Top-down fatigue cracks are predicted using a fracture mechanics. The approach or methodology is used to calculate crack initiation and then uses an incremental growth in crack depth from traffic loads. The following paragraphs provide a brief explanation of the models and equations.

- Crack Initiation: The time to crack initiation, t_0, is calculated with the regression equation displayed in equation 27 and is based on an energy parameter, traffic, and climate variables.

$$t_0 = \frac{K_{L1}}{1+e^{\left(K_{L2}100\left[\frac{a_0}{2A_0}\right]+K_{l3}[HT]+K_{L4}[LT]+K_{L5}[Log_{10}AADTT]\right)}} \tag{Eq. 27}$$

Where:

$a_0/2A_0$ = Energy parameter.

$$\frac{a_0}{2A_0} = 0.1796 + 1.5 * 10^{-5}E_1 - 0.69m - 7.169 * 10^{-4}H_a \tag{Eq. 28}$$

HT = Annual number of days above 32°C.

LT = Annual number of days below 0°C.

E_1, m = Relaxation modulus power law function parameters for aged asphalt.

H_a = Total asphalt layer thickness.

$K_{L1}, K_{L2}, K_{L3}, K_{L4}, K_{L5}$ = Regression calibration coefficients with values of: K_{L1} = 64,271,618; K_{L2} = 0.2855; K_{L3} = 0.011; K_{L4} = 0.0149; and K_{L5} = 3.266. Figure 38 is a screen shot displaying the regression calibration

50

coefficients for calculating the time to crack initiation in number of days for top-down fatigue cracking.

AC Cracking Bottom Up	AC Cracking Top Down	AC Fatigue	AC Rutting	IRI	Subgrade Rutting	Thermal Fracture Level 1	Thermal Fracture Level 2	Thermal Fracture L

Top down AC cracking C1	2.5219	✓
Top down AC cracking C2	0.8069	✓
Top down AC cracking C3	1	✓
Top down AC cracking kL1	64271618	✓
Top down AC cracking kL2	0.2855	✓
Top down AC cracking kL3	0.011	✓
Top down AC cracking kL4	0.01488	✓
Top down AC cracking kL5	3.266	✓
Top down AC cracking standard deviation	0.3657 * TOP + 3.6563	✓

Figure 38. Screen Shot of the PMED Software Displaying the Global Regression Coefficients for Calculating the Time to Crack Initiation for Top-Down Fatigue Cracks.

- Crack Propagation: The propagation of the cracks that initiate at the surface is like the transverse cracking model based on fracture mechanics. A modified Paris law is used to propagate the cracks downward through the asphalt layers using the pseudo-JR integral as displayed in equation 29.

$$\frac{dc}{dN} = A'(J_R)^{n'}$$
(Eq. 29)

Where:

C = Crack length or depth, dc is the change or growth in crack depth.

N = Number of load cycles.

J_R = Pseudo J-integral

A', n' = Fracture properties of the asphalt mixture or layer.

The pseudo-JR integral is displayed in equation 30 and defined as the increment in dissipated work per unit crack surface area and is related or determined by the three models of the stress intensity factors and Poisson's ratio and the representative elastic modulus for the asphalt

51

surface layer. Stress intensity factors are defined for single and dual tires and used to estimate the downward propagation of crack depth for each month throughout the pavement design life.

$$J_R = \frac{1-\mu^2}{E_R}(K_I^2 + K_{II}^2) + \frac{1+\mu}{E_R}K_{III}^2 \qquad \text{(Eq. 30)}$$

Where:

E_R = Representative elastic modulus.

μ = Poisson's ratio.

K_I = Stress intensity factor in mode I, opening mode.

K_{II} = Stress intensity factor in mode II, in-plane shear.

K_{III} = Stress intensity factor in mode III, out-of-plane shear.

The asphalt fracture parameters (A' and n') are displayed in equation 31 and equation 32. Like for bottom-up fatigue cracks, the volumetric properties of air voids and asphalt content have a significant impact on the fracture parameters and on the occurrence of top-down fatigue cracks.

$$A' = 10^{-(1.2752n+1.713)} \qquad \text{(Eq. 31)}$$

$$n' = -9.00498 + 1.0627\varphi + \frac{2.8713}{m} - 40.8788\left(\frac{1}{E_1}\right) + 18.868\frac{P_b}{V_a+P_b} \qquad \text{(Eq. 32)}$$

Where:

V_a = Average air voids, percent.

P_b = Average asphalt content by total weight of mix, percent.

E_1, m = Relaxation modulus power law function parameters for aged asphalt.

φ = Shape parameter of the aggregate power law function.

The transfer function for predicting the area of top-down fatigue cracks includes a sigmoidal function and is based on the maximum area of top-down fatigue cracks, the scaling shape parameters, and calibration coefficients, as well as the time to crack initiation. Equation 33 displays the top-down fatigue cracking transfer function.

$$L(t) = L_{Max}e^{-\left(\frac{c_1 p}{t-c_3 t_0}\right)^{c_2\beta}} \qquad \text{(Eq. 33)}$$

Where:

L_{Max} = Maximum area of top-down cracking, percent.

t = Analysis month in days.

t_0 = Time to crack initiation, in days.

$\rho\ and\ \beta$ = Scaling shaper parameters.

$$\rho = \alpha_2 + \alpha_1 N_f \quad\quad\quad\quad\quad \text{(Eq. 34)}$$

$$\beta = 0.4201\big(Log_{10}N_f\big)^{-1.2801} \quad\quad\quad\quad\quad \text{(Eq. 35)}$$

N_f = Number of months to failure, defined at the time fro the cracks to propagate to 40 mm.

α_1, α_2 = Climate parameters.

c_1, c_2, c_3 =Calibration coefficients with global values of: c_1 = 2.5219; c_2 = 0.8069; and c_3 = 1.0. Figure 38 is a screen shot displaying the global calibration coefficients for predicting the area of top-down fatigue cracks.

6.2 Fatigue Cracking Data Review

Two types of cracks in the wheel path are recorded in the LTPP database: alligator cracks which are measured on an area basis and longitudinal cracks which are measured on a length basis. Both crack types were extracted from the LTPP database and converted to a percent total lane area basis which is the outcome from the PMED software. As discussed above, bottom-up and top-down fatigue cracks are predicted by the PMED software. The LTPP database, however, does not distinguish between bottom-up and top-down fatigue cracks. Thus, all cracks recorded in the wheel path (alligator and longitudinal) were combined for the initial data review.

Figure 39 displays the cumulative distribution of the percent total lane area for fatigue cracking, while Table 9 compares the average (mean) and median percent cracking measurements. As displayed in Figure 39 and Table 10, fatigue cracking is skewed to 0 for the two data sets, new flexible and asphalt overlays, with higher areas of fatigue cracking exhibited on the new flexible pavement sites.
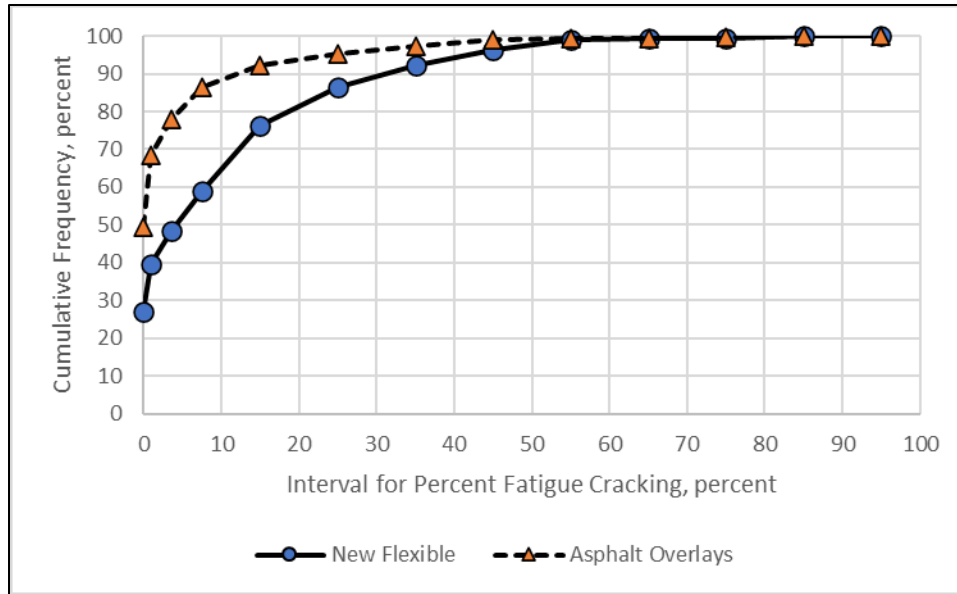
Figure 39. Cumulative Distribution of Total Fatigue Cracks for the LTPP Sites Used in the Verification and Calibration Process.

Table 9. Mean, Median and Standard Deviation of the Measured Fatigue Cracking

Statistical Value	Type of Section or Dataset New Flexible	Type of Section or Dataset Asphalt Overlays
Number of Sections	18	48
Number of Measurements	190	342
Mean of Measured Percent Total Lane Area, percent	15	5
Median of Measured Percent Total Lane Area, percent	9	0
Standard Deviation of Measured Percent Total Lane Area	18	11

Figure 40 displays the increase in fatigue cracks with test section age for new flexible pavements. Some sections started to exhibit fatigue cracks in less than 10 years, while other sites did not exhibit fatigue cracks until after 30 years. Figure 41 displays the growth or increase in fatigue cracks over time for selected sites with minimal and excessive fatigue cracks. These LTPP sites represent a wide range of cracking growth patterns.[9] Another

---

[9] The intent of this comment is not to compare the fatigue cracks measured on the LTPP test sections between states, but to categorize and identify the sections with different increases in fatigue cracks over time. Traffic, asphalt layer thickness, asphalt layer properties, aggregate base stiffness, and other parameters have an impact on fatigue cracking.

observation from Figure 41 is the variability in fatigue cracking measurements over time for a specific section.

Repairs and patches (localized maintenance) are recorded in the LTPP database. Some of the sections included repairs and/or patches which can explain large decreases in the measured fatigue cracks. As an example, Figure 42 displays the measured fatigue cracks over time and identifies the age when localized maintenance was applied to the pavement surface for two sections (25-1002 and 33-1001).
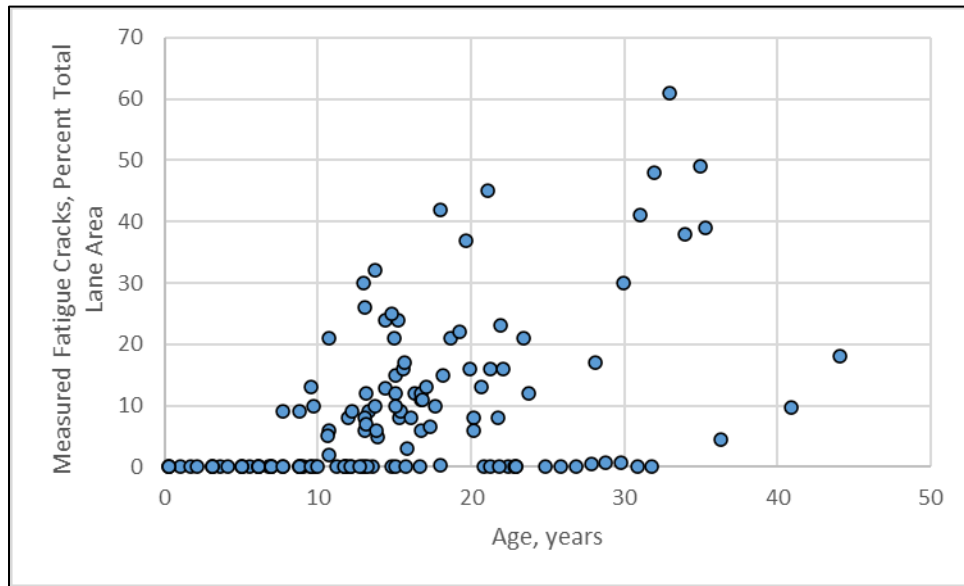
Figure 40. Increase in Measured Percent Total Lane Area Fatigue Cracks with Test Section Age for New Flexible Pavements.
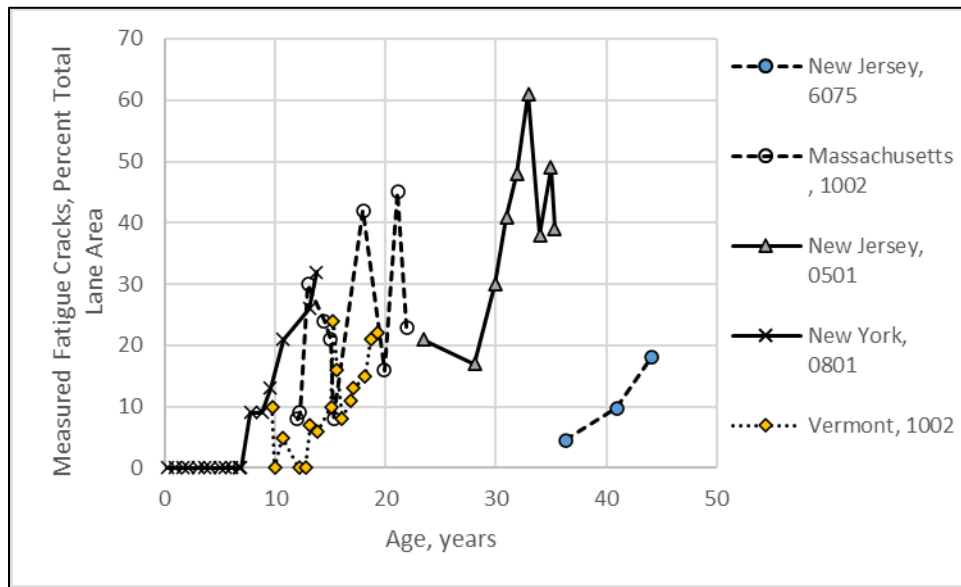
Figure 41. Increase in Measured Percent Total Lane Area Fatigue Cracks with Test Section Age for Selected LTPP New Flexible Pavement Sites.
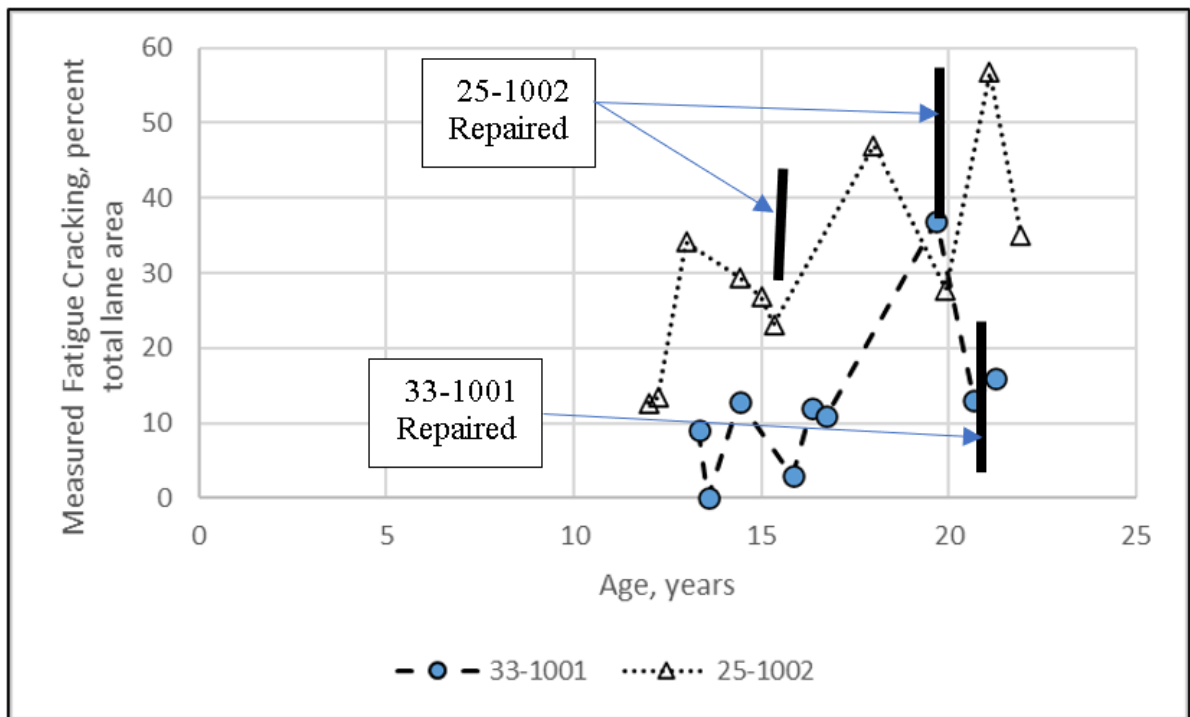
Figure 42. Measured Fatigue Cracks with Repairs Recorded Over Time in the LTPP Database for Selected New Flexible Pavement Sites.

It is difficult to define the reason for the maintenance repair or patch, but the repair/patch probably replaced some area with fatigue cracks. In addition, it is good practice to remove

more than just the cracked area when patching an asphalt pavement, so it is difficult to accurately define the cracked area replaced by the patch. For simplicity: the patched area was added to the area with recorded fatigue cracks for small patches, while for large patches, 50 percent of the area was added to the area with recorded fatigue cracks.

Overall, the measurement error is large, which needs to be considered in assessing the accuracy of the fatigue cracking transfer functions for bottom-up and top-down fatigue cracks.

6.3 Verification of the Fatigue Cracking Transfer Functions Global Coefficients

The PMED software predicts bottom-up and top-down fatigue cracks, but the LTPP cracking data does not distinguish between the two types of fatigue cracks. The first step in the verification process to assess the fatigue transfer functions is to separate top-down from bottom-up measured fatigue cracks. The procedure suggested by Von Quintus, et al. was used to segregate the total fatigue cracking into top-down and bottom-up (Von Quintus, et al., 2017). This procedure also identifies sites with potential mixture and/or construction anomalies or deficiencies.

The area of top-down and bottom-up fatigue cracks was predicted for the new flexible and asphalt overlay sites using the global calibration coefficients for bottom-up and top-down fatigue cracks. The new flexible and asphalt overlay sites, however, were kept separate because of reflection cracking. Reflection transverse cracks are discussed and evaluated in Chapter 7.

The remainder of this section of Chapter 6 separately discusses the verification of the global bottom-up and top-down fatigue cracking transfer functions.

6.3.1 Verification of Bottom-Up Fatigue Cracking Transfer Function Coefficients

The "best" available data from the LTPP database was used to determine the inputs for the asphalt wearing surface for the new flexible sites. Input level 1 was used for many traffic, climate, and layer inputs. Input level 3 for dynamic modulus and fatigue strength coefficients to predict bottom-up fatigue cracks was used because these asphalt properties are not included in the LTPP database.

Figure 43 displays a graphical comparison of the measured and predicted area of bottom-up fatigue cracking values for the new flexible pavement sites, while Figure 44 compares the predicted bottom-up fatigue cracking to the residual error. As displayed, some sections exhibited greater than 10 percent cracks, but very low areas of fatigue cracks were predicted resulting in a large negative bias.

The statistical parameters comparing predicted and measured bottom-up fatigue cracks using the global fatigue strength coefficients (see Figure 36) and the 2018 global calibration coefficients (see Figure 37 and equation 24) in v3.0 are listed in Table 10. The s_e/s_y and standard error of the estimate terms are considered good with a low bias, while the R-squared

is considered poor with a weak relationship. In addition, the hypothesis tests for the slope equal to 1 and the bias equal to 0 based on the paired t-test were rejected, but the hypothesis test for the intercept equal to 0 was accepted.
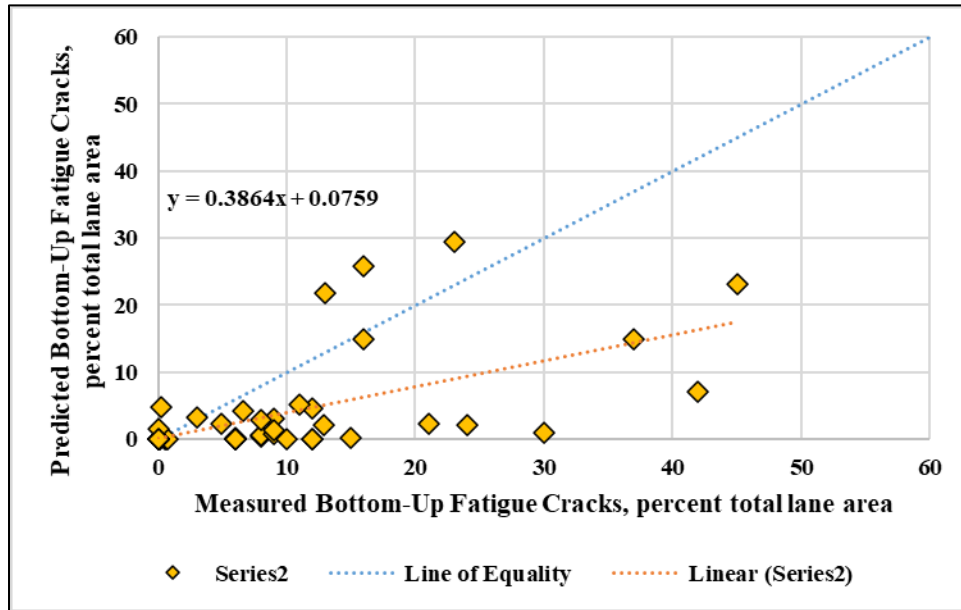
Figure 43. Predicted and Measured Bottom-Up Fatigue Cracks Using the 2018 Global Calibration Coefficients.
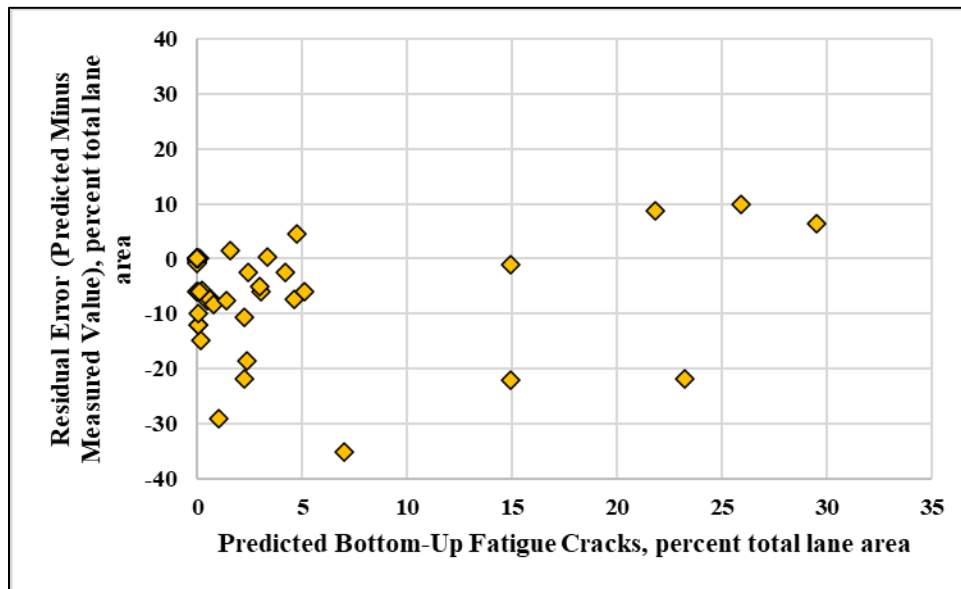
Figure 44. Predicted Bottom-Up Cracking Values Using the 2018 Global Calibration Coefficients as Compared to the Residual Error.

58

Table 10. Evaluation of Results for Assessing the 2018 Global Calibration Coefficients to Predict Bottom-Up Fatigue Cracks.

Statistical Parameters for Bottom-Up Fatigue Cracking Model/Transfer Function	PMED, Version 3.0; New Flexible Pavement Sites
Number of Total Sections	18
Number of Observations	135
Goodness-of-Fit: R-squared	0.413 (Poor, Weak Relationship)
Goodness-of-Fit: Se/Sy	0.464 (Good)
Goodness-of-Fit: SEE, percent cracked slabs	4.301 (Good)
Goodness-of-Fit: Standard Deviation of Residuals	7.120
Goodness-of-Fit: Slope	0.386
Goodness-of-Fit: Intercept	0.882
Bias[10]	-2.94 (Low)
Hypothesis Test; H_0 p-value: Slope = 1.0	Reject (p-value: 0.0000)
Hypothesis Test; H_0 p-value: Intercept = 0.0	Accept (P-value: 0.882)
Hypothesis Test; H_0 p-value: Paired t-test; Bias = 0.	Reject (p-value: 0.00015)

A reason why some of the statistical parameters show a good assessment is that the measured bottom-up fatigue cracks are skewed to 0. The bias between the predicted and measured values was 0.03 percent total lane area for the measured bottom-up fatigue cracks being less than 5 percent total lane area. For the measured bottom-up fatigue cracks greater than 5 percent total lane area, however, the bias to 9.38 percent – a high bias value. In addition, the slope between the measured and predicted values is low (see Figure 43 and Table 10). As such, the bottom-up fatigue cracking transfer function calibration coefficients need to be evaluated and adjusted. The next section of Chapter 6 discusses the recalibration of the bottom-up fatigue cracking transfer function.

6.3.2 Verification of Top-Down Fatigue Cracking Transfer Function Coefficients

The "best" available data from the LTPP database was used to determine the inputs for the asphalt wearing surface for the new flexible sites. Input level 1 was used for many traffic, climate, and layer inputs. Input level 3 for dynamic modulus, creep compliance and strength to predict top-down cracking was used because these asphalt properties are not included in the LTPP database. The regression coefficients to determine the initiation of top-down cracks (see equation 27) is also unavailable in the LTPP database, so the global default values were used.

Figure 45 displays a graphical comparison of the measured and predicted area of top-down fatigue cracking values for the new flexible pavement sites, while Figure 46 compares the predicted top-down fatigue cracks to the residual error. As displayed, several sections exhibited high levels of top-down fatigue cracks but none were predicted, while other sections exhibited no top-down fatigue cracks but top-down cracks were predicted with the PMED software.

---

[10] See text in report on discussion of the bias across the range of measured bottom-up fatigue cracks because the bottom-up fatigue cracking data are skewed to 0.

The statistical parameters between the predicted and measured average top-down fatigue cracking values using the 2018 global calibration coefficients in v3.0 are listed in Table 11. The R-squared is considered poor (weak relationship), while the s_e/s_y and standard error of the estimate terms are considered fair and good. In addition, the hypothesis for the slope equal to 1 and the bias equal to 0 were both rejected, as well as for the bias using the paired t-test. As such, the top-down fatigue cracking transfer function calibration coefficients need to be evaluated and adjusted. The next section of Chapter 6 discusses the assessment and recalibration of the top-down fatigue cracking transfer function.
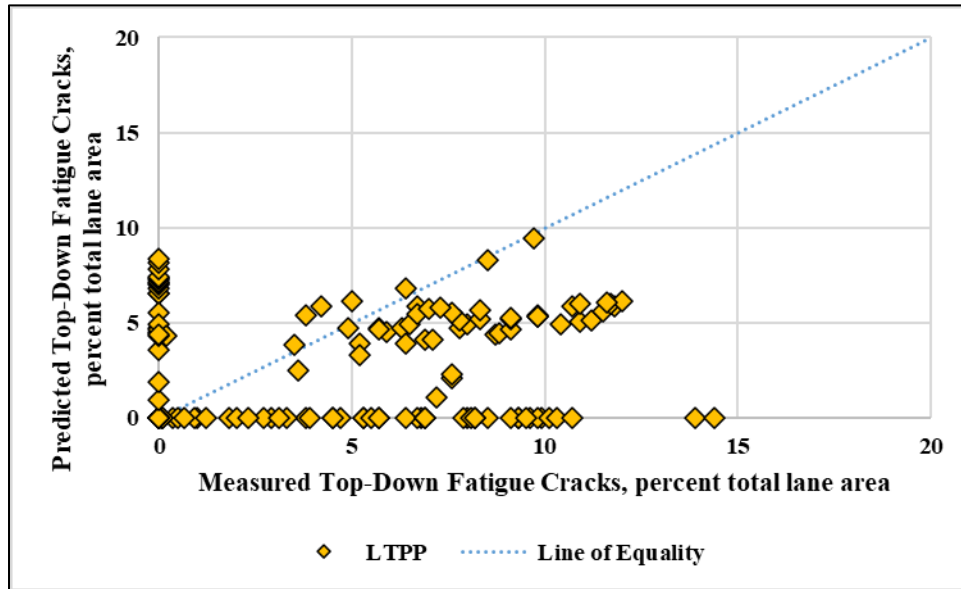
Figure 45. Predicted and Measured Top-Down Fatigue Cracks Using the 2018 Global Calibration Coefficients.
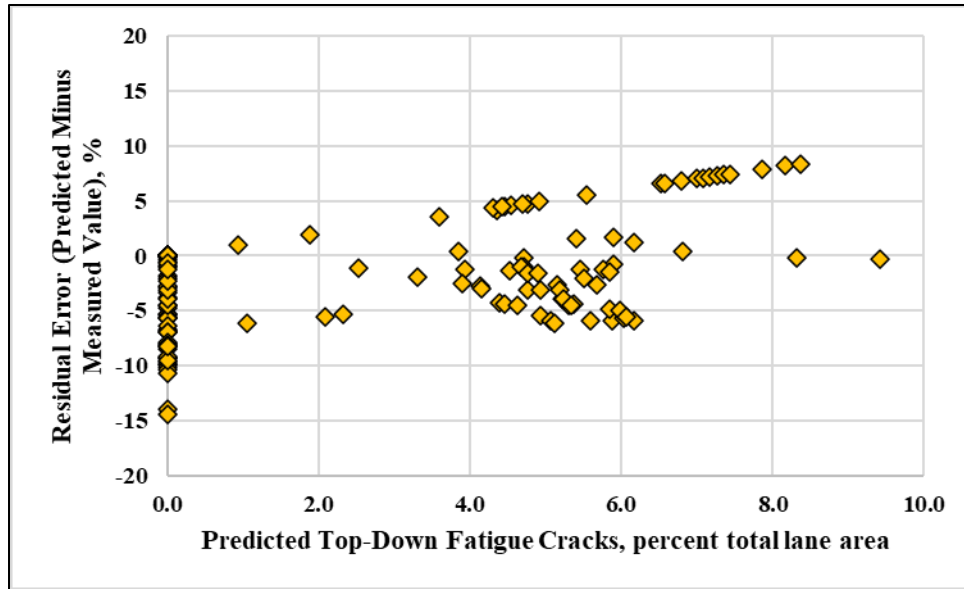
Figure 46. Predicted Top-Down Cracks Using the 2018 Global Calibration Coefficients as Compared to the Residual Error.

Table 11. Evaluation of Results for Assessing the 2018 Global Calibration Coefficients to Predict Top-Down Fatigue Cracks.

Statistical Parameters for Top-Down Fatigue Cracking Model/Transfer Function	PMED, Version 3.0; New Flexible Pavement Sites
Number of Total Sections	18
Number of Observations	135
Goodness-of-Fit: R-squared	0.0046 (Very Poor, Weak Relationship)
Goodness-of-Fit: Se/Sy	0.697 (Fair)
Goodness-of-Fit: SEE, percent cracked slabs	2.879 (Good)
Goodness-of-Fit: Standard Deviation of Residuals	4.869
Goodness-of-Fit: Slope	0.047
Goodness-of-Fit: Intercept	2.640
Bias	-2.129 (Low)
Hypothesis Test; H_0 p-value: Slope = 1.0	Reject (p-value: 0.0000)
Hypothesis Test; H_0 p-value: Intercept = 0.0	Reject (p-value: 0.0000)
Hypothesis Test; H_0 p-value: Paired t-test; Bias = 0.	Reject (p-value: 0.0000)

6.4 Calibration of the Fatigue Cracking Transfer Functions Global Coefficients

The CAT was used to optimize the regional bottom-up and top-down fatigue cracking calibration coefficients for the new flexible pavement sites. The following paragraphs discuss adjusting the calibration coefficients for bottom-up and top-down fatigue cracks.

6.4.1 Calibration of Bottom-Up Fatigue Cracking Transfer Function Coefficients

The CAT was used to optimize the bottom-up calibration coefficients and did result in changes to one of the global calibration coefficients. The global laboratory-derived calibration coefficients were not adjusted in the optimization process for the CAT because this requires laboratory measured values on some of the asphalt mixtures. The following are the optimized local calibration coefficients.

- C_1 = 1.11, which is different from the global 2018 calibration coefficient of 1.31.

- C_2 = 2018 global calibration coefficient that is dependent on asphalt layer thickness.

Figure 47 displays a graphical comparison of the measured and predicted bottom-up fatigue cracking values, while Figure 48 compares the predicted bottom-up fatigue cracking values to the residual error (predicted minus measured value). The statistical parameters between the

predicted and measured average bottom-up fatigue cracking values using the revised C_1 value of 1.11 in v3.0 are listed in Table 12.

The R-squared and s_e/s_y terms are considered very good and good, with a low bias. The standard error of the estimate is considered fair with a value like the global standard error. The hypothesis tests for the slope equal to 1, the intercept equal to 0, and the bias equal to 0 using the paired t-test were all accepted.
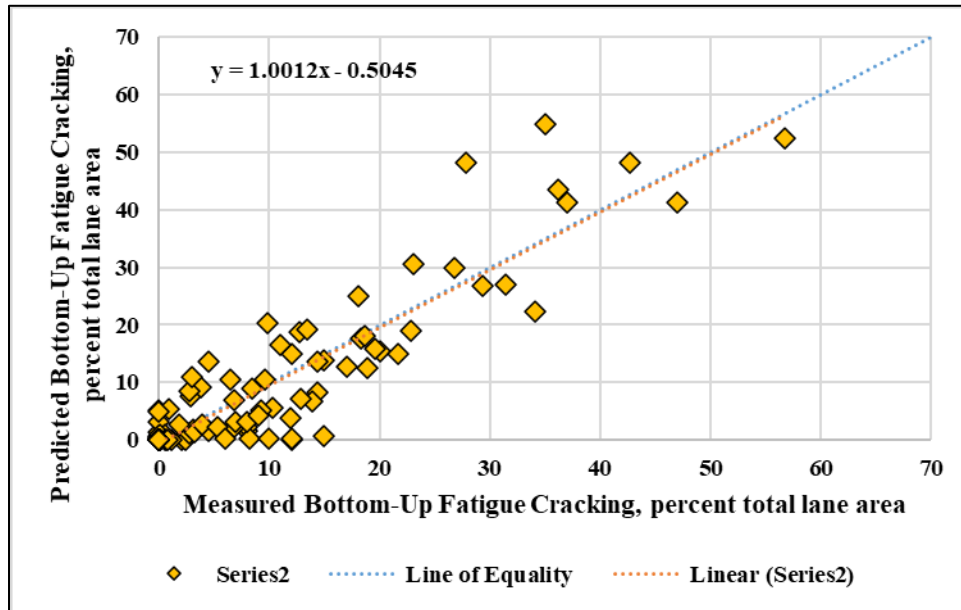
Figure 47. Predicted and Measured Bottom-Up Fatigue Cracks Using the Optimized Regional Calibration Coefficients.
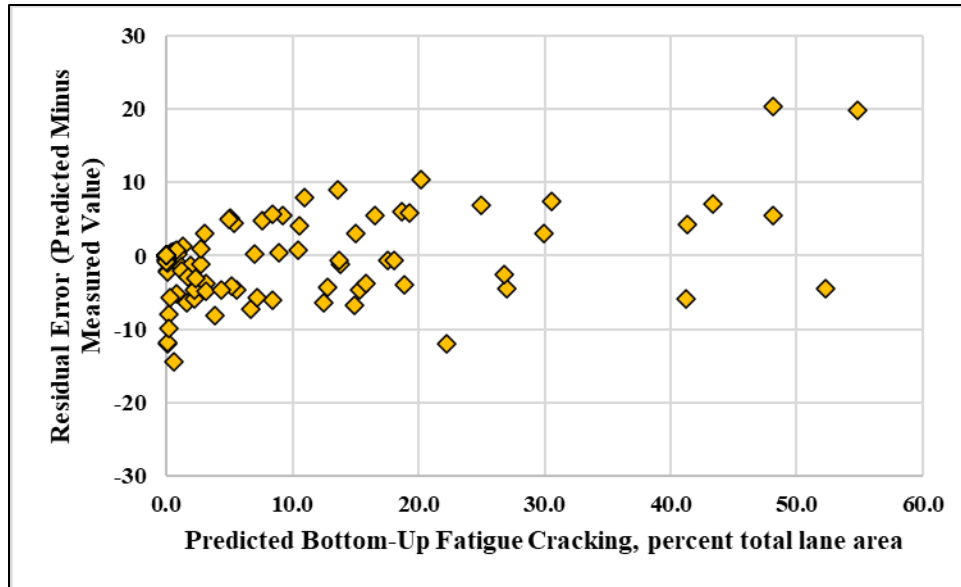
Figure 48. Predicted Bottom-Up Cracking Values Using the Optimized Regional Calibration Coefficients as Compared to the Residual Error.

Table 12. Statistical Results for the Optimized Regional Calibration Coefficients to Predict Bottom-Up Fatigue Cracks.

Statistical Parameters for Bottom-Up Fatigue Cracking Model/Transfer Function	PMED, Version 3.0; New Flexible Pavement Sites
Number of Total Sections	18
Number of Observations	97
Goodness-of-Fit: R-squared	0.817 (Very Good)
Goodness-of-Fit: Se/Sy	0.482 (Good)
Goodness-of-Fit: SEE, percent cracked slabs	5.70 (Fair)
Goodness-of-Fit: Standard Deviation of Residuals	5.67
Goodness-of-Fit: Slope	1.001
Goodness-of-Fit: Intercept	-0.504
Bias	-4.93 (Low)
Hypothesis Test; H_0 p-value: Slope = 1.0	Accept (p-value: 0.981)
Hypothesis Test; H_0 p-value: Intercept = 0.0	Accept (p-value: 0.509)
Hypothesis Test; H_0 p-value: Paired t-test; Bias = 0.	Accept (p-value: 0.396)

Figure 49 displays a comparison of the calculated bottom-up fatigue damage index and the measured bottom-up percent total lane area cracked. The R-squared value of 0.60 (displayed on Figure 49) is considered fair (but is close to the good category). Figure 50 displays a comparison of the predicted and measured time-series cracking data for three sections with different levels of cracking. These comparisons suggest a good simulation of the time-series cracking data considering the variability and error in the measured values. The variability in the measured values is typical of other sites in the LTPP database.
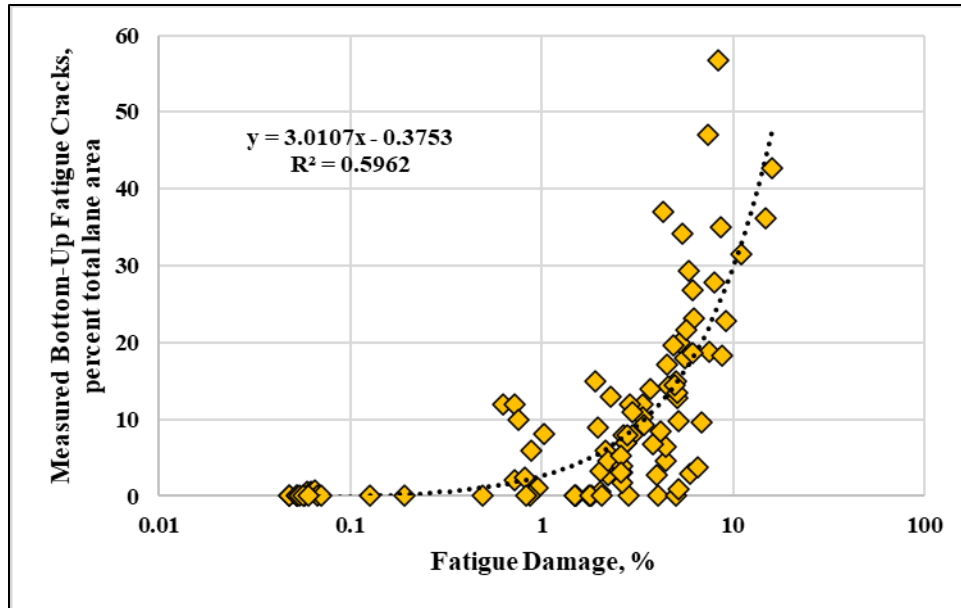
Figure 49. Total Fatigue Damage Index and Measured Bottom-Up Fatigue Cracks.
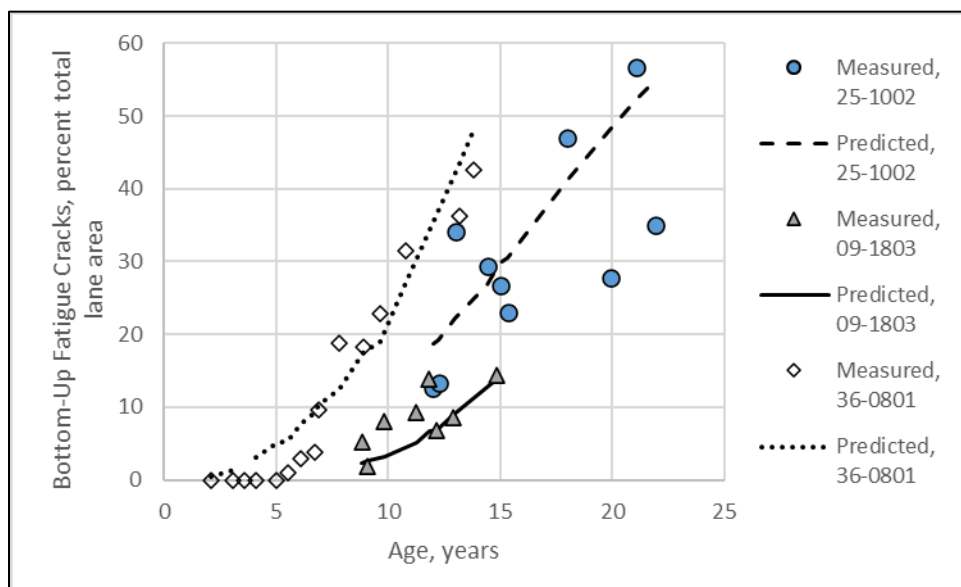
Figure 50. Graphical Comparison of the Predicted and Measured Bottom-Up Fatigue Cracks for Three Sites with the Updated Calibration Coefficients.

Thus, the 2024 bottom-up fatigue cracking calibration coefficient (C_1) and the 2018 C_2 coefficient are considered adequate for use in design for bottom-up fatigue cracks using v3.0 in Massachusetts.

6.4.2 Calibration of Top-Down Fatigue Cracking Transfer Function Coefficients

The CAT was used to optimize the top-down calibration coefficients. Both the C_1 and C_2 coefficients were adjusted from the global calibration coefficients (see Figure 38 and equation 33). The coefficients of the regression equation for crack initiation (see Figure 38 and equation 27) were not adjusted in the optimization process for the CAT. The following are the optimized local calibration coefficients.

- C_1 = 3.0, which is different from the 2018 global calibration coefficient of 2.5219)

- C_2 = 0.60, which is different from the 2018 global calibration coefficient of 0.8069).

The statistical parameters comparing the predicted and measured top-down fatigue cracks using the revised C_1 value of 3.0 and C_2 value of 0.60 in v3.0 are listed in Table 13. The R-squared, s_e/s_y, and standard error of the estimate terms are considered good and very good, with a low bias. The hypothesis tests for the slope equal to 1 and the intercept equal to 0 were accepted, while the bias equal to 0 using the paired t-test was rejected. As such, the top-down fatigue cracking transfer function calibration coefficients are suggested for use in Massachusetts.
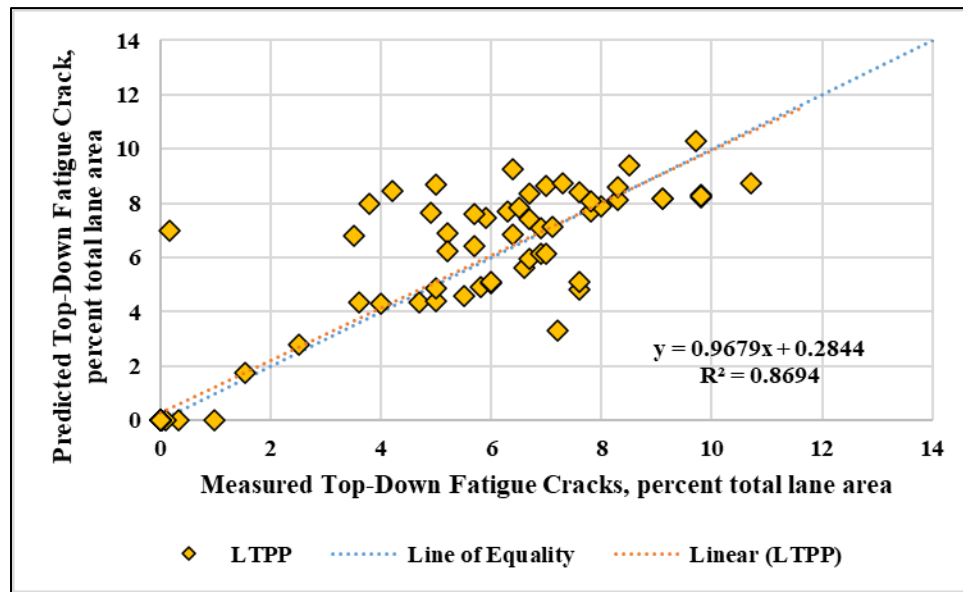
Figure 51. Predicted and Measured Top-Down Fatigue Cracks Using the Optimized Regional Calibration Coefficients.
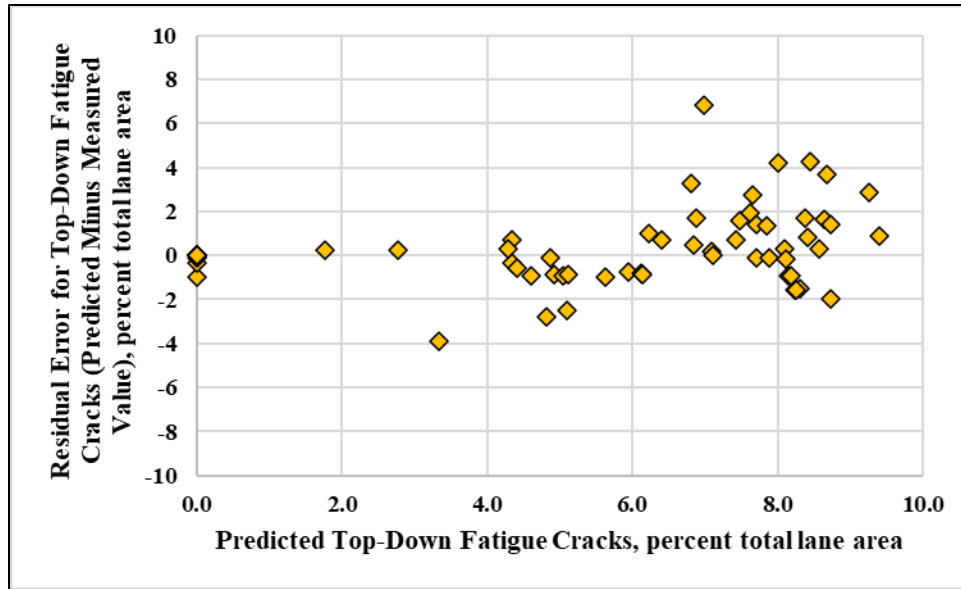
Figure 52. Predicted Top-Down Cracks Using the Optimized Regional Calibration Coefficients as Compared to the Residual Error.

Table 13. Statistical Results for the Optimized Regional Calibration Coefficients to Predict Top-Down Fatigue Cracks.

Statistical Parameters for Top-Down Fatigue Cracking Model/Transfer Function	PMED, Version 3.0; New Flexible Pavement Sites
Number of Total Sections	18
Number of Observations	97
Goodness-of-Fit: R-squared	0.869 (Very Good)
Goodness-of-Fit: Se/Sy	0.375 (Good)
Goodness-of-Fit: SEE, percent cracked slabs	1.327 (Good)
Goodness-of-Fit: Standard Deviation of Residuals	1.241
Goodness-of-Fit: Slope	0.968
Goodness-of-Fit: Intercept	0.284
Bias	0.162 (Very Good)
Hypothesis Test; H_0 p-value: Slope = 1.0	Accept (p-value: 0.611)
Hypothesis Test; H_0 p-value: Intercept = 0.0	Accept (p-value: 0.363)
Hypothesis Test; H_0 p-value: Paired t-test; Bias = 0.	Reject (p-value: 0.00112)

6.5 Reliability Equation for Fatigue Cracking

The MEPDG estimates pavement design reliability, using the estimate of fatigue cracks, percent total lane area, based on the average input values and the standard deviation of residual errors for percent total lane area. Predicted fatigue cracking standard deviation of residual errors prediction equation was determined as follows:

1. Divide the predicted transverse cracking into 4 or more intervals.

2. For each interval, determine mean predicted transverse cracking and standard deviation of residual errors (i.e., standard deviation of predicted minus measured transverse cracking values that fall within the given interval).

3. Develop a linear or nonlinear model to fit the mean predicted transverse cracking and standard deviation of the residual errors.

6.5.1 Reliability Equation for Bottom-Up Fatigue Cracks

The resulting standard deviation of the residual errors for bottom-up fatigue cracks from the 2024 regional calibration data using v3.0 and the optimized regional calibration coefficients is included in equation 36 and graphically displayed in Figure 53.

$$\sigma_{BUC} = 3.5537 + 0.1496(FC_{BUC}) \qquad \text{(Eq. 36)}$$

Where:

σ_{BUC} = Bottom-up fatigue crack standard deviation of residuals, percent total lane area.

FC_{BUC} = Predicted bottom-up fatigue cracks, percent total lane area.
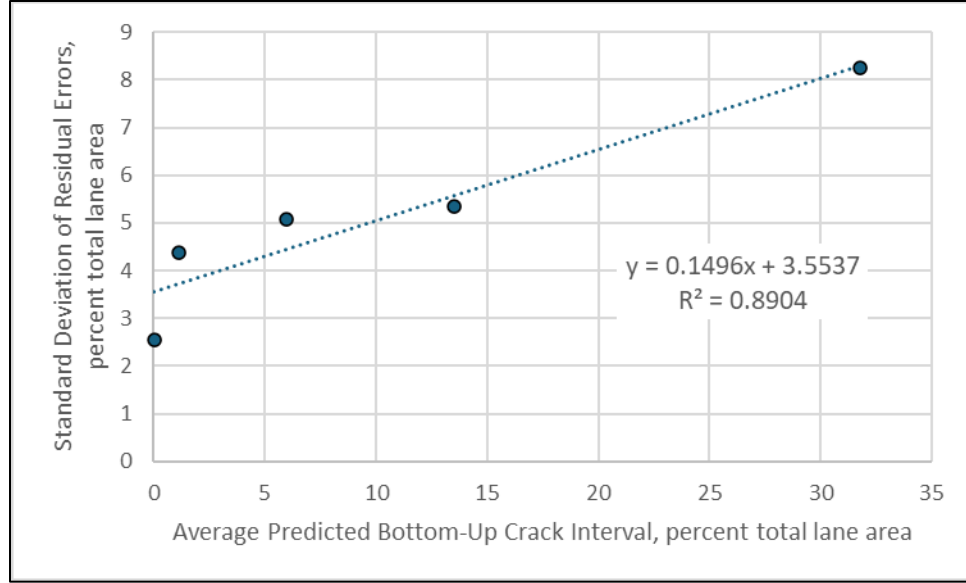
Figure 53. Standard Deviation of Residual Errors Equation for Estimating Reliability for Bottom-Up Fatigue Cracks.

6.5.2 Reliability Equation of Top-Down Fatigue Cracking

The resulting standard deviation of the residual errors for top-down fatigue cracks from the 2024 regional calibration data using v3.0 and the optimized regional calibration coefficients is included in equation 37 and graphically displayed in Figure 54. As displayed, the 2024 reliability equation is a lot lower than for the 2018 global reliability equation. A reason for this statistical difference and lower standard deviation of residual error values is many of the sites included in this update exhibited no top-down fatigue cracks.

$$\sigma_{TDC} = 0.3667 + 0.1797(FC_{TDC}) \qquad \text{(Eq. 37)}$$

Where:

σ_{TDC} = Top-down fatigue crack standard deviation of residuals, percent total lane area.

FC_{TDC} = Predicted top-down fatigue cracks, percent total lane area.
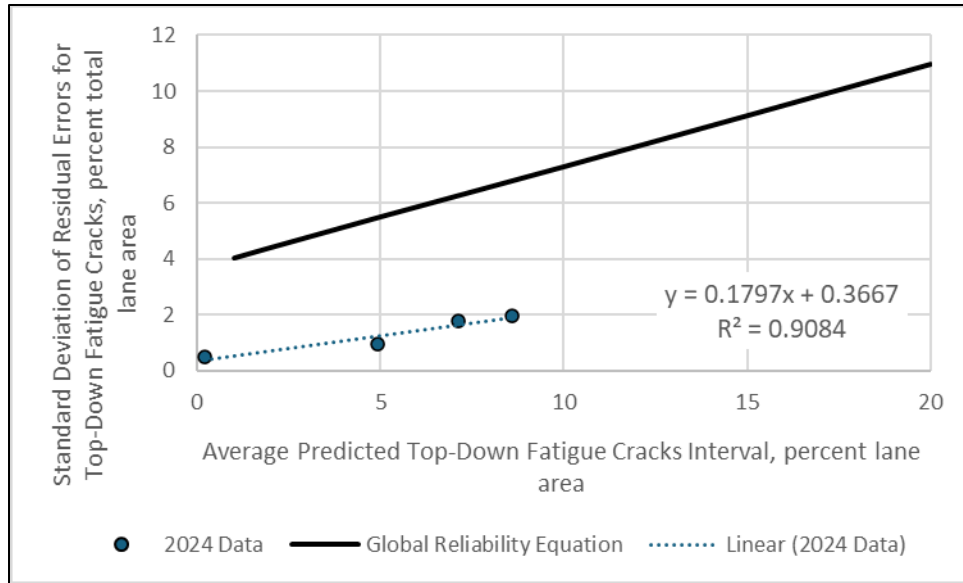
Figure 54. Standard Deviation of Residual Errors Equation for Estimating Reliability for Top-Down Fatigue Cracks.

7.0 Reflection Cracking

7.1 Reflection Cracking Transfer Functions

The PMED software predicts the reflection of bottom-up fatigue cracks and transverse cracks from the existing asphalt layer into and through the asphalt overlay. The reflection cracking model for fatigue and transverse cracks integrated in the MEPDG is an extension of the Paris Law model utilized for the transverse cracking model (see Chapter 5). Crack increments, *c,* are computed in bending and shear due to traffic (as displayed in equation 38) and in direct tension due to temperature changes (as displayed in equation 39):

$$\frac{dc}{dN} = A[k_1(\Delta K_B)^n + k_2 (\Delta K_S)^n] \tag{Eq. 38}$$

$$\frac{dc}{dT} = A\, k_3 \, (K_T)^n \tag{Eq. 39}$$

Where, *A* and *n* are the asphalt mixture/layer fracture properties obtained from indirect creep compliance tests as displayed in equation 40 and equation 41, K_B, K_S and K_T are the stress intensity functions in bending, shear, and direct tension, respectively, and k_1, k_2 and k_3 are stress intensity regression coefficients. Table 14 summarizes the stress intensity regression coefficients for bottom-up fatigue and transverse cracking, while Figure 55 includes a screen shot displaying the stress intensity regression coefficients for bottom-up fatigue cracking and Figure 56 includes a screen shot for the stress intensity regression coefficients for transverse cracking.

$$A = g_2 + \frac{g_3}{m_{Mix}}(Log[D_i]) + g_4(Log[\sigma_t]) \tag{Eq. 40}$$

$$n = g_0 + \frac{g_1}{m_{Mix}}\pi r^2 \tag{Eq. 41}$$

Where:

g_0, g_1, g_2, g_3, g_4 = Mixture regression coefficients.

m_{mix} = The log-log slope of the asphalt mixture creep compliance versus loading time relationship for the current temperature and loading time.

D_1 = Coefficient of the asphalt mixture creep compliance expressed in the power law form.

σ_t = Tensile strength of the asphalt mixture at the specific temperature.

The incremental damage indices ΔDI_i for month *i* are computed in accordance with equation 42.

$$\Delta DI_i = \sum_1^m A[c_1 k_1(K_B)^n + c_2 k_2 (K_S)^n + c_3 k_3 (K_T)^n] \tag{Eq. 42}$$

71

The load transfer efficiency (LTE) of transverse and bottom-up fatigue cracks impact the stress intensity factors for shear. The LTE is not included in the LTPP database for flexible pavements. The LTE was defined through global calibration and found to be related to crack severity.[11] For low severity transverse and fatigue cracks, the global LTE is 0.80, while medium severity cracks the global LTE is 0.40, and for high severity cracks the LTE is 0.10.

The c_1, c_2, and c_3 variables are the calibration coefficients for the damage indices resulting from the bending, shear, and thermal stress intensity modes. Table 14 summarizes the global calibration coefficients. The damage from the stress intensity factors is accumulated over m months into the cracking index DI in accordance with equation 43.

$$DI = \sum_{i=1}^{m} \Delta DI_i \qquad \text{(Eq. 43)}$$

Equation 44 is used to compute the reflection cracking rate on an area or length of cracks basis.

$$RCR = C \left(\frac{100}{c_4 + e^{c_5 logDI}} \right) \qquad \text{(Eq. 44)}$$

Where, C is the total area or length of cracks in the pavement surface before the overlay and c_4 and c_5 are calibration factors with default values listed in Table 14 for bottom-up fatigue and transverse cracks.

---

[11] Most of the transverse and fatigue cracks recorded in the LTPP database are classified as low severity. Relatively few LTPP sections used in the global calibration process exhibited medium severity cracks and fewer sections exhibited high severity cracks. Thus, the default LTE values included in the PMED software for medium and high severity cracks are an estimate.

Table 14. Global Calibration Coefficients to Predict Bottom-Up Fatigue and Transverse Reflective Cracks.

Reflection Cracking Variable Name	Term or Coefficient	Bottom-Up Fatigue Reflective Cracks	Transverse Reflective Cracks
Damage Index Stress Intensity Coefficient	k_1	0.012	0.012
Damage Index Stress Intensity Coefficient	k_2	0.005	0.005
Damage Index Stress Intensity Coefficient	k_3	1.0	1.0
Damage Index Calibration Coefficient	c_1	0.38	3.22
Damage Index Calibration Coefficient	c_2	1.66	25.7
Damage Index Calibration Coefficient	c_3	2.72	0.1
Transfer Function Calibration Coefficient	c_4	105.4	133.4
Transfer Function Calibration Coefficient	c_5	-7.02	-72.4

Figure 55. PMED Scree Shot for the Asphalt Mixture Regression Coefficients and Global Calibration Coefficients for Bottom-Up Fatigue Cracks.

Figure 56. PMED Screen Shot for the Asphalt Mixture Regression Coefficients and Global Calibration Coefficients for Transverse Cracks.

7.2 Verification of the Reflection Cracking Transfer Function Global Coefficients

Verification and calibration of the reflection cracking transfer function was completed using the same process used for the 2018 global recalibration. The process is briefly summarized below:

1. Use the results from new flexible pavement calibration for the existing layers. The regional calibration coefficients and layer properties discussed in Chapter 5 for transverse cracks and in Chapter 6 for bottom-up and top-down fatigue cracks were used in the verification of the reflection cracking transfer function.

2. The measured fatigue cracks recorded in the LTPP database just prior to the asphalt overlay placement are grouped into bottom-up and top-down fatigue cracks. The bottom-up fatigue cracks observed at the surface are assumed to have propagated through the entire asphalt layers of the existing pavement. Top-down fatigue cracks are assumed to be confined within the asphalt layers. Top-down cracks can propagate downward through thinner asphalt pavements, but the assumption is that the load transfer efficiency (LTE) of top-down cracks is approximately 100 percent, regardless of their severity. For the initial verification, top-down cracks are not used to determine

74

the damage of the existing asphalt layers; only the area of bottom-up fatigue cracks are used to determine the fatigue damage (bottom-up) of the existing asphalt layers.

3. The load transfer efficiency (LTE) of fatigue and transverse cracks has a significant impact on the prediction of fatigue and transverse cracks. The fatigue cracks LTE is not measured but is a calibration parameter. The transverse cracks LTE can be measured from deflection basin data, in accordance with the MEDPG Manual of Practice. However, deflection basin measurements across cracks were not measured in the LTPP program, so the transverse crack LTE is a calibration parameter.

4. The fatigue and transverse crack LTEs are first estimated on a section basis by determining the LTE value to "best" match, as possible, the measured cracks.

5. The average fatigue crack LTE and transverse crack LTE are determined and then used in the verification and calibration process. The average fatigue and transverse crack LTEs included in the MEPDG Manual of Practice were found to be correlated to crack severity. The PMED software includes these values as the default LTEs. The fatigue and transverse crack default LTEs were used in the initial verification as part of this regional study. The fatigue and transverse cracks recorded for the sections used in this regional study were of a minor severity.

6. The average fatigue and transverse crack LTEs were then used in the updated verification process using the default calibration coefficients for reflection cracks (see Figure 55 and Figure 56). If the verification results imply improvements are needed, the CAT is used to adjust the reflection cracking calibration coefficients.

The following sections describe the verification of the bottom-up fatigue reflection and transverse reflection crack transfer functions.

7.2.1 Bottom-Up Fatigue Cracks Reflection Cracking Transfer Function

The CAT was used to determine the statistical parameters between the predicted and measured fatigue reflection cracks using the global calibration coefficients (see Table 14 and Figure 55) and the representative LTE values.

Figure 57 displays a graphical comparison of the measured and predicted fatigue cracks in asphalt overlays, while Figure 58 compares the predicted fatigue cracks to the residual error (predicted minus measured value). Table 15 summarizes the statistical parameters using the 2018 calibration coefficients. As summarized, the s_e/s_y, R^2, and the SEE statistical parameters for percent total lane area fatigue cracks suggest a poor to good simulation of the observed fatigue cracking.
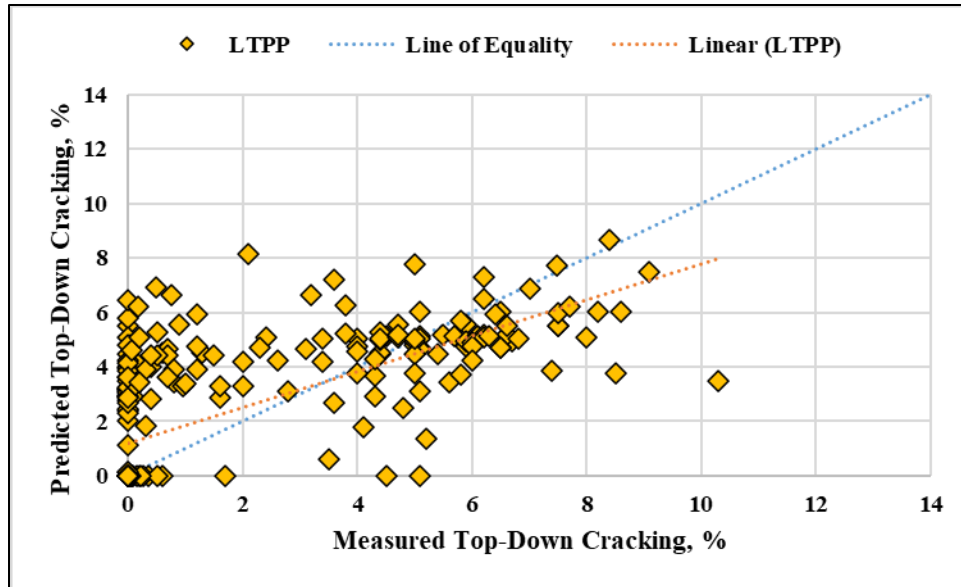
Figure 57. Predicted and Measured Percent Fatigue Cracks of the Asphalt Overlay using the 2018 Global Reflective Fatigue Cracking Calibration Coefficients.
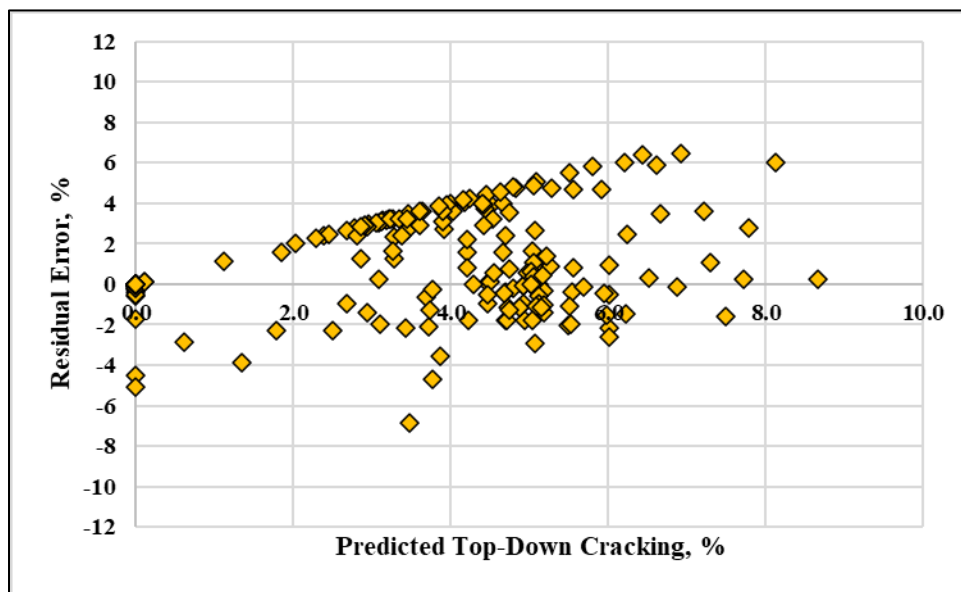
Figure 58. Predicted Total Fatigue Cracks of the Asphalt Overlays using the 2018 Global Reflective Fatigue Cracking Calibration Coefficients as Compared to the Residual Error.

Table 15. Evaluation of Results for Verifying the 2018 Global Calibration Coefficients to Predict Total Fatigue Crack (New and Reflective) in Asphalt Overlays.

Statistical Parameters for Total Fatigue Cracking (New and Reflective Cracks) Transfer Functions	PMED, Version 3.0; Asphalt Overlays
Number of Total Sections	66
Number of Observations	303
Goodness-of-Fit: R-squared	0.478 (Poor)
Goodness-of-Fit: Se/Sy	0.706 (Fair)
Goodness-of-Fit: SEE, percent cracked slabs	1.78 (Good)
Goodness-of-Fit: Standard Deviation of Residuals	1.98
Goodness-of-Fit: Slope	0.659
Goodness-of-Fit: Intercept	1.20
Bias	0.618 (Low)
Hypothesis Test; H_0 p-value: Slope = 1.0	Reject
Hypothesis Test; H_0 p-value: Intercept = 0.0	Reject
Hypothesis Test; H_0 p-value: Paired t-test; Bias = 0.	Reject

Overall, the verification results suggest the fatigue cracking reflection cracking model and transfer function provide a fair goodness of fit for explaining the measured total area of bottom-up fatigue cracks; includes new fatigue cracks in the asphalt overlay and fatigue cracks reflection through the asphalt overlay. The CAT was used to try and improve on the calibration coefficients for the fatigue reflection cracking transfer function. No significant improvement in the comparison of the predicted versus measured values was obtained. In addition, the hypothesis tests were still all rejected. There were cases were the hypotheses for the slope and paired t-test were accepted but the statistical parameters for the goodness of fit were increased resulting in mostly a poor fit or weak relationship between the measured and predicted values. Thus, the 2018 global calibration coefficients are suggested for use in Massachusetts.

7.2.2 Transverse Cracks Transfer Function Reflection Cracking

The CAT was used to determine the statistical parameters between the predicted and measured transverse reflection cracks using the global calibration coefficients (see Table 14 and Figure 56) and the representative LTE values for transverse cracks.

Figure 59 displays a graphical comparison of the measured and predicted transverse cracks in asphalt overlays, while Figure 60 compares the predicted transverse cracks to the residual error (predicted minus measured value). Table 16 summarizes the statistical parameters using the 2018 calibration coefficients. As summarized, the s_e/s_y, R^2, and the SEE statistical parameters for the length of transverse cracks suggest a fair to good simulation of the observed transverse cracking.
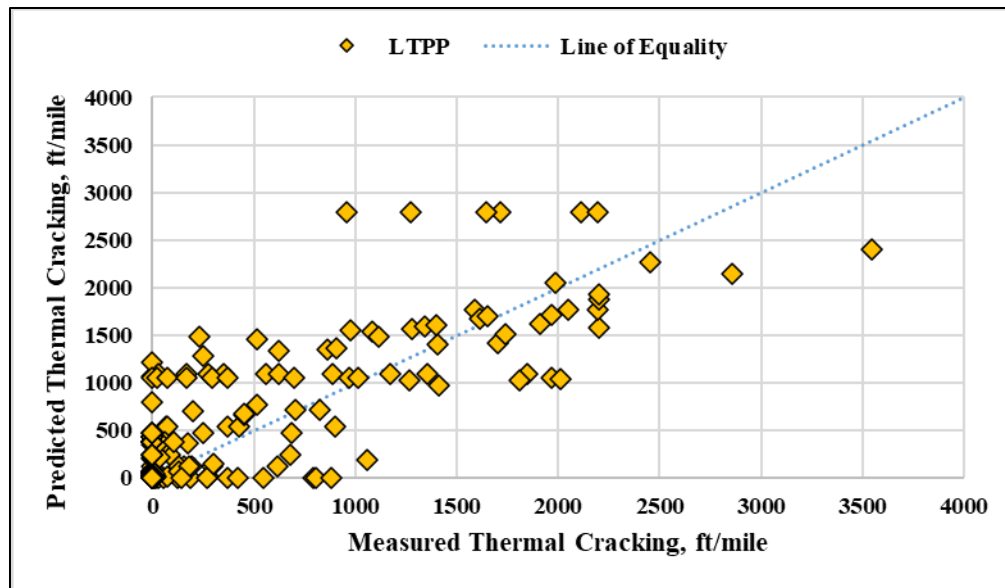
Figure 59. Predicted and Measured Transverse Cracks in Asphalt Overlays using the 2018 Fatigue Reflective Cracking Calibration Coefficients.
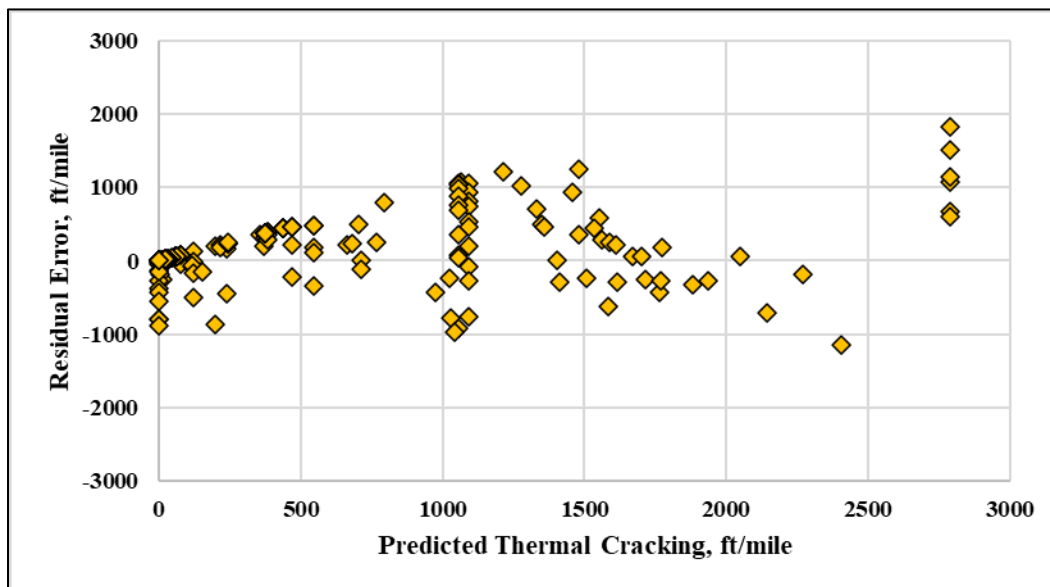
Figure 60. Predicted Length of Transverse Cracks in Asphalt Overlays using the 2018 Global Calibration Coefficients as Compared to the Residual Error.

Table 16. Evaluation of Results for Verifying the 2018 Global Calibration Coefficients to Predict Total Transverse Cracks (New and Reflective) in Asphalt Overlays.

Statistical Parameters for Total Transverse Cracking (New and Reflective Cracks) Transfer Functions	PMED, Version 3.0; Asphalt Overlays
Number of Total Sections	66
Number of Observations	248
Goodness-of-Fit: R-squared	0.672 (Good)
Goodness-of-Fit: Se/Sy	0.528 (Good)
Goodness-of-Fit: SEE, percent cracked slabs	389.7 (Fair)
Goodness-of-Fit: Standard Deviation of Residuals	403.1
Goodness-of-Fit: Slope	0.840
Goodness-of-Fit: Intercept	173.5
Bias	114.8 (Low)
Hypothesis Test; H_0 p-value: Slope = 1.0	Reject
Hypothesis Test; H_0 p-value: Intercept = 0.0	Accept
Hypothesis Test; H_0 p-value: Paired t-test; Bias = 0.	Reject

Overall, the verification results suggest the reflective transverse cracking model and transfer function provide a fair goodness of fit for explaining the measured length of transverse cracks; includes new transverse cracks in the asphalt overlay and transverse cracks reflecting through the asphalt overlay. The CAT was not used to try and improve on the calibration coefficients for the transverse reflection cracking transfer function.

7.3 Reliability Equation for Fatigue and Transverse Reflective Cracking of Asphalt Overlays

The MEPDG estimates pavement design reliability, using the estimate of total cracks in the overlay (new and reflective) based on the average input values and the standard deviation of residual errors for total fatigue or transverse cracks (new and reflective). The standard deviation of residual errors prediction equation for bottom-up fatigue and transverse cracks were developed as follows:

1. Divide the predicted fatigue and transverse reflective cracks into 4 or more intervals.

2. For each interval, determine mean predicted fatigue or transverse cracks and standard deviation of residual errors (i.e., standard deviation of predicted minus measured cracks that fall within the given interval).

3. Develop a linear or nonlinear model to fit the mean predicted cracking and standard deviation of the residual errors.

7.3.1 Fatigue Reflective Crack Reliability Equation

The resulting standard deviation of the residual errors from the 2024 calibration update using v3.0 is displayed in Figure 61, in comparison to the 2018 global reliability equation. As displayed, the standard deviation of the residuals for the 2024 data is less in comparison to the 2018 global standard deviation of residuals equation. The 2024 reliability equation shown in equation 45 is suggested for use in Massachusetts.

$$\sigma_{RC-BUC} = 1.8387(FC_{RC-BUC})^{0.2093} \qquad \text{(Eq. 45)}$$

Where:

$\sigma_{RC\text{-}BUC}$ = Standard deviation of residuals for the bottom-up reflective fatigue cracks, percent total lane area.

$FC_{RC\text{-}BUC}$ = Predicted bottom-up fatigue reflective cracks, percent total lane area.
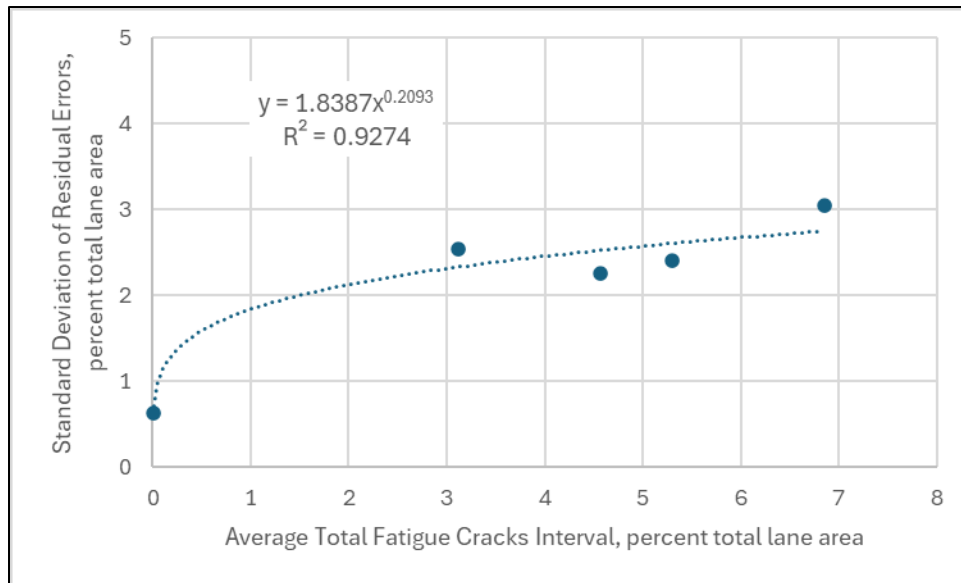
Figure 61. Standard Deviation of Residual Errors Equation for Estimating Reliability for Bottom-Up Reflective Fatigue Cracks in Asphalt Overlays.

7.3.2 Transverse Reflective Crack Reliability Equation

The resulting standard deviation of the residual errors from the 2024 calibration update using v3.0 is displayed in Figure 62, in comparison to the and the 2018 global reliability equation. As displayed, the standard deviation of the residuals for the 2024 data is less in comparison to the 2018 global standard deviation of residuals equation. The 2024 reliability equation shown in equation 46 is suggested for use in Massachusetts.

$$\sigma_{RC-TC} = 69.61(TC_{RC-TC})^{0.2893} \qquad \text{(Eq. 46)}$$

Where:

$\sigma_{RC\text{-}TC}$ = Standard deviation of residuals for total transverse cracks (new and reflective), ft./mi.

$TC_{RC\text{-}TC}$ = Predicted total transverse cracks (new and reflective), ft./mi.
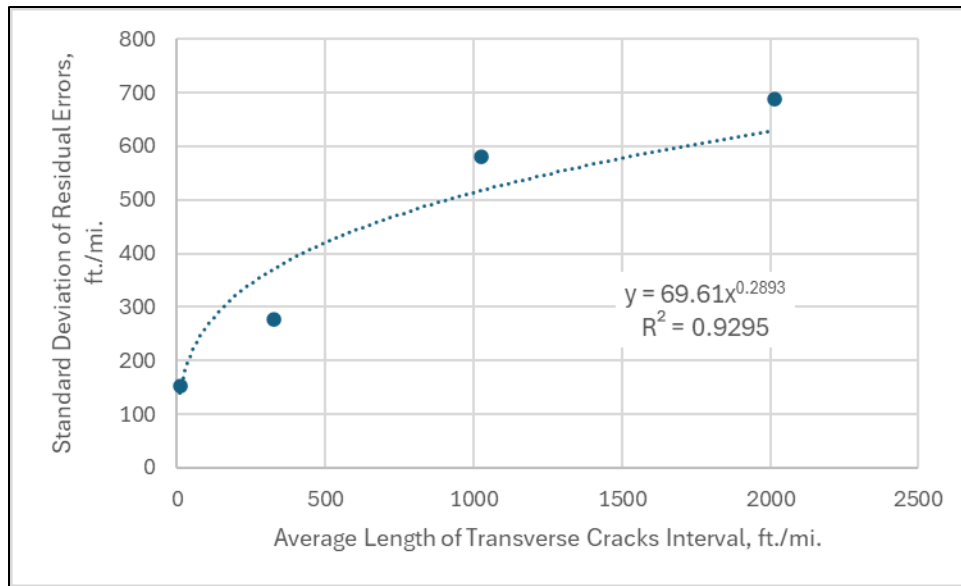
Figure 62. Standard Deviation of Residual Errors Equation for Estimating Reliability for Reflective Total Transverse Cracks in Asphalt Overlays.

This page left blank intentionally

8.0 Smoothness

8.1 Smoothness Regression Equation

A detailed description of the smoothness or IRI regression equation and prediction process is presented in the MEPDG Manual of Practice (AASHTO, 2020). IRI of new flexible pavements and asphalt overlays of flexible pavements is predicted using the regression equation displayed in equation 33:

$$IRI = IRI_i + C_1(RD) + C_2(FC_{Total}) + C_3(TC) + C_4(SF) \qquad \text{(Eq. 47)}$$

Where:

$IRIi$ = Initial IRI.

RD = Predicted average rut depth.

FC_{Total} = Predicted average total area of fatigue cracking that includes new fatigue cracks and fatigue cracks that reflect through an asphalt overlay from the existing asphalt layers.

TC = Predicted average total length of transverse cracks that includes new transverse cracks and transverse cracks that reflect through an asphalt overlay from the existing asphalt layer.

SF = Site Factor.

C_1, C_2, C_3, C_4 = Smoothness regression model coefficients. A screen shot of the IRI regression coefficients are displayed in Figure 63.

C_1 = The impact of rutting on IRI, the global default value is 40.0.

C_2 = The impact of fatigue cracking on IRI, the global default value is 0.40.

C_3 = The impact of transverse cracks on IRI; the global default value is 0.008.

C_4 = The impact of the site factors (climate and soils) on IRI; the global default value is 0.015.

$$SF = Age^{1.5}(Ln[(Precp + 1)(FI + 2)p_{02}] + Ln[(Precp + 1)(PI + 1)p_{0.075}]) \quad \text{(Eq. 48)}$$

Age = Pavement age in years.

$Precp$ = Average annual rainfall or precipitation in inches.

FI = Freezing index in degree F-days.

P_{02} = Percent subgrade material passing the No. 02 mm sieve.

$P_{0.075}$ = Percent subgrade material passing the No. 0.075 mm sieve.

Figure 63. PMED Screen Shot for the IRI Global Regression Coefficients.

8.2 IRI Data Review

The International Roughness Index (IRI) data extracted from the LTPP database and reviewed for consistency and to identify potential errors, outliers, and any bias between the two datasets. Figure 64 displays the cumulative frequency diagram of the average IRI value measured for the LTPP new flexible and asphalt overlay sections. The LTPP data sets exhibit different characteristics. Table 17 compares the mean, median, and standard deviation of the IRI measurements. s displayed in Figure 64 and Table 17, the new flexible sections have higher IRI values (rougher pavement).

The other important variable to consider is the maintenance/repair made to the sections within the monitoring period. Table 2 listed the sections where some maintenance activity was recorded. The maintenance feature in the PMED software was used to simulate the first maintenance activity and the change in the average IRI measurements over time. The IRI measurements after the second maintenance activity were excluded from the comparison between the predicted and measured IRI values for the verification and calibration process because the PMED software only allows one maintenance activity within the design period.
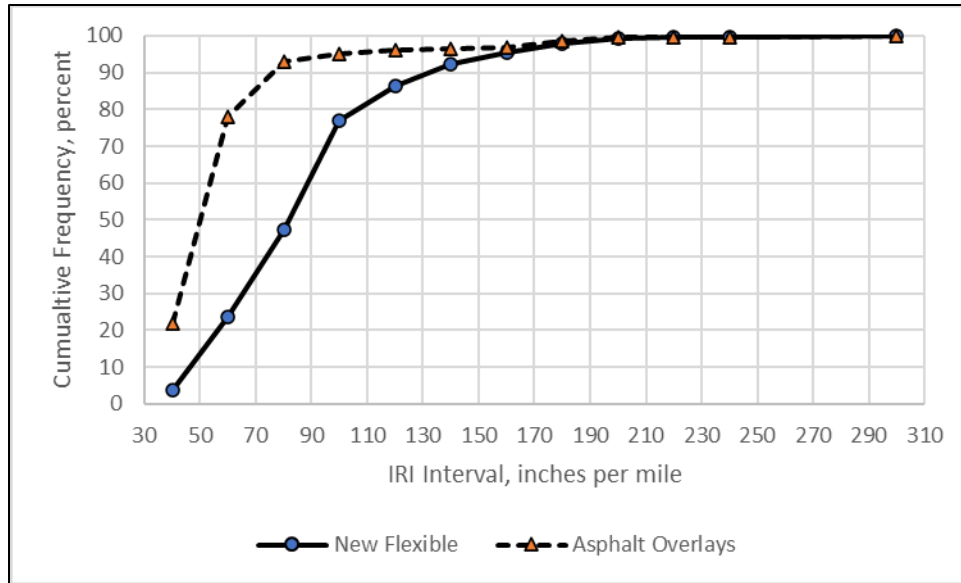
Figure 64. Cumulative Frequency Diagram of the IRI Measurements for the LTPP Sections.

Table 17. Mean, Median, and Standard Deviation of the IRI Measurements of the LTPP Sections.

Statistical Value	Type of Roadway Segment New Flexible	Type of Roadway Segment Asphalt Overlays
Number of Sections	18	48
Number of Observations	419	559
Average Measured IRI, inches per mile	98.9	65.4
Median Measured IRI, inches per mile	92	58
Standard Deviation of IRI Value, inches per mile	42.2	29.7

8.3 Verification of the IRI Regression Coefficients

The CAT was used to determine the statistical parameters between the predicted and measured IRI values using the global calibration coefficients. Table 18 summarizes the statistical parameters using the global calibration coefficients derived for version 3.0. As summarized, the s_e/s_y, R^2, and the SEE statistical parameters for percent cracked slabs suggest a good simulation of the observed or measured IRI. In addition, the bias is considered low.

Figure 65 displays a graphical comparison of the measured and predicted IRI values, while Figure 66 compares the predicted IRI to the residual error (predicted minus measured value). The data displayed in Figure 65 and Figure 66 were labeled as new flexible and asphalt overlay

sections. No systematic difference in the residual errors or significant bias was observed between the two datasets when the difference in age is taken into consideration. Thus, the two datasets were combined.
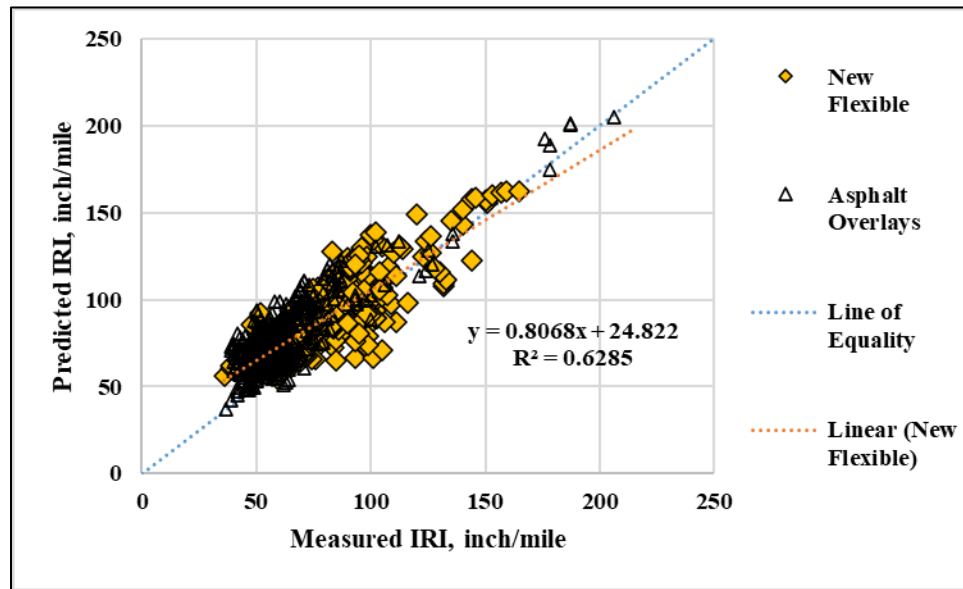
Figure 65. Predicted and Measured IRI Values using V3.0 with the 2018 Global Regression Model Coefficients.
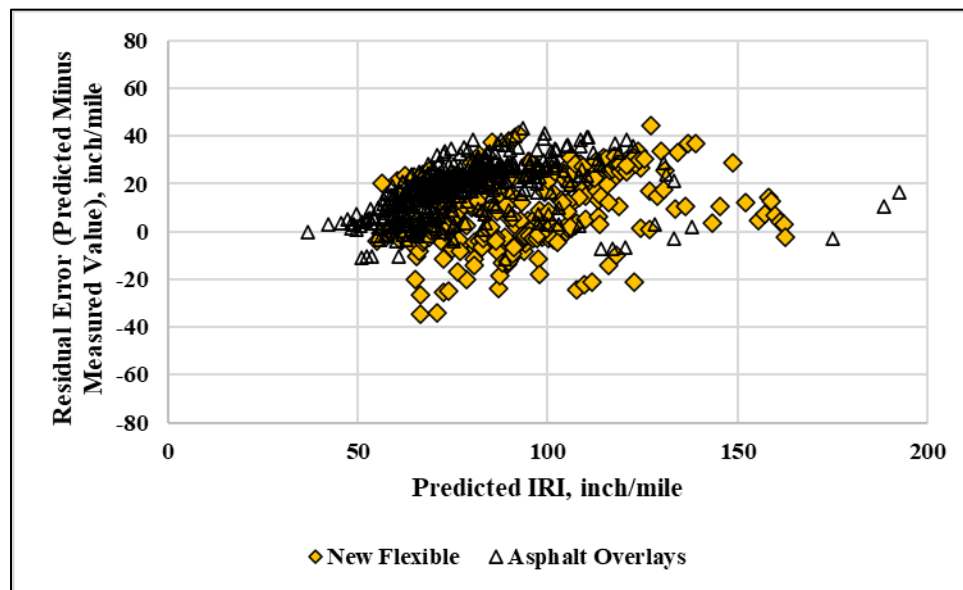
Figure 66. Residual Error versus Predicted IRI using V3.0 with the 2018 Global Regression Model Coefficients.

Table 18. Evaluation of Results Using the Global 2018 Regression Model Coefficients to Calculate IRI for all Sections.

Statistical Parameters for IRI Regression Equation	PMED, Global, Version 3.0
Number of Total Sections	66
Number of Observations	567
Goodness-of-Fit R-squared	0.719 (Good)
Goodness-of-Fit Se/Sy	0.480 (Good)
Goodness-of-Fit SEE, IRI, inches per mile	12.48 (Good)
Goodness-of-Fit Standard Deviation of Residuals	13.41
Goodness-of-Fit Slope	0.802
Goodness-of-Fit Intercept	27.84
Bias	13.69 (Low)
Hypothesis Test: H_0 p-value: Slope = 1.0	Reject (p-value: 0.000)
Hypothesis Test: H_0 p-value: Intercept = 0.0	Reject (p-value: 0.000)
Hypothesis Test: H_0 p-value: Paired t-test; Bias = 0.	Reject (p-value: 0.000)

8.4 Calibration of the IRI Regression Coefficients

The CAT was used to optimize the regional IRI regression model coefficients for the new flexible and asphalt overlay sections. No improvement was found relative to the verification results. If the regression coefficients were revised to reduce the intercept so the hypothesis test was accepted, the standard error increased while the R-squared decreased.

Figure 65 exhibits the IRI global regression equation overpredicts the IRI at relative low values or smooth pavements, while little bias was determined for higher measured IRI values or rougher pavements, closer to the IRI threshold or design value. The same was true for the new flexible pavement data set.

Overall, the verification results suggest the IRI regression equation provides the "best" overall fit for explaining the measured IRI values. No adjustment to the 2018 global regression model coefficients was required for the IRI regression equation. The following lists the IRI regression equation model coefficients suggested for use in Massachusetts.

C_1 = 40.0; the impact of rutting on IRI.

C_2 = 0.40; the impact of fatigue cracking on IRI.

C_3 = 0.008; the impact of transverse cracks on IRI.

C_4 = 0.015; the impact of the site factors (climate and soils) on IRI.

8.5 Reliability Equation for Smoothness Regression Equation

The MEPDG estimates pavement design reliability, using the average predicted IRI value based on the average input values and the standard deviation of residual errors for IRI. Predicted IRI standard deviation of residual errors prediction equation was developed as follows:

1. Divide the predicted IRI into 4 or more intervals.

2. For each interval, determine the mean predicted IRI and standard deviation of residual errors (i.e., standard variation of predicted – measured IRI for all predicted IRI values that fall within the given interval).

3. Develop a linear or nonlinear model to fit the mean predicted IRI and standard deviation of the residual errors.

The 2024 regional standard deviation of residuals is displayed in equation 49 and in Figure 67 in comparison to the 2018 global IRI reliability equation. The regional standard deviation of residuals is less than the 2018 global values for relatively smooth pavements but greater than the 2018 global values for rougher pavements. The 2024 regional standard deviation of residuals equation is suggested for use in design in Massachusetts.

$$\sigma_{IRI} = 9.1082 * \text{Ln}(IRI) - 27.288 \qquad \text{(Eq. 49)}$$

Where:

σ_{IRI} = IRI standard deviation of residuals, inches per mile.

IRI = Predicted IRI, inches per mile.
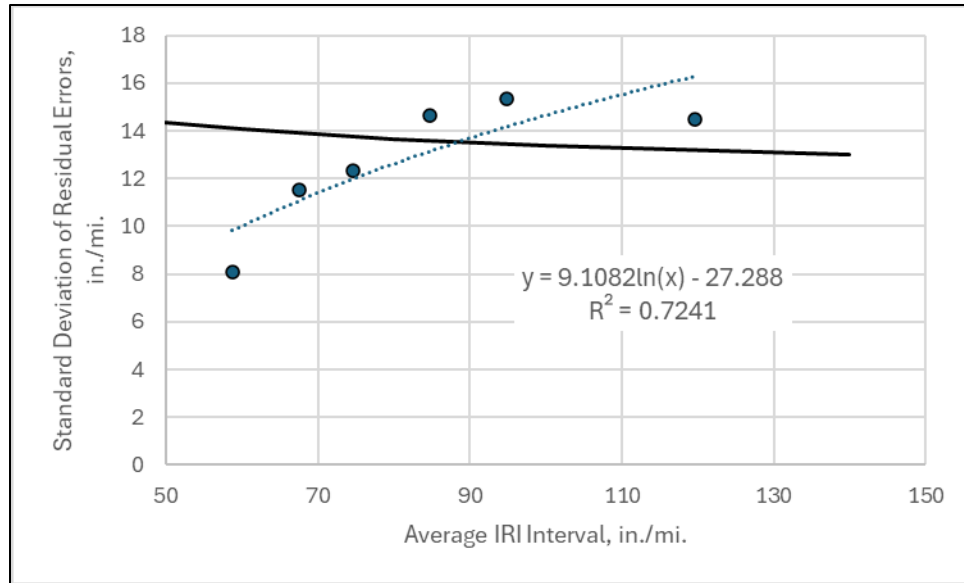
Figure 67. Standard Deviation of Residual Errors Equation for Estimating IRI Reliability.

This page left blank intentionally.

9.0 Summary and Recommendations

This section of the report provides a summary of the regional calibration coefficients suggested for use in Massachusetts and includes some recommendations for future verification efforts.

9.1 Regional Calibration Coefficients

Table 19 through Table 25 list the 2024 regional calibration coefficients by distress type for new flexible pavements and asphalt overlays. The global calibration coefficients for version 3 of the PMED software are also included in the respective tables for a comparison to the regional calibration coefficients. In summary, it is suggested that MassDOT use these regional calibration coefficients for designing and/or evaluating flexible pavements, because they represent the performance of flexible pavements and asphalt overlays built in Massachusetts and adjacent states.

[Note: The cells highlighted in the tables identify the calibration coefficients for which the 2024 regional values differ from the global values derived in 2018 for flexible pavements.]

Table 19. Recommended Rut Depth Transfer Function Calibration Coefficients and Reliability Equation.

Layer Type	Model Coefficients	2018 Global Coefficients	2024 Regional Values
Asphalt	β_{1r}	0.40	0.40
Asphalt	β_{2r}	0.52	0.52
Asphalt	β_{3r}	1.36	1.36
Asphalt	$\sigma_{RD\text{-}Asphalt}$	$= 0.24\left(RD_{Asphalt}\right)^{0.8026} + 0.001$	=0.060
Aggregate Base	β_{S1}	1.0	1.0
Aggregate Base	$\sigma_{RD\text{-}Aggr.Base}$	$= 0.1477\left(RD_{Aggr.Base}\right)^{0.6711} + 0.001$	=0.0079
Subgrade Soil	β_{S1}	1.0	1.0
Subgrade Soil	$\sigma_{RD\text{-}Subgr.}$	$= 0.1235\left(RD_{Subgr.}\right)^{0.5012} + 0.001$	=0.029

Table 20. Recommended Transverse Cracking Transfer Function Calibration Coefficients and Reliability Equation.

Layer Type	Model Coefficients	2018 Global Coefficients	2024 Regional Values
Asphalt Wearing Surface	β_t	1.0	1.0
Asphalt Wearing Surface	$\sigma_{\text{TC-Level3}}$	$= 0.2386(TC) + 168$	$= 0.2386(TC) + 168$

Table 21. Recommended Bottom-Up Fatigue Cracking Transfer Function Calibration Coefficients and Reliability Equation.

Layer Type	Model Coefficients	2018 Global Coefficients	2024 Regional Values
Lower Asphalt Layer or Asphalt Base	C_1	1.31	1.11
Lower Asphalt Layer or Asphalt Base	C_2: $h_{ac} < 5$ in.	2.1585	2.1585
Lower Asphalt Layer or Asphalt Base	C_2: 5 in. < h_{ac} < 12 in	$= 0.867 + (0.2583 * h_{ac})$	$= 0.867 + (0.2583 * h_{ac})$
Lower Asphalt Layer or Asphalt Base	C_2: $h_{ac} > 12$ in	3.9666	3.9666
Lower Asphalt Layer or Asphalt Base	C_3	6,000	6,000
Lower Asphalt Layer or Asphalt Base	$\sigma_{\text{FC-BUC}}$	$= 1.13 + \dfrac{13}{e^{(7.57-15.5Log(FC_{BUC}+0.0001))}}$	$= 3.5537 + (0.1496 * FC_{BUC})$

Table 22. Recommended Top-Down Fatigue Cracking Transfer Function Calibration Coefficients and Reliability Equation.

Layer Type	Model Coefficients	2018 Global Coefficients	2024 Regional Values
Asphalt Wearing Surface	C_1	2.5219	3.00
Asphalt Wearing Surface	C_2	0.9069	0.60
Asphalt Wearing Surface	C_3	1.0	1.0
Asphalt Wearing Surface	$\sigma_{\text{FC-TDC}}$	$= 3.6563 + (0.3657 * FC_{TDC})$	$= 0.3667 + (0.1797 * FC_{TDC})$

Table 23. Recommended Fatigue Reflective Cracking Transfer Function Calibration Coefficients and Reliability Equation.

Layer Type	Model Coefficients	2018 Global Coefficients	2024 Regional Values
Asphalt Overlay	C_4	105.4	105.4
Asphalt Overlay	C_5	-7.02	-7.02
Asphalt Overlay	$\sigma_{RC\text{-}BUC}$	$= 1.1097(FC_{BUC})^{0.6804} + 1.23$	$= 1.8387(FC_{BUC})^{0.2093}$
Asphalt Overlay	$LTE_{FC\text{-}BUC}(1)$	0.80	0.80

(1) All fatigue cracks exhibited on the LTPP test sections prior to overlay for these sites were classified as low severity. Thus, only one LTE value is provided and suggested for use.

Table 24. Recommended Transverse Reflective Cracking Transfer Function Calibration Coefficients and Reliability Equation.

Layer Type	Model Coefficients	2018 Global Coefficients	2024 Regional Values
Asphalt Overlay; MAAT < 57°F[1]	C_4	133.4	133.4
Asphalt Overlay; MAAT < 57°F[1]	C_5	-72.4	-72.4
Asphalt Overlay; MAAT < 57°F[1]	$\sigma_{RC\text{-}TC\text{-}Level3}$	$= 70.0(TC_{RC})^{0.2994} + 30.12$	$= 69.61(TC_{RC})^{0.2893}$
Asphalt Overlay; MAAT < 57°F[1]	$LTE_{TC\text{-}Level\ 3}[2]$	0.80	0.85

(1) All LTPP sites included in the verification-calibration effort were located in climates with a MAAT<57°F.

(2) All transverse cracks exhibited on the LTPP test sections prior to overlay for these sites were classified as low severity. Thus, only one LTE value is provided and suggested for use.

Table 25. Recommended IRI Regression Model Coefficients and Reliability Equation.

Pavement Type	Model Coefficients	2018 Global Coefficients	2024 Regional Values
New Asphalt Pavement and Asphalt Overlays	C_1-Rut Depth	40.0	40.0
New Asphalt Pavement and Asphalt Overlays	C_2-Fatigue Cracks	0.40	0.40
New Asphalt Pavement and Asphalt Overlays	C_3-Transverse Cracks	0.008	0.008
New Asphalt Pavement and Asphalt Overlays	C_4-Site Factor	0.015	0.015
New Asphalt Pavement and Asphalt Overlays	$\sigma_{FC\text{-}TDC}$	$= 25.1148 * Ln(IRI) - 87.95062$	$= 9.1082 * Ln(IRI) - 27.288$

9.2 Suggestions for Design and Future Calibration Updates

The following provides suggestions for future calibration updates.

1. A verification of the calibration coefficients should be planned periodically using the distress data collected on roadway sections with time. AASHTOWare is planning to update the global calibration coefficients and/or release future enhancements affecting the calibration coefficients on a 5-year cycle; the next update is scheduled for fiscal year 2027. Thus, a 5+ year cycle would be suggested for MassDOT.

2. The accuracy of the top-down fatigue cracking model and transfer function is dependent on the asphalt mixture properties of the wearing surface and time to crack initiation variable (K_{L1}). The time to crack initiation is determined from a regression equation, and is dependent on traffic, climate, and the relaxation modulus power law parameters (see equation 27). However, the gradation or aggregate blend and air voids of the asphalt wearing surface have an impact on when the top-down fatigue cracks occur or can be observed. The K_{L1} parameter translates the laboratory property to field observations. It is suggested that additional roadway segments in Massachusetts be used to confirm or validate the K_{L1} parameter as related to the properties of the wearing surface (air voids, asphalt content, gradation, etc.).

3. The performance indicator measurement error is considered the greatest component of the total standard error of the estimate, especially when the values of the performance indicator are low. Variability of the distress measurements should be considered in assessing the adequacy of the calibration coefficients to fit future time-series data and in determining the number of sites to be used for calibration.

4. The number of new flexible pavement projects used in the 2024 regional calibration (18) is a minimum number. Additional sections should be identified and used. The standard deviation of the residuals is normally underestimated for relatively few projects, especially when the observed values of the performance indicators are skewed towards 0 or the lower range of values.

This page left blank intentionally.

10.0 References

AASHTO (2010). Guide for the Local Calibration of the Mechanistic-Empirical Pavement Design Guide, First Edition, Publication Code: LCG-1, ISBN: 978-1-56051-449-7, American Association of State Highway and Transportation Officials, Washington, DC.

AASHTO (2020). Mechanistic-Empirical Pavement Design Guide, A Manual of Practice, Third Edition with Supplement, MEPDG-3, Publication Code 978-1-56051-748-1, American Association of State Highway and Transportation Officials, Washington, DC.

NCHRP (2004). *Development of 2002 Guide for the Design of New and Rehabilitated Pavement Structure*, NCHRP Project 1-37A, National Cooperative Highway Research Program, National Academies of Science, Washington, DC.

Von Quintus, Harold L. and James S. Moulthrop (2007). *Performance Prediction Models: Volume I – Research Report*, Publication Number FHWA/MT-06-014/8158-1, Montana Department of Transportation, Helena, MT.

Von Quintus, Harold, Chuck Schwartz, Ramon Bonaquist, Jagannath Mallela, and Regis Carvalho (2012). *Calibration of Rutting Models for HMA Structural and Mixture Design*, Report Number 719, National Cooperative Highway Research Program, Transportation Research Board of the National Academies, Washington, DC.

Von Quintus, Harold, Michael Darter, Biplab Bhattacharya, and Leslie Titus-Glover (2015). *Implementation and Calibration of the MEPDG in Georgia*, Report Number FHWA/GA-014-11-17, Georgia Department of Transportation, Materials Research and Testing, Forest Park, Georgia.

Von Quintus, Harold, Dinesh Ayyala, and Hyung Lee (2017). *Characterization Existing Asphalt Concrete Layer Damage for Mechanistic Pavement Rehabilitation Design*, Publication Number FHWA-HRT-17-059; Federal Highway Administration, Turner-Fairbank Highway Research Center; McLean, Virginia.

Von Quintus, H.L., A.T. Papagiannakis, A.E. Masad, E. Alrashydah, and W. Brink (2020). *Calibration and Validation of Flexible Pavement ME Design using Texas Data*, Draft Final Report, Grant #46-8MTIA007, Texas Department of Transportation, Austin, Texas.

This page left blank intentionally.

Appendix A: Pavement Cross Section and Structure for Flexible Pavement Sites

This Appendix A includes a listing and description of the pavement structure for the flexible pavements that were used in the regional calibration with v3.0.

STATE CODE	SHRP ID NUMBER	CONSTRUCTION or OVERLAY DATE	LAYER NO	LAYER TYPE	REPR THICKNESS	MATL CODE	COMMENT
9	0901	7/1/1970	1	SS		203	Original Construction
9	0901	7/1/1970	2	GS	10	306	Original Construction
9	0901	7/1/1970	3	GS	8	308	Original Construction
9	0901	7/1/1970	4	TB	5.8	319	Original Construction
9	0901	7/1/1970	5	AC	5.2	1	Original Construction
9	0901	7/1/1970	6	AC	1.1	1	Original Construction
9	0901	6/1/1997	5	AC	3.8	1	Mill 2.6 inches.
9	0901	6/1/1997	7	AC	1.2	1	Overlay
9	0901	6/1/1997	8	AC	2.3	1	Overlay
9	0902	7/1/1970	1	SS		203	Original Construction
9	0902	7/1/1970	2	GS	10	302	Original Construction
9	0902	7/1/1970	3	GS	8.5	308	Original Construction
9	0902	7/1/1970	4	TB	6.4	319	Original Construction
9	0902	7/1/1970	5	AC	4	1	Original Construction
9	0902	7/1/1970	6	AC	1.7	1	Original Construction
9	0902	6/1/1997	5	AC	3.4	1	Mill 2.3 inches
9	0902	6/1/1997	7	AC	1.2	1	Overlay
9	0902	6/1/1997	8	AC	2.6	1	Overlay
9	0903	7/1/1970	1	SS		203	Original Construction
9	0903	7/1/1970	2	GS	11	306	Original Construction
9	0903	7/1/1970	3	GS	8	308	Original Construction
9	0903	7/1/1970	4	TB	6.3	319	Original Construction
9	0903	7/1/1970	5	AC	4.2	1	Original Construction
9	0903	7/1/1970	6	AC	1.8	1	Original Construction
9	0903	6/1/1997	5	AC	3.5	1	Mill 2.5 inches
9	0903	6/1/1997	7	AC	1.1	1	Overlay
9	0903	6/1/1997	8	AC	2.2	1	Overlay
9	0960	7/1/1970	1	SS		203	Original Construction
9	0960	7/1/1970	2	GS	10	306	Original Construction
9	0960	7/1/1970	3	GS	8.3	308	Original Construction
9	0960	7/1/1970	4	TB	6.4	319	Original Construction
9	0960	7/1/1970	5	AC	4.2	1	Original Construction
9	0960	7/1/1970	6	AC	1.8	1	Original Construction
9	0960	6/1/1997	5	AC	3.3	1	Mill 2.7 inches
9	0960	6/1/1997	7	AC	0.9	1	Overlay
9	0960	6/1/1997	8	AC	2.3	13	Overlay
9	0961	7/1/1970	1	SS		203	Original Construction

STATE CODE	SHRP ID NUMBER	CONSTRUCTION or OVERLAY DATE	LAYER NO	LAYER TYPE	REPR THICKNESS	MATL CODE	COMMENT
9	0961	7/1/1970	2	GS	12	306	Original Construction
9	0961	7/1/1970	3	GS	8	308	Original Construction
9	0961	7/1/1970	4	TB	6.4	319	Original Construction
9	0961	7/1/1970	5	AC	4	1	Original Construction
9	0961	7/1/1970	6	AC	2.2	1	Original Construction
9	0961	6/1/1997	5	AC	3.6	1	Mill 2.6 inches
9	0961	6/1/1997	7	AC	1	1	Overlay
9	0961	6/1/1997	8	AC	2.3	13	Overlay
9	0962	7/1/1970	1	SS		203	Original Construction
9	0962	7/1/1970	2	GS	10.8	306	Original Construction
9	0962	7/1/1970	3	GS	6.5	308	Original Construction
9	0962	7/1/1970	4	TB	6.2	319	Original Construction
9	0962	7/1/1970	5	AC	2.9	1	Original Construction
9	0962	7/1/1970	6	AC	2.1	1	Original Construction
9	0962	6/1/1997	5	AC	2.4	1	Mill 2.6 inches
9	0962	6/1/1997	7	AC	1.4	1	Overlay
9	0962	6/1/1997	8	AC	2.3	13	Overlay
9	1803	7/1/1985	1	SS		211	Original Construction
9	1803	7/1/1985	2	GB	12	302	Original Construction
9	1803	7/1/1985	3	AC	4.1	1	Original Construction
9	1803	7/1/1985	4	AC	3	1	Original Construction
9	1803	6/1/2000	5	AC	0.6	1	Overlay
9	1803	6/1/2000	6	AC	1.2	1	Overlay
23	0501	11/1/1970	1	SS		216	Original Construction
23	0501	11/1/1970	2	GS	9	302	Original Construction
23	0501	11/1/1970	3	GB	4.4	304	Original Construction
23	0501	11/1/1970	4	AC	3.3	1	Original Construction
23	0501	11/1/1970	5	AC	2.8	1	Original Construction
23	0501	11/1/1970	6	AC	2	1	Original Construction
23	0501	11/1/1970	7	AC	0.4	2	Original Construction
23	0502	11/1/1970	1	SS		216	Original Construction
23	0502	11/1/1970	2	GS	9	302	Original Construction
23	0502	11/1/1970	3	GB	4	304	Original Construction
23	0502	11/1/1970	4	AC	3.5	1	Original Construction
23	0502	11/1/1970	5	AC	2.7	1	Original Construction
23	0502	11/1/1970	6	AC	2.2	1	Original Construction
23	0502	11/1/1970	7	AC	0.6	2	Original Construction
23	0502	6/16/1995	8	AC	3.6	13	Overlay
23	0503	11/1/1970	1	SS		216	Original Construction
23	0503	11/1/1970	2	GS	9	302	Original Construction

STATE CODE	SHRP ID NUMBER	CONSTRUCTION or OVERLAY DATE	LAYER NO	LAYER TYPE	REPR THICKNESS	MATL CODE	COMMENT
23	0503	11/1/1970	3	GB	4.4	304	Original Construction
23	0503	11/1/1970	4	AC	3.6	1	Original Construction
23	0503	11/1/1970	5	AC	3	1	Original Construction
23	0503	11/1/1970	6	AC	2.1	1	Original Construction
23	0503	11/1/1970	7	AC	0.5	2	Original Construction
23	0503	6/16/1995	8	AC	3.5	13	Overlay
23	0503	6/16/1995	9	AC	2	13	Overlay
23	0504	11/1/1970	1	SS		216	Original Construction
23	0504	11/1/1970	2	GS	9	302	Original Construction
23	0504	11/1/1970	3	GB	4.4	304	Original Construction
23	0504	11/1/1970	4	AC	3.1	1	Original Construction
23	0504	11/1/1970	5	AC	2.9	1	Original Construction
23	0504	11/1/1970	6	AC	2.1	1	Original Construction
23	0504	11/1/1970	7	AC	0.5	2	Original Construction
23	0504	6/16/1995	8	AC	3.7	1	Overlay
23	0504	6/16/1995	9	AC	2	1	Overlay
23	0505	11/1/1970	1	SS		216	Original Construction
23	0505	11/1/1970	2	GS	9	302	Original Construction
23	0505	11/1/1970	3	GB	4.4	304	Original Construction
23	0505	11/1/1970	4	AC	3	1	Original Construction
23	0505	11/1/1970	5	AC	2.7	1	Original Construction
23	0505	11/1/1970	6	AC	2.2	1	Original Construction
23	0505	11/1/1970	7	AC	0.5	2	Original Construction
23	0505	6/16/1995	8	AC	2.7	1	Overlay
23	0506	11/1/1970	1	SS		216	Original Construction
23	0506	11/1/1970	2	GS	9	302	Original Construction
23	0506	11/1/1970	3	GB	4.2	304	Original Construction
23	0506	11/1/1970	4	AC	3.3	1	Original Construction
23	0506	11/1/1970	5	AC	2.9	1	Original Construction
23	0506	11/1/1970	6	AC	2.1	1	Original Construction
23	0506	11/1/1970	7	AC	0.5	2	Original Construction
23	0506	6/16/1995	6	AC	1.2	1	Mill 1.4 inches
23	0506	6/16/1995	8	AC	2	1	Overlay
23	0506	6/16/1995	9	AC	2.1	1	Overlay
23	0507	11/1/1970	1	SS		216	Original Construction
23	0507	11/1/1970	2	GS	9	302	Original Construction
23	0507	11/1/1970	3	GB	4.4	304	Original Construction
23	0507	11/1/1970	4	AC	3	1	Original Construction
23	0507	11/1/1970	5	AC	2.9	1	Original Construction
23	0507	11/1/1970	6	AC	2.1	1	Original Construction

STATE CODE	SHRP ID NUMBER	CONSTRUCTION or OVERLAY DATE	LAYER NO	LAYER TYPE	REPR THICKNESS	MATL CODE	COMMENT
23	0507	11/1/1970	7	AC	0.4	2	Original Construction
23	0507	6/16/1995	6	AC	1	1	Mill 1.5 inches
23	0507	6/16/1995	8	AC	2.3	1	Overlay
23	0507	6/16/1995	9	AC	3.2	1	Overlay
23	0507	6/16/1995	10	AC	2.1	1	Overlay
23	0508	11/1/1970	1	SS		216	Original Construction
23	0508	11/1/1970	2	GS	9	302	Original Construction
23	0508	11/1/1970	3	GB	4.6	304	Original Construction
23	0508	11/1/1970	4	AC	3.2	1	Original Construction
23	0508	11/1/1970	5	AC	3	1	Original Construction
23	0508	11/1/1970	6	AC	2.2	1	Original Construction
23	0508	11/1/1970	7	AC	0.4	2	Original Construction
23	0508	6/16/1995	6	AC	1.6	1	Mill 1.0 inches
23	0508	6/16/1995	8	AC	2	13	Overlay
23	0508	6/16/1995	9	AC	2.9	13	Overlay
23	0508	6/16/1995	10	AC	1.9	13	Overlay
23	0509	11/1/1970	1	SS		214	Original Construction
23	0509	11/1/1970	2	GS	9	302	Original Construction
23	0509	11/1/1970	3	GB	4.4	304	Original Construction
23	0509	11/1/1970	4	AC	3.1	1	Original Construction
23	0509	11/1/1970	5	AC	2.7	1	Original Construction
23	0509	11/1/1970	6	AC	2.1	1	Original Construction
23	0509	11/1/1970	7	AC	0.5	2	Original Construction
23	0509	6/16/1995	6	AC	1.1	1	Mill 1.5 inches
23	0509	6/16/1995	8	AC	1.7	13	Overlay
23	0509	6/16/1995	9	AC	2.1	13	Overlay
23	0559	11/1/1970	1	SS		214	Original Construction
23	0559	11/1/1970	2	GS	9	302	Original Construction
23	0559	11/1/1970	3	GB	4.4	304	Original Construction
23	0559	11/1/1970	4	AC	3.4	1	Original Construction
23	0559	11/1/1970	5	AC	3	1	Original Construction
23	0559	11/1/1970	6	AC	2.1	1	Original Construction
23	0559	11/1/1970	7	AC	0.3	2	Original Construction
23	0559	6/16/1995	8	AC	1.3	1	Overlay
23	0559	6/16/1995	9	AC	1.8	1	Overlay
23	1001	11/1/1972	1	SS		203	Original Construction
23	1001	11/1/1972	2	GB	12	306	Original Construction
23	1001	11/1/1972	3	AC	3	1	Original Construction
23	1001	11/1/1972	4	AC	5.4	1	Original Construction
23	1001	11/1/1972	5	AC	0.5	2	Original Construction

STATE CODE	SHRP ID NUMBER	CONSTRUCTION or OVERLAY DATE	LAYER NO	LAYER TYPE	REPR THICKNESS	MATL CODE	COMMENT
23	1001	6/6/1995	4	AC	4.1	1	Mill 1.8 inches
23	1001	6/6/1995	6	AC	2.4	1	Overlay
23	1001	6/6/1995	7	AC	1.5	1	Overlay
23	1009	9/1/1970	1	SS		205	Original Construction
23	1009	9/1/1970	2	GS	25.8	308	Original Construction
23	1009	9/1/1970	3	GB	4.8	304	Original Construction
23	1009	9/1/1970	4	AC	4.7	1	Original Construction
23	1009	9/1/1970	5	AC	1	1	Original Construction
23	1009	8/22/1993	6	AC	1.2	1	Overlay
23	1009	8/22/1993	7	AC	1.5	1	Overlay
23	1012	8/1/1985	1	SS		214	Original Construction
23	1012	8/1/1985	2	GS	19.8	306	Original Construction
23	1012	8/1/1985	3	GB	13.2	302	Original Construction
23	1012	8/1/1985	4	AC	8	1	Original Construction
23	1012	8/1/1985	5	AC	1.3	1	Original Construction
23	1026	7/1/1973	1	SS		215	Original Construction
23	1026	7/1/1973	2	GB	17.6	302	Original Construction
23	1026	7/1/1973	3	AC	6.2	1	Original Construction
23	1026	7/1/1973	4	AC	1	1	Original Construction
23	1026	9/15/1996	5	AC	1	78	Overlay
23	1026	9/15/1996	6	AC	1.6	1	Overlay
23	1028	11/1/1972	1	SS		203	Original Construction
23	1028	11/1/1972	2	GB	19.6	308	Original Construction
23	1028	11/1/1972	3	AC	5.3	1	Original Construction
23	1028	11/1/1972	4	AC	1.3	1	Original Construction
23	1028	9/6/1994	5	AC	0.3	78	Overlay
23	1028	9/6/1994	6	AC	1.6	1	Overlay
25	1002	5/1/1982	1	SS		204	Original Construction
25	1002	5/1/1982	2	GS	8.4	308	Original Construction
25	1002	5/1/1982	3	GB	4	304	Original Construction
25	1002	5/1/1982	4	AC	6.4	1	Original Construction
25	1002	5/1/1982	5	AC	1.4	1	Original Construction
25	1003	9/1/1974	1	SS		205	Original Construction
25	1003	9/1/1974	2	GB	12.7	302	Original Construction
25	1003	9/1/1974	3	AC	5.4	1	Original Construction
25	1003	9/1/1974	4	AC	1.2	1	Original Construction
25	1004	7/1/1974	1	SS		265	Original Construction
25	1004	7/1/1974	2	GB	25.6	307	Original Construction
25	1004	7/1/1974	3	AC	8.2	1	Original Construction

STATE CODE	SHRP ID NUMBER	CONSTRUCTION or OVERLAY DATE	LAYER NO	LAYER TYPE	REPR THICKNESS	MATL CODE	COMMENT
25	1004	7/1/1974	4	AC	1.4	1	Original Construction
25	1004	6/1/2001	3	AC	7.8	1	Mill 1.8 inches
25	1004	6/1/2001	5	AC	2.2	13	Overlay
25	1004	9/1/2002	5	AC	2.2	13	Overlay
25	1004	9/1/2002	6	AC	1.2	1	Overlay
33	1001	1/1/1981	1	SS		204	Original Construction
33	1001	1/1/1981	2	GS	14.4	308	Original Construction
33	1001	1/1/1981	3	GB	19.3	302	Original Construction
33	1001	1/1/1981	4	AC	7.2	1	Original Construction
33	1001	1/1/1981	5	AC	1.2	1	Original Construction
33	1001	9/1/2003	4	AC	5.6	1	Mill 2.8 inches
33	1001	9/1/2003	6	AC	1.2	1	Overlay
33	1001	9/1/2003	7	AC	0.1	83	Overlay
33	1001	7/15/2009	8	AC	1.8	1	Overlay
33	1001	7/15/2009	9	AC	1.1	1	Overlay
33	1001	7/1/2016	10	AC	0.6	71	Surface Treatment
34	0501	11/1/1968	1	SS		216	Original Construction
34	0501	11/1/1968	2	GS	66	308	Original Construction
34	0501	11/1/1968	3	GB	10	302	Original Construction
34	0501	11/1/1968	4	AC	6	1	Original Construction
34	0501	11/1/1968	5	AC	3.5	1	Original Construction
34	0502	11/1/1968	1	SS		216	Original Construction
34	0502	11/1/1968	2	GS	41	308	Original Construction
34	0502	11/1/1968	3	GB	10.4	302	Original Construction
34	0502	11/1/1968	4	AC	5.8	1	Original Construction
34	0502	11/1/1968	5	AC	2.9	1	Original Construction
34	0502	8/18/1992	6	AC	1.7	13	Overlay
34	0503	-	1	SS		216	Original Construction
34	0503	-	2	GS	15	308	Original Construction
34	0503	-	3	GS	4	308	Original Construction
34	0503	-	4	GB	11.3	302	Original Construction
34	0503	-	5	AC	6.2	1	Original Construction
34	0503	-	6	AC	3	1	Original Construction
34	0503	8/18/1992	7	AC	3	13	Overlay
34	0503	8/18/1992	8	AC	1.7	13	Overlay
34	0504	11/1/1968	1	SS		216	Original Construction
34	0504	11/1/1968	2	GS	17	308	Original Construction
34	0504	11/1/1968	3	GS	4	308	Original Construction
34	0504	11/1/1968	4	GB	10.7	302	Original Construction

STATE CODE	SHRP ID NUMBER	CONSTRUCTION or OVERLAY DATE	LAYER NO	LAYER TYPE	REPR THICKNESS	MATL CODE	COMMENT
34	0504	11/1/1968	5	AC	5.7	1	Original Construction
34	0504	11/1/1968	6	AC	3	1	Original Construction
34	0504	8/18/1992	7	AC	2.9	1	Overlay
34	0504	8/18/1992	8	AC	1.8	1	Overlay
34	0505	11/1/1968	1	SS		216	Original Construction
34	0505	11/1/1968	2	GS	16	308	Original Construction
34	0505	11/1/1968	3	GS	4	308	Original Construction
34	0505	11/1/1968	4	GB	10	302	Original Construction
34	0505	11/1/1968	5	AC	6.1	1	Original Construction
34	0505	11/1/1968	6	AC	3	1	Original Construction
34	0505	8/18/1992	6	AC	3	1	Overlay
34	0505	8/18/1992	7	AC	1.8	1	Overlay
34	0506	11/1/1968	1	SS		214	Original Construction
34	0506	11/1/1968	2	GB	10	302	Original Construction
34	0506	11/1/1968	3	AC	6.5	1	Original Construction
34	0506	11/1/1968	4	AC	3	1	Original Construction
34	0506	8/18/1992	4	AC	0.9	1	Mill 2.1 inches
34	0506	8/18/1992	5	AC	2	1	Overlay
34	0506	8/18/1992	6	AC	1.9	1	Overlay
34	0507	11/1/1968	1	SS		216	Original Construction
34	0507	11/1/1968	2	GS	54	308	Original Construction
34	0507	11/1/1968	3	GB	10	302	Original Construction
34	0507	11/1/1968	4	AC	5.3	1	Original Construction
34	0507	11/1/1968	5	AC	3	1	Original Construction
34	0507	8/18/1992	5	AC	1	1	Mill 2.0 inches
34	0507	8/18/1992	6	AC	2.6	1	Overlay
34	0507	8/18/1992	7	AC	2.9	1	Overlay
34	0507	8/18/1992	8	AC	1.9	1	Overlay
34	0508	11/1/1968	1	SS		216	Original Construction
34	0508	11/1/1968	2	GS	18	308	Original Construction
34	0508	11/1/1968	3	GS	4	308	Original Construction
34	0508	11/1/1968	4	GB	11.3	302	Original Construction
34	0508	11/1/1968	5	AC	5.8	1	Original Construction
34	0508	11/1/1968	6	AC	3	1	Original Construction
34	0508	8/18/1992	6	AC	0.9	1	Mill 2.1 inches
34	0508	8/18/1992	7	AC	2.5	13	Overlay
34	0508	8/18/1992	8	AC	3.3	13	Overlay
34	0508	8/18/1992	9	AC	1.8	13	Overlay
34	0509	11/1/1968	1	SS		216	Original Construction
34	0509	11/1/1968	2	GS	18	308	Original Construction

STATE CODE	SHRP ID NUMBER	CONSTRUCTION or OVERLAY DATE	LAYER NO	LAYER TYPE	REPR THICKNESS	MATL CODE	COMMENT
34	0509	11/1/1968	3	GS	4	308	Original Construction
34	0509	11/1/1968	4	GB	11.3	302	Original Construction
34	0509	11/1/1968	5	AC	6.2	1	Original Construction
34	0509	11/1/1968	6	AC	3.2	1	Original Construction
34	0509	8/18/1992	6	AC	1.1	1	Mill 2.1 inches
34	0509	8/18/1992	7	AC	2.6	13	Overlay
34	0509	8/18/1992	8	AC	1.8	13	Overlay
34	0559	11/1/1968	1	SS		216	Original Construction
34	0559	11/1/1968	2	GS	30	308	Original Construction
34	0559	11/1/1968	3	GB	10.5	302	Original Construction
34	0559	11/1/1968	4	AC	5.6	1	Original Construction
34	0559	11/1/1968	5	AC	3	1	Original Construction
34	0559	8/18/1992	5	AC	1	1	Mill 2.0 inches
34	0559	8/18/1992	6	AC	2.5	1	Overlay
34	0559	8/18/1992	7	AC	1.9	13	Overlay
34	0560	11/1/1968	1	SS		216	Original Construction
34	0560	11/1/1968	2	GS	4	308	Original Construction
34	0560	11/1/1968	3	GB	10.5	302	Original Construction
34	0560	11/1/1968	4	AC	5.6	1	Original Construction
34	0560	11/1/1968	5	AC	2.9	1	Original Construction
34	0560	8/18/1992	5	AC	1	1	Mill 1.9 inches
34	0560	8/18/1992	6	AC	2.3	1	Overlay
34	0560	8/18/1992	7	AC	1	20	Overlay
34	0801	6/1/1993	1	SS		204	Original Construction
34	0801	6/1/1993	2	GB	7.8	304	Original Construction
34	0801	6/1/1993	3	AC	3.6	1	Original Construction
34	0802	6/1/1993	1	SS		204	Original Construction
34	0802	6/1/1993	2	GB	11.6	304	Original Construction
34	0802	6/1/1993	3	AC	6.7	1	Original Construction
34	0859	6/1/1993	1	SS		204	Original Construction
34	0859	6/1/1993	2	GB	6.3	304	Original Construction
34	0859	6/1/1993	3	AC	3.7	1	Original Construction
34	0859	6/1/1993	4	AC	3	1	Original Construction
34	0860	6/1/1993	1	SS		204	Original Construction
34	0860	6/1/1993	2	GB	8.6	304	Original Construction
34	0860	6/1/1993	3	AC	6	1	Original Construction
34	0860	6/1/1993	4	AC	2	1	Original Construction
34	0860	6/1/1993	5	AC	2.2	1	Original Construction
34	0901	3/1/1970	1	SS		214	Original Construction

STATE CODE	SHRP ID NUMBER	CONSTRUCTION or OVERLAY DATE	LAYER NO	LAYER TYPE	REPR THICKNESS	MATL CODE	COMMENT
34	0901	3/1/1970	2	GS	5	308	Original Construction
34	0901	3/1/1970	3	GS	5	308	Original Construction
34	0901	3/1/1970	4	TB	7.4	319	Original Construction
34	0901	3/1/1970	5	AC	1.5	1	Original Construction
34	0901	4/22/1998	4	TB	6.5	319	Mill 2.4 inches
34	0901	4/22/1998	6	AC	2.7	1	Overlay
34	0901	4/22/1998	7	AC	2.2	1	Overlay
34	0902	3/1/1970	1	SS		214	Original Construction
34	0902	3/1/1970	2	GS	5	308	Original Construction
34	0902	3/1/1970	3	GS	5	308	Original Construction
34	0902	3/1/1970	4	TB	6.7	319	Original Construction
34	0902	3/1/1970	5	AC	3	1	Original Construction
34	0902	4/22/1998	5	AC	0.6	1	Mill 2.4 inches
34	0902	4/22/1998	6	AC	2.5	1	Overlay
34	0902	4/22/1998	7	AC	2.6	1	Overlay
34	0903	3/1/1970	1	SS		214	Original Construction
34	0903	3/1/1970	2	GS	5	308	Original Construction
34	0903	3/1/1970	3	GS	5	308	Original Construction
34	0903	3/1/1970	4	TB	7.4	319	Original Construction
34	0903	3/1/1970	5	AC	1.4	1	Original Construction
34	0903	4/22/1998	5	AC	0	1	Mill 1.4 inches
34	0903	4/22/1998	6	AC	3.3	1	Overlay
34	0903	4/22/1998	7	AC	2.1	1	Overlay
34	0960	3/1/1970	1	SS		214	Original Construction
34	0960	3/1/1970	2	GS	5	310	Original Construction
34	0960	3/1/1970	3	GS	5	310	Original Construction
34	0960	3/1/1970	4	TB	6.4	319	Original Construction
34	0960	3/1/1970	5	AC	3	1	Original Construction
34	0960	4/22/1998	5	AC	0.9	1	Mill 2.1 inches
34	0960	4/22/1998	6	AC	2.1	1	Overlay
34	0960	4/22/1998	7	AC	2.7	1	Overlay
34	0961	3/1/1970	1	SS		214	Original Construction
34	0961	3/1/1970	2	GS	5	308	Original Construction
34	0961	3/1/1970	3	GS	5	308	Original Construction
34	0961	3/1/1970	4	TB	6.3	319	Original Construction
34	0961	3/1/1970	5	AC	3	1	Original Construction
34	0961	4/11/1998	4	TB	5.6	319	Mill 3.7 inches
34	0961	4/11/1998	6	AC	3.8	1	Overlay
34	0961	4/11/1998	7	AC	2.6	1	Overlay

STATE CODE	SHRP ID NUMBER	CONSTRUCTION or OVERLAY DATE	LAYER NO	LAYER TYPE	REPR THICKNESS	MATL CODE	COMMENT
34	0962	3/1/1970	1	SS		215	Original Construction
34	0962	3/1/1970	2	GS	5	308	Original Construction
34	0962	3/1/1970	3	GS	5	308	Original Construction
34	0962	3/1/1970	4	TB	6.6	319	Original Construction
34	0962	3/1/1970	5	AC	2.4	1	Original Construction
34	0962	4/22/1998	5	AC	0.9	1	Mill 1.5 inches
34	0962	4/22/1998	6	AC	1.5	1	Overlay
34	0962	4/22/1998	7	AC	2.7	13	Overlay
34	1003	12/1/1973	1	SS	54	282	Original Construction
34	1003	12/1/1973	2	GS	24.9	308	Original Construction
34	1003	12/1/1973	3	GB	7.4	308	Original Construction
34	1003	12/1/1973	4	AC	5.9	1	Original Construction
34	1003	12/1/1973	5	AC	1.6	1	Original Construction
34	1003	4/8/1994	4	AC	5.5	1	Mill 2.0 inches
34	1003	4/8/1994	6	AC	2.2	1	Overlay
34	1011	3/1/1970	1	SS		204	Original Construction
34	1011	3/1/1970	2	GS	24.2	308	Original Construction
34	1011	3/1/1970	3	GB	6.9	308	Original Construction
34	1011	3/1/1970	4	AC	7.6	1	Original Construction
34	1011	3/1/1970	5	AC	1.4	1	Original Construction
34	1011	4/28/1998	4	AC	6.6	1	Mill 2.4 inches
34	1011	4/28/1998	6	AC	2.1	13	Overlay
34	1011	4/28/1998	7	AC	1.8	1	Overlay
34	1030	7/1/1969	1	SS	54	205	Original Construction
34	1030	7/1/1969	2	GS	23.4	306	Original Construction
34	1030	7/1/1969	3	GB	6.8	304	Original Construction
34	1030	7/1/1969	4	AC	4.2	1	Original Construction
34	1030	7/1/1969	5	AC	1.8	1	Original Construction
34	1030	7/1/1997	4	AC	3.1	1	Mill 2.9 inches
34	1030	7/1/1997	6	AC	1.9	13	Overlay
34	1030	7/1/1997	7	AC	2.7	1	Overlay
34	1031	-	1	SS		204	Original Construction
34	1031	-	2	GB	11	304	Original Construction
34	1031	-	3	AC	5.5	1	Original Construction
34	1031	-	4	AC	1.8	1	Original Construction
34	1031	-	3	AC	4.3	1	Mill 3.0 inches
34	1031	-	5	AC	3	1	Overlay
34	1031	-	6	AC	2	13	Overlay
34	1033	5/1/1974	1	SS	120	267	Original Construction

STATE CODE	SHRP ID NUMBER	CONSTRUCTION or OVERLAY DATE	LAYER NO	LAYER TYPE	REPR THICKNESS	MATL CODE	COMMENT
34	1033	5/1/1974	2	GS	13.8	304	Original Construction
34	1033	5/1/1974	3	TB	6.2	319	Original Construction
34	1033	5/1/1974	4	AC	1.2	1	Original Construction
34	1033	9/11/1997	4	AC	0.5	1	Mill 0.7 inches
34	1033	9/11/1997	5	AC	2	13	Overlay
34	1033	9/1/2003	6	AC	0.3	11	Seal Coat
34	1034	9/1/1985	1	SS		204	Original Construction
34	1034	9/1/1985	2	TB	8.7	319	Original Construction
34	1034	9/1/1985	3	AC	3	1	Original Construction
34	1638	9/1/1985	1	SS		211	Original Construction
34	1638	9/1/1985	2	TB	7.4	331	Original Construction
34	1638	9/1/1985	3	AC	6.8	1	Original Construction
34	1638	9/1/1985	4	AC	2.4	1	Original Construction
34	6057	6/1/1961	1	SS	74.4	261	Original Construction
34	6057	6/1/1961	2	GB	7.5	304	Original Construction
34	6057	6/1/1961	3	AC	6.1	1	Original Construction
34	6057	6/1/1961	4	AC	1.8	1	Original Construction
36	0801	8/1/1994	1	SS	168	214	Original Construction
36	0801	8/1/1994	2	GB	8.4	304	Original Construction
36	0801	8/1/1994	3	AC	3.8	1	Original Construction
36	0801	8/1/1994	4	AC	1.2	1	Original Construction
36	0802	8/1/1994	1	SS	156	216	Original Construction
36	0802	8/1/1994	2	GB	10	304	Original Construction
36	0802	8/1/1994	3	AC	4.6	1	Original Construction
36	0802	8/1/1994	4	AC	2.1	1	Original Construction
36	0802	8/1/1994	5	AC	0.9	1	Original Construction
36	0859	8/1/1994	1	SS	156	214	Original Construction
36	0859	8/1/1994	2	GB	12.5	304	Original Construction
36	0859	8/1/1994	3	AC	3.9	1	Original Construction
36	0859	8/1/1994	4	AC	1.4	1	Original Construction
36	0859	8/1/1994	5	AC	1.2	1	Original Construction
36	1008	11/1/1980	1	SS		143	Original Construction
36	1008	11/1/1980	2	GS	12	308	Original Construction
36	1008	11/1/1980	3	TB	9.7	319	Original Construction
36	1008	11/1/1980	4	AC	1.1	1	Original Construction
36	1008	8/1/1989	5	AC	1.3	1	Overlay
36	1011	6/1/1984	1	SS		265	Original Construction
36	1011	6/1/1984	2	GB	15.1	304	Original Construction
36	1011	6/1/1984	3	AC	8.6	1	Original Construction

STATE CODE	SHRP ID NUMBER	CONSTRUCTION or OVERLAY DATE	LAYER NO	LAYER TYPE	REPR THICKNESS	MATL CODE	COMMENT
36	1011	6/1/1984	4	AC	1.2	1	Original Construction
36	1011	9/14/1993	5	AC	2.8	1	Overlay
36	1011	9/14/1993	6	AC	1.6	1	Overlay
36	1643	5/1/1978	1	SS		211	Original Construction
36	1643	5/1/1978	2	GS	7.2	304	Original Construction
36	1643	5/1/1978	3	TB	8.2	319	Original Construction
36	1643	5/1/1978	4	AC	2.2	1	Original Construction
36	1643	9/15/1996	5	AC	1.8	1	Overlay
36	1643	9/15/1996	6	AC	1.1	1	Overlay
36	1644	8/1/1980	1	SS	66	203	Original Construction
36	1644	8/1/1980	2	GS	14.5	308	Original Construction
36	1644	8/1/1980	3	TB	6.3	321	Original Construction
36	1644	8/1/1980	4	AC	1.3	1	Original Construction
36	1644	8/1/1980	5	AC	1	1	Original Construction
36	1644	6/19/1996	4	AC	0.6	1	Mill 1.7 inches
36	1644	6/19/1996	6	AC	1.6	1	Overlay
36	1644	6/19/1996	7	AC	1.4	1	Overlay
50	1002	8/1/1984	1	SS		255	Original Construction
50	1002	8/1/1984	2	GB	25.8	304	Original Construction
50	1002	8/1/1984	3	AC	5.5	1	Original Construction
50	1002	8/1/1984	4	AC	3	1	Original Construction
50	1004	9/1/1984	1	SS		103	Original Construction
50	1004	9/1/1984	2	GS	21.6	309	Original Construction
50	1004	9/1/1984	3	GB	24.6	304	Original Construction
50	1004	9/1/1984	4	AC	5	1	Original Construction
50	1004	9/1/1984	5	AC	3	1	Original Construction
50	1004	7/15/2001	5	AC	1.5	1	Mill 1.5 inches
50	1004	7/15/2001	6	AC	0.9	13	Overlay
50	1004	7/15/2001	7	AC	1.8	13	Overlay
50	1681	9/1/1963	1	SS		267	Original Construction
50	1681	9/1/1963	2	GS	12	306	Original Construction
50	1681	9/1/1963	3	GS	21.6	308	Original Construction
50	1681	9/1/1963	4	TB	3.4	321	Original Construction
50	1681	9/1/1963	5	AC	2.4	1	Original Construction
50	1681	9/8/1991	6	AC	4.5	1	Overlay
50	1683	9/23/1991	1	SS		215	New Construction
50	1683	9/23/1991	2	GS	12	306	Original Construction
50	1683	9/23/1991	3	GS	24	308	Original Construction
50	1683	9/23/1991	4	TB	2.8	321	Original Construction

STATE CODE	SHRP ID NUMBER	CONSTRUCTION or OVERLAY DATE	LAYER NO	LAYER TYPE	REPR THICKNESS	MATL CODE	COMMENT
50	1683	9/23/1991	5	AC	2.6	1	Original Construction
50	1683	5/1/2012	6	AC	4.7	1	Overlay

Appendix B: Laboratory-Estimated Plastic Strain Coefficients for the Flexible Pavement Sites

This Appendix B identifies the rut depth category (defined in Chapter 4) that was assumed for the different asphalt layers used in the verification/calibration of the rut depth transfer functions.

STATE CODE	SHRP ID NUMBER	Laboratory-Derived Plastic Strain Coefficients Asphalt Layers, New Flexible K1r	Laboratory-Derived Plastic Strain Coefficients Asphalt Layers, New Flexible K2r	Laboratory-Derived Plastic Strain Coefficients Asphalt Layers, New Flexible K3r	Laboratory-Derived Plastic Strain Coefficients Asphalt Overlay Layers K1r	Laboratory-Derived Plastic Strain Coefficients Asphalt Overlay Layers K2r	Laboratory-Derived Plastic Strain Coefficients Asphalt Overlay Layers K3r
09	0901	-2.45	3.01	0.22	-2.45	3.01	0.22
09	0902	-2.45	3.01	0.22	-2.45	3.01	0.22
09	0903	-2.45	3.01	0.22	-2.45	3.01	0.22
09	0960	-2.45	3.01	0.22	-2.45	3.01	0.22
09	0961	-2.45	3.01	0.22	-2.45	3.01	0.22
09	0962	-2.45	3.01	0.22	-2.45	3.01	0.22
09	1803	-2.45	3.01	0.22	-2.45	3.01	0.22
-	-	-	-	-	-	-	-
23	0501	-2.85	3.01	0.38	-	-	-
23	0502	-2.85	3.01	0.38	-2.45	3.01	0.22
23	0503	-2.85	3.01	0.38	-2.45	3.01	0.22
23	0504	-2.85	3.01	0.38	-2.45	3.01	0.22
23	0505	-2.85	3.01	0.38	-2.45	3.01	0.22
23	0506	-2.85	3.01	0.38	-2.45	3.01	0.22
23	0507	-2.85	3.01	0.38	-2.45	3.01	0.22
23	0508	-2.85	3.01	0.38	-2.45	3.01	0.22
23	0509	-2.85	3.01	0.38	-2.45	3.01	0.22
23	0559	-2.85	3.01	0.38	-2.45	3.01	0.22
23	1001	-2.85	3.01	0.38	-2.45	3.01	0.22
23	1009	-2.45	3.01	0.22	-2.45	3.01	0.22
23	1012	-2.85	3.01	0.38	-	-	-
23	1026	-2.85	3.01	0.38	-2.45	3.01	0.22
23	1028	-2.85	3.01	0.38	-2.45	3.01	0.22
-	-	-	-	-	-	-	-
25	1002	-2.45	3.01	0.22	-	-	-
25	1003	-2.45	3.01	0.22	-	-	-
25	1004	-2.45	3.01	0.22	-2.45	3.01	0.22
-	-	-	-	-	-	-	-
33	1001	-2.45	3.01	0.22	-2.85	3.01	0.38
-	-	-	-	-	-	-	-
34	0501	-2.45	3.01	0.22	-2.45	3.01	0.22
34	0502	-2.45	3.01	0.22	-2.45	3.01	0.22

STATE CODE	SHRP ID NUMBER	Laboratory-Derived Plastic Strain Coefficients Asphalt Layers, New Flexible K1r	Laboratory-Derived Plastic Strain Coefficients Asphalt Layers, New Flexible K2r	Laboratory-Derived Plastic Strain Coefficients Asphalt Layers, New Flexible K3r	Laboratory-Derived Plastic Strain Coefficients Asphalt Overlay Layers K1r	Laboratory-Derived Plastic Strain Coefficients Asphalt Overlay Layers K2r	Laboratory-Derived Plastic Strain Coefficients Asphalt Overlay Layers K3r
34	0503	-2.45	3.01	0.22	-2.45	3.01	0.22
34	0504	-2.45	3.01	0.22	-2.45	3.01	0.22
34	0505	-2.45	3.01	0.22	-2.45	3.01	0.22
34	0506	-2.45	3.01	0.22	-2.45	3.01	0.22
34	0507	-2.45	3.01	0.22	-2.45	3.01	0.22
34	0508	-2.45	3.01	0.22	-2.45	3.01	0.22
34	0509	-2.45	3.01	0.22	-2.45	3.01	0.22
34	0559	-2.45	3.01	0.22	-2.45	3.01	0.22
34	0560	-2.45	3.01	0.22	-2.45	3.01	0.22
34	0801	-2.45	3.01	0.22	-	-	-
34	0802	-2.45	3.01	0.22	-	-	-
34	0859	-2.45	3.01	0.22	-	-	-
34	0860	-2.45	3.01	0.22	-	-	-
34	0901	-2.45	3.01	0.22	-2.45	3.01	0.22
34	0902	-2.45	3.01	0.22	-2.45	3.01	0.22
34	0903	-2.45	3.01	0.22	-2.45	3.01	0.22
34	0959	-2.45	3.01	0.22	-2.45	3.01	0.22
34	0960	-2.45	3.01	0.22	-2.45	3.01	0.22
34	0961	-2.45	3.01	0.22	-2.45	3.01	0.22
34	0962	-2.45	3.01	0.22	-2.45	3.01	0.22
34	1003	-2.85	3.01	0.38	-2.45	3.01	0.22
34	1011	-2.45	3.01	0.22	-2.45	3.01	0.22
34	1030	-2.85	3.01	0.38	-2.45	3.01	0.22
34	1033	-2.45	3.01	0.22	-2.45	3.01	0.22
34	1034	-2.45	3.01	0.22	-	-	-
34	1638	-2.45	3.01	0.22	-	-	-
34	6057	-2.45	3.01	0.22	-	-	-
-	-	-	-	-	-	-	-
36	0801	-2.45	3.01	0.22	-	-	-
36	0802	-2.45	3.01	0.22	-	-	-
36	0859	-2.45	3.01	0.22	-	-	-
36	1008	-2.85	3.01	0.38	-2.45	3.01	0.22
36	1011	-2.45	3.01	0.22	-2.45	3.01	0.22
36	1643	-2.85	3.01	0.38	-2.45	3.01	0.22
36	1644	-2.45	3.01	0.22	-2.45	3.01	0.22

STATE CODE	SHRP ID NUMBER	Laboratory-Derived Plastic Strain Coefficients Asphalt Layers, New Flexible K1r	Laboratory-Derived Plastic Strain Coefficients Asphalt Layers, New Flexible K2r	Laboratory-Derived Plastic Strain Coefficients Asphalt Layers, New Flexible K3r	Laboratory-Derived Plastic Strain Coefficients Asphalt Overlay Layers K1r	Laboratory-Derived Plastic Strain Coefficients Asphalt Overlay Layers K2r	Laboratory-Derived Plastic Strain Coefficients Asphalt Overlay Layers K3r
-	-	-	-	-	-	-	-
50	1002	-2.85	3.01	0.38	-	-	-
50	1004	-2.45	3.01	0.22	-2.45	3.01	0.22
50	1681	-2.45	3.01	0.22	-2.45	3.01	0.22
50	1683	-2.85	3.01	0.38	-2.85	3.01	0.38
-	-	-	-	-	-	-	-

Appendix C: Laboratory-Estimated Fracture Strength Coefficients for the Flexible Pavement Sites

This Appendix C identifies the fracture strength coefficients (defined in Chapters 5 and 6) that were assumed for the different asphalt layers used in the verification/calibration of the bottom-up fatigue and transverse cracking transfer functions.

STATE CODE	SHRP ID NUMBER	Fatigue Strength Coefficient, k1f	Aggregate Thermal Coefficient
09	0901	3.75	5.0E-06
09	0902	3.75	5.0E-06
09	0903	3.75	5.0E-06
09	0960	3.75	5.0E-06
09	0961	3.75	5.0E-06
09	0962	3.75	5.0E-06
09	1803	3.75	6.5E-06
-	-	-	-
23	0501	3.75	5.0E-06
23	0502	3.75	5.0E-06
23	0503	3.75	5.0E-06
23	0504	3.75	5.0E-06
23	0505	3.75	5.0E-06
23	0506	3.75	5.0E-06
23	0507	3.75	5.0E-06
23	0508	3.75	5.0E-06
23	0509	3.75	5.0E-06
23	0559	3.75	5.0E-06
23	1001	3.75	5.0E-06
23	1009	1.00	5.0E-06
23	1012	3.75	4.0E-06
23	1026	3.75	5.0E-06
23	1028	3.75	6.5E-06
-	-	-	-
25	1002	1.00	6.5E-06
25	1003	2.50	6.5E_06
25	1004	3.75	5.5E-06
-	-	-	-
33	1001	1.00	5.5E-06
-	-	-	-
34	0501	1.00	6.5E-06
34	0502	2.50	5.5E-06
34	0503	2.50	5.5E-06
34	0504	2.50	5.5E-06
34	0505	2.50	5.5E-06
34	0506	2.50	5.5E-06
34	0507	2.50	5.5E-06
34	0508	2.50	5.5E-06
34	0509	2.50	5.5E-06
34	0559	2.50	5.5E-06

STATE CODE	SHRP ID NUMBER	Fatigue Strength Coefficient, k1f	Aggregate Thermal Coefficient
34	0560	2.50	5.5E-06
34	0801	3.75	5.0E-06
34	0802	3.75	5.0E-06
34	0859	3.75	5.0E-06
34	0860	3.75	5.0E-06
34	0901	1.00	5.0E-06
34	0902	1.00	5.0E-06
34	0903	1.00	5.0E-06
34	0959	1.00	5.0E-06
34	0960	1.00	5.0E-06
34	0961	1.00	5.0E-06
34	0962	1.00	5.0E-06
34	1003	1.00	5.0E-06
34	1011	1.00	6.5E-06
34	1030	1.00	5.0e-06
34	1033	1.00	5.5E-06
34	1034	2.50	5.0E-06
34	1638	3.75	5.0E-06
34	6057	3.75	5.5E-06
-	-	-	-
36	0801	2.50	5.0E-06
36	0802	2.50	5.0E-06
36	0859	2.50	5.0E-06
36	1008	3.75	5.0E-06
36	1011	3.75	5.0E-06
36	1643	3.75	6.50E-06
36	1644	3.75	6.50E-06
-	-	-	-
50	1002	2.50	6.50E-06
50	1004	2.50	6.5E-06
50	1681	3.75	5.0E-06
50	1683	3.75	5.0E-06